THÈSE

Pour obtenir le grade de

DOCTEUR DE L'UNIVERSITÉ GRENOBLE ALPES

Spécialité : BIS - Biotechnologie, instrumentation, signal et imagerie pour la biologie, la médecine et l'environnement

Arrêté ministériel : 25 mai 2016

Présentée par

Sebastian KÖHLER

Thèse dirigée par **Donald MARTIN**, professeur des universités, Université Grenoble Alpes
et codirigée par **Marco MACCARINI**, chargé de recherche, CNRS
et **Giovanna FRAGNETO,** directrice de recherche, Institut Laue-Langevin

préparée au sein des Laboratoires **Techniques de l'Ingénierie Médicale et de la Complexité - Informatique, Mathématiques et Applications**
et **Institut Laue-Langevin**
dans **l'École Doctorale Ingénierie pour la Santé la Cognition et l'Environnement**

Étude de bicouches lipidiques amarrées destinées à l'incorporation de protéines membranaires

Investigation of tethered lipid bilayer systems for membrane protein incorporation

Thèse soutenue publiquement le **26 juin 2020**,
devant le jury composé de :

Madame Jayne LAWRENCE
Professeur, University of Manchester, Rapporteur
Monsieur Thierry CHARITAT
Professeur, Université de Strasbourg, Rapporteur
Monsieur Tommy NYLANDER
Professeur, University of Lund, Examinateur
Madame Judith PETERS
Professeur, Université Grenoble Alpes, Présidente

Acknowledgements

Without the help of several people, this thesis would not have been possible. First of all, I want to thank my supervisors Marco Maccarini, Giovanna Fragneto and Donald Martin for giving me the opportunity to work in such an interesting multi-disciplinary field. Don as the director of this project always had enthusiastic advice, especially on electrochemical topics. My thanks go to Giovanna for the great guidance, organisation and help during all experiments, and for giving me the opportunity to attend several interesting conferences as well as perform experiments in different places. I want to thank Marco for supporting me on a daily basis. His encouragement and suggestions were truly helpful and indispensable for the success of my work.

The biological part of my thesis would not have been possible without Jean-Pierre Alcaraz, who not only produced the protein for my project, but also always took the time to answer the many questions that a physicist has about biology.

The neutron reflectometry experiments at the ILL and ISIS were successful due to the support of the great instrument scientists. I'm grateful for the help from Thomas Saerbeck and Samantha Micciulla at D17, Philipp Gutfreund and Armando Maestro at FIGARO and Mario Campana at SURF.

Simon Wood was a great help for all technical questions, not only related to D17 and FIGARO, but also whenever a question about sample environment or how to generally make something came up.

Yuri Gerelli contributed to this work in many indirect ways. He provided great support for the instruments and equipment of the PSCM, but was also helping with general advice concerning scientific life. He was the one who always had answers to all the small questions related to membrane biophysics.

I want to thank David Hess for his unrelenting support in the chemistry labs. No matter if it was evening or weekend, David could always be counted on.

Of course I have to mention all the great people that I met in Grenoble: Gauthier and Pierre in the SyNaBi group were able to show me a little bit of French culture. Many colleagues and friends from the ILL made working there an amazing experience. I especially want to thank Aljoša, Tetiana, Andrea, Dominic, Nico, Marco and Loïc who not only made work more enjoyable through scientific and philosophical discussions, but who were also an important part of my personal life. Thank you for making the last three years in Grenoble special.

Finally I want to thank my parents and my sister. In the end, it is because of their care and support that I was able to work on this project in such an impressive environment. Thank you for everything.

Abstract

This thesis investigates the structure of tethered lipid bilayer membranes, which are lipid bilayers chemically grafted to a planar surface. Compared to other model membrane systems they show increased stability, but have a higher complexity in structure, which requires thorough investigation. The structure of tethered lipid bilayers is strongly influenced by the molecular architecture of the grafting molecules. Within the framework of this thesis, two different types of tether architecture were investigated. The first was a lipid bilayer tethered to a gold surface and using a single phytanyl chain to anchor the membrane, while the second used a synthetic, lipid-like molecular structure and was bound to a silicon surface by silane chemistry. Three main objectives for those systems were pursued: (i) to investigate tethered bilayers with high fractions of the lipid cardiolipin, (ii) to investigate the structural differences between tethered membranes having different surface grafting molecules, and (iii) to investigate the incorporation of the membrane protein NhaA into these systems. Cardiolipin has a unique structure characterized by four fatty acid chains, which leads to interesting effects on bilayer structure, as well as interaction with several membrane proteins. Tethered membranes with high cardiolipin fractions of up to 80% were structurally characterized by neutron reflectometry, and their electrophysiological properties were investigated by electrochemical impedance spectroscopy. In both tethered bilayer architectures, cardiolipin containing membranes showed a very condensed structure with high electrical sealing properties. Differences in tether architecture mainly affected the structure of the water-filled sub-membrane space. The tethered bilayers grafted to a gold surface showed very low water content below the membrane, while the sub-membrane space of bilayers grafted to a silicon surface was highly hydrated. Finally, NhaA was successfully incorporated into both tether architecture systems at high fractions without damaging the tethered lipid bilayer structure significantly. This makes tethered membranes containing elevated amounts of cardiolipin a promising model membrane system for protein incorporation and offers possibilities for further technological uses of tethered lipid bilayers.

Résumé

Cette thèse a pour but l'étude de la structure de bicouches lipidiques greffées chimiquement sur une surface plane et utilisées comme modèles de membranes cellulaires. Ces systèmes, comparés à d'autres systèmes de membranes modèles, présentent une stabilité accrue et une structure plus complexe, nécessitant une étude approfondie. La structure des bicouches lipidiques amarrées est fortement influencée par l'architecture moléculaire des composés utilisés pour greffer la bicouche lipidique à la surface. Cette thèse porte sur l'étude de deux systèmes d'ancrage sur des surfaces différentes. Le premier système est une bicouche lipidique liée à une surface d'or utilisant une seule chaîne alkyle pour ancrer la membrane. Le second système utilise une structure moléculaire synthétique semblable à un lipide pour ancrer la membrane et lie à une surface de silicium par chimie du silane. Cette thèse a trois objectifs pour ces systèmes d'ancrage: (i) étudier les bicouches amarrées avec des fractions élevées du lipide cardiolipine, (ii) étudier la structure des membranes attachées sur une surface via l'utilisation de différentes molécules de greffage, et (iii) étudier l'incorporation de la protéine membranaire NhaA dans ces systèmes. Le lipide cardiolipine a une structure unique contenant quatre chaînes d'acides gras. Cela conduit à des propriétés intéressantes des bicouches le contenant ainsi qu'à une interaction avec plusieurs protéines membranaires. La structure des bicouches amarrées avec des fractions de cardiolipine élevées pouvant atteindre 80 % a été étudié. Les deux systèmes étudiés pourraient être utilisés pour former des bicouches lipidiques avec des fractions élevées de cardiolipine, bien que le cardiolipine est généralement présent dans les membranes naturelles à de faibles fractions de l'ordre de 10 %. La nanostructure des membranes avec différentes fractions de cardiolipine a été caractérisée par réflectométrie neutronique, et leurs propriétés électrophysiologiques ont été étudiées par spectroscopie d'impédance électrochimique. Ces membranes amarrées de cardiolipine ont montré une structure très condensée avec de très bonnes propriétés d'étanchéité électrique. Ces résultats sont importants pour des utilisations technologiques des bicouches lipidiques captives. Enfin, l'incorporation de la protéine membranaire NhaA dans tels systèmes membranaires a été étudiée. NhaA a été incorporée avec succès dans les deux systèmes à des fractions élevées sans perturber de manière significative la structure bicouche lipidique. Cela fait des membranes amarrées contenant des quantités élevées de cardiolipine un système de membrane modèle prometteur pour l'incorporation de protéines.

Contents

Acronyms

APTES 3-aminopropyltriethoxysilane

AuMW gold matched water

Chol cholesterol

CL cardiolipin

DLP double length phytanyl

DOPC 1,2-dioleoyl-sn-glycero-3-phosphocholine

DPEPC diphytanyl-ether-phosphatidylcholine

DPN DSPE-PEG-NHS

DSPE 1,2-distearoyl-sn-glycero-3-phosphoethanolamine

EIS electrochemical impedance spectroscopy

GDPE glycero diphytanyl ether

ILL Institut Laue-Langevin

NhaA sodium proton antiporter A

NR neutron reflectometry

OxMW silicon oxide matched water

PC phosphatidylcholine

PEG poly ethylene glycol

QCM-D quartz crystal microbalance with dissipation monitoring

SiMW silicon matched water

SLB solid-supported lipid bilayer

SLD scattering length density

stBLM sparsely tethered bilayer lipid membrane

tBLM tethered bilayer lipid membrane

TOF time of flight

Chapter 1

Introduction

The aim of the work presented in this thesis is the structural characterization of tethered lipid bilayers of different composition and the investigation of membrane protein incorporation. This very specific topic is motivated by developments in different research fields ranging from biology through physics to bio-engineering. At the heart of this work lie lipid bilayers. They are the constituting feature of all cell membranes and thus the structures that define the borders of all living beings.

The basic concept that some form of membrane surrounds cells and separates them from their environment dates back more than 250 years [1]. A detailed understanding of the structure of these membranes is, however, a relatively recent development. Although first ideas about the lipid bilayer nature of cell membranes were proposed at the end of the 19th century, it took until 1972, when Singer and Nicholson developed the fluid mosaic model [2], to arrive at the current understanding and concepts of the cell membrane. A cell membrane consists of many different components which assemble into a complex structure as sketched in fig. 1.1 on the left. Its basic building unit are lipids, molecules that possess a hydrophobic chain region and a hydrophilic headgroup (fig. 1.1, right). The lipids arrange into a double layer structure with the hydrophobic region facing inwards. This creates a barrier for water that separates the interior of the cell from the outside world. Cell membranes, however, are much more complex than this basic building block. While the membrane itself is mainly built up of hundreds of different lipids, sterols, membrane proteins, peptides, sugars and various other components, the shape of the cell membrane is strongly influenced by the cytoskeletal structure below the membrane, as well as the external carbohydrate glycocalyx [3]. Within the fluid mosaic model, the different components are well structured across the cell membrane, but can diffuse in the lateral direction, which leads to fluid-like behaviour for molecules in the bilayer.

While the complex nature of cell membranes gives rise to obviously fascinating properties, as it forms the basis of advanced life, their fundamental biophysical properties are frustratingly difficult to measure in situ. Hence model membrane systems are needed to determine the role or structure of any single component of the cell membrane. These sim-

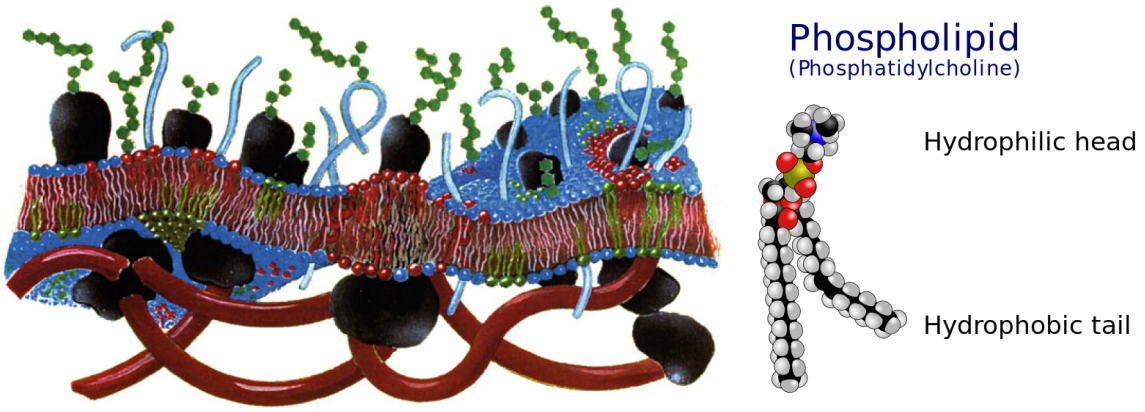

Figure 1.1: Left: Sketch of the cell membrane [4]. Right: space filling model representation of a phospholipid [5].

plified systems consist of only a small part of the components that constitute a natural cell membrane and thus show only a limited number of its properties. They are, however, much easier to characterize with biophysical methods and can serve to shed light on isolated processes. Many different model systems have been developed over the years that show different properties and model different features of a cell membrane (see sec. 2.1). The main motivation behind the use of different model membrane systems is twofold. Firstly, a membrane model must be adapted to the biological process or structure that is to be investigated. Depending on the nature of the investigated topic, different features of a cell membrane must be matched or approximated for its observation. Secondly, a model system should be adapted for accessibility by different experimental methods. While very complex systems that are close to a natural cell membrane can be produced, they are useless if no information can be extracted from them with the available experimental equipment. Some characterization methods require the membranes to conform to a particular geometry, many model membrane systems are therefore specifically designed with these constraints in mind. Multiple model membrane systems of varying shape have been developed over the years. Lipid bilayers are one of the simplest model membrane systems and can range from spherical systems like vesicles, micelles or bicelles to planar systems like free standing bilayers, bilayer stacks or single bilayers on a flat surface [6]. Among these, planar model membrane systems have the advantage of being very well suited for investigation with nanostructural and electrochemical characterization methods.

In light of the considerations outlined above, a planar model membrane system consisting of tethered lipid bilayer membranes (tBLMs) was selected for this work. tBLMs consist of lipid bilayers that are chemically grafted to a planar surface. The grafting molecules consist of a hydrophobic anchor that inserts into the lipid bilayer and is connected to the surface by a hydrophilic chain-like molecule. This type of system is explained in detail in sec. 2.1. Structurally, tBLMs can imitate all biological properties that planar model system exhibit in general. Additionally, the inserted grafting molecules can mimic situations

in which structures attach to a membrane in vivo. This may be the case for cytoskeletal attachment points in the cell membrane, or in situations such as neurotransmitter binding, in which protein anchors inserting into a membrane induce fusion of vesicles with a membrane. Furthermore, the attachment to a planar surface makes tBLMs accessible to a range of experimental methods that are sensitive to interfaces. This will be exploited by the use of neutron reflectometry in this thesis. In addition to this favourable structure for experimental investigation, tBLMs are highly robust both in time and against external influences. This allows long term studies and treatment that would damage other types of model system. Moreover, the robustness of tBLMs opens up a field of bio-technological devices. Bio-sensors and other devices that make use of model membrane systems are required to function over extended periods of time. As most other model membrane systems lack the required stability, the development of tBLMs has led to advances in the field of biologically inspired devices. All three reasons make them an interesting model membrane system to investigate.

tBLMs offer a broad freedom in design because there are multiple different ways to create them and many different specific compositions of the molecules that connect the lipid bilayer to the surface. This is an obvious advantage that has been exploited in a multitude of studies. Despite this rapid expansion in their use and investigation, the nanostructural details of many tBLM systems have often not been precisely defined. This is important however, as the exploitation of tBLMs for more sophisticated applications requires a detailed understanding of the nanostructure of tBLMs. The so-called DLP tethers, which will be introduced in detail in section 2.3 are a case in point. They make use of a gold surface as a support, which provides access to electrochemical characterization methods. Despite a 20-year history of development, the nanostructural properties of DLP-tether systems are not commonly described, even if their electrophysiological properties are widely exploited. This is a strong motivation for the research contained in this thesis, as knowledge of the structural properties will advance the interpretation of experimental results obtained using this system. Furthermore, because of the large number of different architectures, many different ways to prepare tBLMs and many specific structures remain unexplored. This offers the possibility of improving existing systems by alteration of components and experimental procedures. This is the motivation for choosing to characterize the second tBLM tethering system that is described in sec. 2.4. It differs from the DLP tBLMs in the structure of the molecules used to graft the bilayer to the surface. The architecture is similar to tBLM systems that have been described previously, but differs in surface functionalization which may make it interesting for specific applications. These DSPE-PEG-NHS tBLMs are supported by a silicon surface, which is easier to procure than gold surfaces at the requisite quality and facilitates the interpretation of data obtained from scattering experiments.

tBLMs have been exploited since the 1990s to investigate the functional properties of membrane proteins [7]. Generally, most membrane proteins require a lipid bilayer environment to function, thus for their investigation, model membrane systems are needed. This is particularly the case for ion transporting membrane proteins that have the important role of translocating ions across lipid bilayer membranes. Naturally, a lipid bilayer barrier is needed

to be able to determine any movement across it. A tBLM provides the ideal basic building block for constructing these complex ion-transporting model membrane systems. Due to their robust nature, they can withstand the processes of incorporating ion-transporting membrane proteins. These processes require disruption, but not dissolution, of lipids in the bilayer and often involve the use of detergents. The connection to a surface by the tethering molecules provides the robustness needed for the construction of this complete tBLM + protein system, which other planar model systems lack. This property is exploited in this thesis to investigate a specific ion transport protein, the sodium proton antiporter NhaA. NhaA is an electrogenic transporter, which means that it transports more ions in one direction across the membrane than in the other. This property makes it interesting for the third range of applications for tBLMs mentioned above: the use in biomimetic devices.

Within the Nanobiotechnology and Biomimetic Systems research group at the University of Grenoble (SyNaBi), a biomimetic device is being developed that makes use of this ion transport across a membrane. The concept consists of two compartments that are divided by a lipid bilayer with incorporated NhaA. The protein transports sodium ions across the membrane, creating a trans-membrane potential. Placement of electrodes in each compartment allows the induced ionic potential to be harvested and transformed into an electrical potential which can be used for electricity generation [8]. This concept may be used in the future for an implantable device that fuels medical implants by making use of substances that are present in the body (sodium ions in this case). The optimization of this system is limited by a lack of detailed understanding of the interaction between NhaA and its lipid bilayer environment. This is important as the structure of a membrane strongly influences the protein incorporation and function. As mentioned previously, the structure of the lipid bilayer environment is determined not only by the lipid composition, but also by the tether architecture when a tBLM is used as a model system. The development of this device serves as a further motivation for the investigation of the properties of tBLM systems and in particular for the choice of NhaA as an electrogenic ion transport protein. Within this thesis, the interaction between NhaA incorporation and the tBLM's lipid composition, as well as the tether architecture, is investigated. The characterization of lipid composition is focused on membranes containing large fractions of cardiolipin (CL), a lipid with unique structure and properties which is introduced further in sec. 2.2.1. This lipid may not only influence the protein incorporation, but also affect the structures of the tBLMs themselves. These considerations lead to the three points of interest tackled in this thesis: the type of tBLM architecture, its lipid composition and the incorporation of NhaA.

A study of tBLM systems requires experimental techniques that are adapted to provide information about interface systems, as the connection to a surface is a defining factor of tBLMs. The choice of a planar surface allows the use of high resolution structural techniques like neutron reflectometry (NR), which is one of the main techniques used in this thesis. NR gives averaged structural information about the tBLM system with sub nanometer precision. This technique can thus be used to characterize the dimensions and composition of different parts of the lipid bilayer and tether layer and, as NR is sensitive to the molecular composition of a system, will also allow the protein presence and degree

of protein incorporation to be determined. Furthermore a planar design, especially with a conductive gold surface as a support, allows for the placement of electrodes on both sides of the system for an electrophysiological characterization using electrochemical impedance spectroscopy (EIS). This is an established method to determine DLP tBLM parameters [9] and therefore enables the comparison of information obtained on cardiolipin containing tBLMs in this thesis to studies with different lipid composition.

The **aims of this thesis** are:

- The investigation of two different tBLM architecture systems and their specific structural properties and differences: DLP tBLMs (introduced in 2.3) and DPN tBLMs (2.4).
- The variation of CL content in both tBLM systems and the characterization of the effects that this has on bilayer structure and properties.
- The incorporation of the ion channel protein NhaA into these tBLM systems, to study if it is affected by CL and which structural changes the incorporation of NhaA causes in both tBLM systems.

Chapter 2 will describe the scientific background of tBLM systems, their properties, the differences between different systems and the fabrication procedures of the two systems used in this thesis. This is followed by an introduction of the membrane protein NhaA and the protein fabrication and incorporation procedures. Chapter 3 is dedicated to the experimental techniques used in this project. An overview of the theoretical background will be given, as well as the experimental details and the data modelling process. Chapter 4 presents a structural characterization of DLP tBLMs with varying CL concentration and the effects of NhaA incorporation using EIS and NR (sec. 4.1). The nanostructural characterization of the effect of CL content on the DPN tBLM system is presented in section 4.2.1, together with the characterization of changes induced by NhaA incorporation. In chapter 5, a summary of the performed studies will be given. The results for the two different tether systems will be compared and an outlook for future developments will be given.

Chapter 2

Sample systems and preparation

2.1 Tethered lipid bilayers as model systems for lipid membranes

Model membrane systems encountered broad interest by enabling the investigation of function, properties or effects of single components, which can not be studied in natural biological systems. This may be because the signal of single components is superimposed by the other components, or because the complexity of natural membranes makes the interpretation of causality very difficult or impossible. Depending on the topic to investigate, a large number of model systems of different characteristics have been developed, most of which fall either into a round shaped vesicle category or are planar membranes. While they all have their application I will focus on different forms of planar lipid membranes here.

Free standing black lipid membranes are probably the most natural model system and one of the first ones to be developed [10]. While they mimic the natural solvent environment quite well, they are very fragile and inaccessible by many methods.

Forming a lipid bilayer on a flat surface (called solid-supported lipid bilayers (SLBs)) makes it possible to study membranes by a large range of methods which are interface or surface sensitive like AFM, SPR or different scattering techniques, and thus increases the amount of information which can be obtained[11]. These membranes are comparably easy to prepare. Usually employed methods are vesicle fusion (see 2.1.1) or Langmuir-Blodgett/Langmuir-Schäfer deposition. While a large proportion of today's knowledge about lipid bilayer structure was obtained using this kind of model system, there are several shortcomings. For long term studies SLBs are not suitable as they tend to deteriorate over a timespan of days. The close proximity to the substrate can also lead to effects like a decreased lipid mobility in the membrane [12]. Furthermore the suitability of SLBs as an environment for membrane protein studies is debatable. The close proximity of the membrane to the surface hinders protein incorporation or at least leads to interaction of the protein with the surface [13]. A way to make SLBs more suitable for protein incorporation is to assemble them

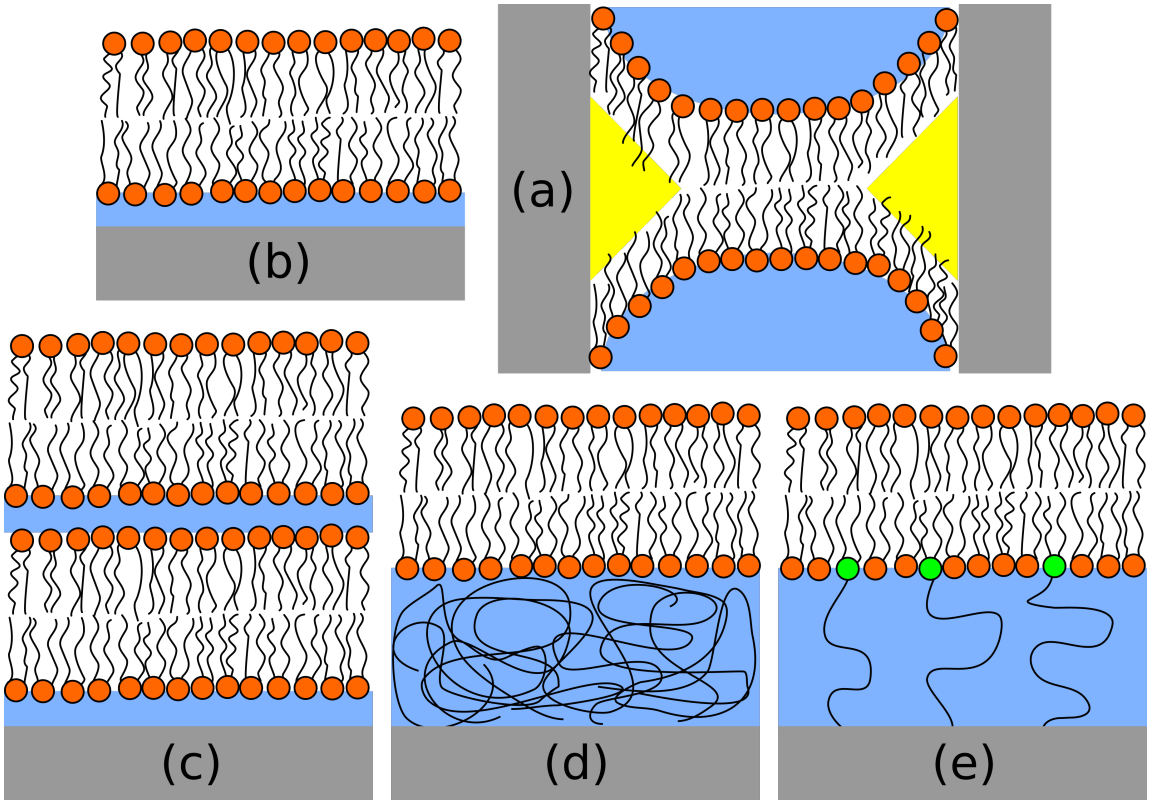

Figure 2.1: Different model membrane systems: a.: Black lipid membrane, b.: Solid supported lipid bilayer, c.: Double lipid bilayer, d.: Cushioned lipid bilayer, e.: Tethered lipid bilayer.

over holes on patterned or randomly organized surfaces [14]. Otherwise the complexity of the model membrane system can be increased in several ways, each of them leading to advantages in different aspects.

Double lipid bilayers or floating lipid bilayers are an interesting model system that is for some aspects more relevant as mimic of natural membranes than supported bilayers. They consist of a second bilayer floating in close proximity above a solid supported bilayer. This proximity to another membrane instead of a rigid substrate causes bilayer-bilayer interactions which are much more resembling of the interactions in biological matter than a flat substrate. While this type of model system has considerable advantages in mimicking some aspects of membrane behaviour (such as the ability to fluctuate), these systems are not easy to produce and the floating bilayer is less stable than SLBs [15].

Another possibility is the addition of a cushioning layer between support and lipid bilayer. This is usually a soft polymer layer, which aims to keep the thermodynamical and structural properties of free standing bilayers[11]. They are more stable than floating bilayers, but still

provide a separation from the surface. By adapting the composition of the support, a series of different preparation methods can be used to produce this type of model system[16].

Finally, by combining a cushioning layer and a chemical bond to the surface, tethered lipid bilayer membranes (tBLMs) can be produced. They offer the same biological relevance as polymer cushioned bilayers from having a separation between membrane and surface, as well as graft the membrane to the surface which leads to highly increased stability, both against external forces and in time [17].

These tBLMs are the main interest of this project, as they offer the possibility to insert membrane proteins, provide an ion reservoir below the membrane and are stable enough for long term studies. In the following sections I will give a general overview of tBLM structure and production, as well as discuss the different tBLM systems used within this project in more detail. The individual experiments and their scientific interpretation will be presented in chapter 4.

tBLMs are a relatively recent model membrane system, with first developments in the 1990s (e.g. [18],[7]). They have seen great interest in the last 20 years. From the first concepts on they have been regarded as an ideal platform for biosensors because of their increased stability, when compared to SLBs [7]. However while there are many functional studies on tBLMs, their detailed structure is still under investigation, mainly because there are so many different structures that rarely any of them has been subject of more than a few studies.

However, apart from a few exceptions, they all exhibit the same general structure. They are connected to the surface by molecules, which consist of a hydrophobic part that inserts into the inner of the membrane or even constitutes large parts of the membrane. Connected to that is a hydrophilic part which creates the water filled space between the membrane and the surface. Finally, a functional group which grafts the tether molecules to the surface is attached to that hydrophilic part. These are the basic components of every tether molecule, but their exact structures differ vastly between different systems. As each of the parts can be altered, tBLMs can be grouped according to their structure in these three parts.

Supporting surface

A few categories of tBLMs have seen increased interest for different reasons. tBLMs can be anchored to different kinds of surfaces. Among the most common are gold [7, 19], silicon [20, 21], and to a lesser extend mercury [22]or quartz [23]. Gold is by far the most used one, mainly for the following two reasons. Firstly, the sulfur-gold chemistry which is usually used to attach the tethers to the surface is very easy to use and forms very stable bonds to the surface [24]. This could be thiols or disulphides. The second reason is the possibility to use the conductive gold surface as an electrode for electrophysiological studies [25]. Most of the work in this project is carried out on gold supported tBLMs.

There is a range of tBLM systems which make use of silicon surfaces with different kinds of surface functionalization for the attachment of tether molecules. Usually a form of silanization is used as it allows the attachment of different functional groups[21, 20]. Silanization

has also been reported as a method to graft tether molecules to surfaces other than silicon. Wagner et al. [23], e.g., used it for tBLM formation on quartz slides. While silicon surfaces lack the possibility to be used as an electrode for electrophysiological studies, they are much easier to prepare in a sufficient quality than gold and offer an easier access by different surface characterization methods. Using a doped silicon substrate even enables the use as an electrode[26, 27]. The DSPE-PEG-NHS tBLMs presented in 2.4 make use of such a silane functionalized silicon surface.

Spacer group

Considering the spacer structure there are two larger classes, which are frequently used and have been developed around the same time: polymer spacers which are mainly poly ethylene glycol (PEG) spacers [7, 28] and peptide spacers [19, 7]. PEG spacers are a further development of polymer cushioned SLBs, where one end of the PEG is connected to the surface and the other end to the membrane inserting part. As such they show generally similar properties in terms of separation from the surface, with the additional feature of increased stability due to being at least partly covalently connected to the surface. PEG forms long very flexible chains, which lead - assuming that the PEG density is not too high on the surface - to coiling below the membrane. In this way, the layer separating the membrane from the surface is usually much thinner than the length of the PEG chain. As another consequence this leads to at partly retained lipid mobility in the lower leaflet, as the flexibility of the chain allows a certain range of movement.

Tether molecules which use peptides as spacers are the second large group. They offer a great deal of flexibility because they can be tailored according to needs by changing the amino acid sequence. This leads to control over length and rigidity and can even be used to produce secondary structures. Peptide tethers showing secondary structures are however still relatively unexplored. Nevertheless, peptide tethers have been shown to lead to stable tBLMs and are a valid alternative to PEG tethers.

Apart from the general structure of the spacer, the length of the same is of high importance to the structure of the sub-membrane space. While the exact dependence differs for different tether systems, an often seen trend is that a longer spacer molecule leads to higher hydration in the sub-membrane space, but also more defects in the lipid bilayer [29].

Membrane inserting anchor

The part of the tether molecule inserting into the membrane is the part which actually connects the lipid bilayer to the surface. As the lipids in a bilayer are connected via hydrophobic interaction, this is also the force which ultimately determines the strength of the bond between membrane and surface. The structure of this part - as for the other parts - can vary widely. Most systems span half of the bilayer, but in a few cases full membrane spanning anchors have been reported [30].

An obvious choice for such a structure is a lipid like shape which is connected to the spacer, and this kind of tether is probably the most common one ([31, 23, 32]). Both an actual lipid structure with head group and two fatty acid chains, as well as lipid like structures which

basically connect two fatty acids to a PEG chain [33] have been used. The most commonly used lipids are DSPE and other phosphatidylethanolamines. These may be connected to different spacer units like PEG[32] or peptides[19]. Like with lipids the fatty acid chains of these lipid like anchors can vary in length and degree of unsaturation. Unsaturation has been related to higher fluidity in the resulting tBLM and is supposed to facilitate protein incorporation [34].

The basic requirement for the anchor part is hydrophobicity, and as such any basic hydrophobic chain can fulfil this purpose. Alkyl chains like phytanyl fulfil this requirement and, when chosen at a length similar to a lipid molecule, they effectively replace some of the lipids in the membrane [7, 28]. While only one chain leads to a weaker anchoring in the membrane [35] this kind of anchor molecules leads to stable tBLMs. The DLP tether system presented in 2.3 makes use of such a structure.

Both these types of anchor molecules replace part or all of the lower leaflet of the lipid bilayer. Molecules which cover both leaflets of the lipid bilayer can be formed from two lipid like molecules connected at the end of the alkyl chains to form such an anchor complex [30, 36]. The use of a membrane protein as a tether molecule which spans the whole bilayer has been reported by Giess et al. [37]. This protein possesses a his-tag which is used as a flexible spacer unit, while the histidine group binds to the surface.

Sparsely tethered lipid bilayers (stBLMs)

One characteristic of tBLMs is the difference in composition between the upper and the lower leaflet of the bilayer. Even with a lower leaflet built from lipid-like tether molecules the mobility of those molecules is reduced due to their attachment to the surface. A type of tBLMs that is closer to symmetric membranes are so called sparsely tethered lipid bilayer membranes (stBLMs). This kind of system composes only part of the lower leaflet from tether molecules, while the gaps are filled up with the lipids making up the bilayer. This provides at least a part of the inner leaflet with the necessary lipid mobility needed for e.g. protein incorporation. The preparation of these stBLMs can, for example, be achieved by only covering a part of the surface with tether molecules. When covering a surface with long polymer tethers, the coiled up molecules can lead to obstruction of a larger part of the surface than just the molecule diameter. In this way the resulting bilayer has a lower fraction of anchors in the lower leaflet than a full surface coverage would suggest. However this method offers little control over the exact amount of tether molecules on the surface. A better control can be achieved by introducing additional molecules which cover the surface. These are molecules which usually have a surface grafting group similar to the actual tether molecule, but are much shorter and do not possess a hydrophobic part that inserts into the membrane. As such they cover part of the surface - in this way preventing tether molecules to cover that space - but do not enter the lower leaflet of the membrane. This leaves only a part of the surface covered with actual tether molecules and hence only part of the the lower leaflet composed of tethers. Compared to the other method, the use of lateral spacer molecules gives a better control over the actual percentage of the surface covered by tether molecules [38]. When aiming towards simple model systems, symmetry of

the membrane is often preferred. While tether molecules can be tailored to have a range of lipid like anchors, their development takes considerable effort and might even be impossible for some lipid species. By using stBLMs, at least an approximation of symmetric bilayers (considering the lipid composition) can be achieved by building only a percentage of the lower leaflet from tether molecules [39]. Depending on the exact fraction of tether molecules in the membrane, proteins of different size can be incorporated into the membrane. For the DLP tethers described in 2.3, a fraction of 10 % tether molecules has been estimated to offer space in between the anchored molecules for proteins up to 40 kDa, and up to 300 kDa with a tether fraction of 1 % [40]. Apart from the available space for proteins, the tether fraction usually strongly affects the water content in the sub membrane space and the defect density in the bilayer. Membranes with high tether content form bilayers without larger defects, but the water content below the membrane can be very low [38]. Conversely, low tether fractions lead to less perfect tBLMs [34] but usually create a sub membrane space with higher hydration. As this balance differs from system to system, an optimal ratio has to be found for every tether system.

stBLM have a generally lower stability than tBLMs with a completely tethered lower monolayer, but can still be stable for extended periods of time [39]. As protein incorporation studies are a vital part of tBLM usage, many tBLMs are actually sparsely tethered. The systems used in this thesis are sparsely tethered to different extents.

2.1.1 Tethered lipid bilayer production

The production of tBLMs generally follows similar rules as all solid supported lipid bilayers. However, there are some specificities due to their nature, which I will explain in the following. Just as with SLBs, it is quite challenging to form a defect-free bilayer on a surface from a solution of lipid molecules. In addition to the formation of the lipid bilayer itself, tBLMs require the additional process of forming the tether layer. While the exact process has to be adapted to each specific tether system there are a few common preparation techniques.

Vesicle fusion

One method is very similar to the vesicle fusion technique for SLBs (e.g.[41]). First a layer of complete tether molecules (i.e. surface grafting group, spacer and anchor part) is grafted to the surface by an appropriate process. Subsequently this monolayer is exposed to an aqueous solution of lipid vesicles of the desired composition and incubated for an amount of time. The vesicles adsorb to the tether layer and fuse with each other over time, just like with SLBs. Differing from the SLB procedure, vesicles do not only rely on adsorption to the surface, which is extremely dependent on lipid properties, but are also attracted by hydrophobic interaction between the anchor parts of the tether monolayer and the vesicles. This makes the method relatively robust, so that even multilamellar vesicles can be used for the formation [42]. It has been shown that this method can be a reliable and reproducible process for tBLM formation [20, 17]. However, this requires a high fraction of tether molecules in the lower leaflet, so that this method is unsuitable for sparsely tBLMs. Furthermore, several types of tether molecules tend to coil once they come into contact

with water, due to the hydrophobic anchor structure at their end. Once this coiling occurs, these molecules have no tethering effect any more and need an organic solvent to reach an uncoiled state again.

One notable variation of the vesicle fusion method incorporates the completely assembled tether molecules into the lipid vesicles with the spacer and surface grafting group protruding from the vesicle. These vesicles are then added to a surface which is functionalized in a way that allows binding of the surface grafting group of the tether molecules. Depending on the surface chemistry, this can make the whole tBLM production a one-step process. Rossi et al. [32] used this to form tBLMs on amine coated surfaces. This method provides a simple process for tBLM production and a precise control over the amount of tether molecules present in the membrane [43]. The tether molecules incorporated in the vesicles have no preferred orientation, however, which leads to some of them protruding outwards from the formed tBLM in the end. Other variations of the vesicle fusion method first graft a part of the tether consisting of the surface grafting group and the spacer to the surface. The vesicles contain a certain fraction of a modified lipid which allows binding to the spacer group, and thus anchoring the vesicles to the surface, which leads again to a lipid bilayer tethered to the surface [44].

Rapid solvent exchange method

A process which avoids the involvement of vesicles is the so called rapid solvent exchange method, which is depicted in fig.2.2. This procedure usually starts with a grafted monolayer of tether molecules as well, but the lipids are added to the system in organic solvent. An incubation period allows the lipids to arrange in the proximity of and in between the anchoring part of the tether molecules. The organic solvent is subsequently replaced with water or buffer solution at rapid speed. This causes a self assembly of the solubilized lipid molecules, filling voids between the anchor molecules and completing the lower leaflet of the lipid bilayer. A second monolayer is formed above which leads to a complete tBLM. The term rapid is relatively uncertain. It has been reported that partial exchange of the solvent still leads to bilayer formation [45]. A variation of this method uses spin coating for the deposition of a layer of organic lipid solution onto the tether molecules. Following evaporation of the solvent the surface is immersed in aqueous solution, which again leads to tBLM formation [21].

Rapid solvent exchange has a lower dependency on lipid composition, which allows for a large freedom in tBLM construction. However, due to the fact that there is no control over which lipids from the solvent form the final bilayer, tBLMs formed by this method do not necessarily have the same lipid composition as the lipid solution they originate from. For the right lipid combinations however, this can lead to tBLMs with higher resistance and lower defect density than bilayers formed through vesicle fusion [39, 38].

Detailed protocols for sample preparation of the two tBLM types used in this project will be given in the respective section describing the tether systems. The different tethering systems that I used in this thesis will be introduced in more detail further below and previous studies performed with them will be presented (2.3.12.4.1).

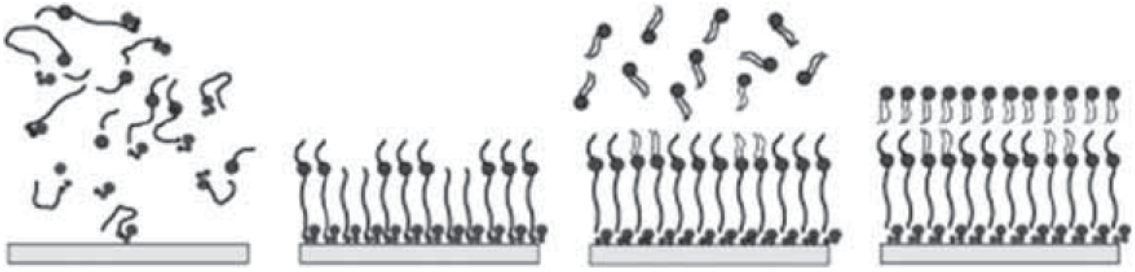

Figure 2.2: Rapid solvent exchange method as applied for the DLP tBLMs introduced in 2.3. Taken from [8]. The necessary steps are: 1.: Addition of the tethering molecules in organic solvent, 2.: After an incubation period the tether molecules react with the surface and form a tethered layer. 3.: Addition of the mobile lipids in organic solution for an incubation period. 4.: Rinsing with buffer solution leads to removal of the organic solvent and self assembly of the tBLM.

2.2 Lipid composition of tethered lipid bilayers

The properties of a lipid bilayer are largely governed by the properties of the lipids it is composed of. This holds equally true for tBLMs. The shape of the individual lipids defines what kind of structure a bilayer can adopt. An important parameter in this regard is the shape of lipids, which can be categorized as the volume of the hydrophilic headgroup in relation to the volume of the chain region. When the relation is in favour of one, usually shapes like micelles of versicles are the preferred form, while when the relation is roughly equal they tend to form planar shapes [4]. This means it is easier to form lamellar model membrane systems from these types of lipids, which is why there is a range of lipids which are used frequently in model membrane studies and are therefore characterized very well. However, by mixing lipids of different shapes, planar membranes can also be created with lipids usually not tending to form planar structures, which can have interesting effects on the bilayer properties.

Another property is the negative or zwitterionic headgroup charge which many lipids possess. They give most membranes a slightly negative net charge at physiological conditions. In the case of model membrane systems this can e.g. make an SLB stay in close proximity to a surface. Apart from influencing the shape of the bilayer, the charge also causes direct interaction of the lipids with different proteins [46]. Finally the degree of unsaturation in the chains also has an effect on the bilayer stability, fluidity and again the interaction with proteins. The combination of these parameters leads to the final shape and properties of the bilayer, from stability or fluidity, to electrophysiological properties like capacitance or ion transduction.

The properties of bilayers with different lipid composition have been studied extensively. This holds especially true for SLBs as the most simple and wide spread planar model membrane system. SLBs have no other components than lipids (apart from the surface) and

thus, SLBs of a certain composition should always have at least roughly similar properties. For tBLMs the situation is more complicated, because the fact that different tether systems have different membrane anchoring units leads to significant differences between properties of tBLMs with the same lipid composition, but different tether architecture. While there has been a large number of studies with different lipid composition on tBLMs as well, they can only be compared exclusively between very similar tether systems, instead of providing the more general information obtained from SLBs.

The origins of tBLMs are in the field of biosensors, therefore many tBLMs are designed with stability in mind, not physiological relevance. Thus, tBLMs of lipids with a composition very different to the majority of naturally occurring lipids are often used. This applies both to the lipid like anchor part of the tether molecules, as well as the lipids used to complete the tBLM themselves. While this is beneficial for applications in bio-engineering, structural studies of the membrane, or protein incorporation studies may lead to different results than one would obtain in membranes of more "natural lipids"

A frequently used type of lipids are phytanyl chain lipids(e.g. [47, 30]). They are known from extremophiles and archaea and can even sustain a stable bilayer under extreme conditions. Use of these lipids has resulted in extremely stable tBLMs which were still a suitable incorporation platform for EIS studies of proteins[20, 48]. The AM199 mixture used in this thesis (a 70:30 mixture of diphytanyl ether phosphatidylcholine (DPEPC) and glycero diphytanyl ether (GDPE)) consists of such phytanyl lipids and has been shown to be suitable for protein incorporation in the past (e.g. for the incorporation of Gramicidin-A [36]).

In general it is easier to produce tBLMs with the lower leaflet completely composed of tethered lipids (as opposed to sparsely tethered bilayers), which is why the lipid composition of this kind of tBLM has been varied more extensively, up to the point of natural lipid compositions like e.g. yeast lipid extracts [49]. These tBLMs are of course highly asymmetric and strongly influenced by the type of tether molecule.

It has to be noted that all studies on tBLMs are describing the lipid composition which is used in their production and not the actual lipid composition of the resulting membrane. It has been shown that the composition of a bilayer formed by vesicle fusion can differ significantly from the composition of the vesicles used in its production [50]. Different lipids have different propensity for different membrane shapes, so that from a mixture of two lipids one may prefer non lamellar structures an thus be present in the final bilayer to a much lower degree. So all lipid compositions of tBLMs have to be seen as estimations.

The lipids used in this project are mainly common and well studied lipids, as suitable for model systems which want to keep the amount of unknown variables as low as possible. Fig. 2.3 shows an overview of the structures of all used lipids. One aim of this thesis was to study the effect of cardiolipin on membrane structure and protein incorporation, thus lipid compositions which are already well characterized are necessary to identify whether tBLMs containing cardiolipin behave differently. Hence, an unusual lipid used in this thesis is cardiolipin, which will be further introduced in section 2.2.1.

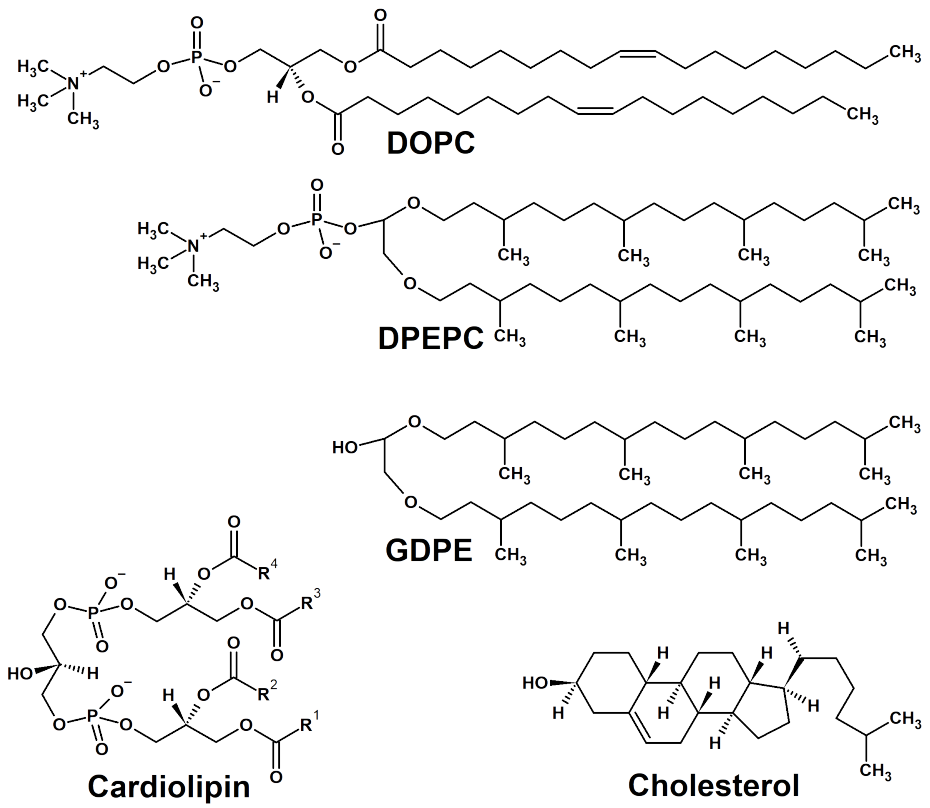

Figure 2.3: Chemical structure of the lipids used in this thesis project. A bovine heart solution of cardiolipin was used for the experiments presented in this thesis, which was composed of different fatty acid chains. A majority contained linoleic acid.

As a basis for most tBLMs in this thesis the phospholipid 1,2-dioleoyl-sn-glycero-3-phosphocholine (DOPC) was used. Phosphocholines in general and DOPC especially are very well characterized, due to their biological importance and their propensity to form planar bilayers [51]. DOPC has a cylindric shape and is in the fluid phase at room temperature. It has two monounsaturated chains and a zwitterionic headgroup. Structurally, DOPC bilayers are one of the best studied lipid bilayer systems [52].

In some cases 1-palmitoyl-2-oleoyl-glycero-3-phosphocholine (POPC) was used, which is very similar to DOPC, but has one saturated and one unsaturated chain. Thus it can be used as a comparison in terms of saturation. It forms SLBs trough vesicle fusion more readily than DOPC, however this can not be directly translated to tBLMs which are not formed by vesicle fusion.

Cholesterol (Chol) is a very common, but special lipid with a steroid chemical structure. It is much less flexible and has unique effects on lipid bilayer packing, shown mainly in an increase in the orientation order in the bilayer. An interesting property for electrophysiological purposes is the lower ion permeability it causes in membranes [53]. At low fractions it

has been shown to cause a lower membrane conductance and increased membrane thickness in tBLMs [54].

DOPC and POPC were purchased from Avanti Polar Lipids (Alabaster, USA). Cardiolipin was purchased from Sigma Aldrich (St. Louis, USA) as an ethanol solution from bovine heart, containing different, mostly polyunsaturated chains with a large fraction of linoleic acid. Cholesterol was obtained as a powder from Sigma Aldrich (St. Louis, USA). The AM199 mixture of DPEPC and GDPE was obtained as a solution in ethanol from SDx Tethered Membranes (Roseville, Au).

2.2.1 Cardiolipin

Most tBLMs investigated in this thesis contain varying fractions of the lipid cardiolipin. It has been first isolated in 1942 [55] from bovine heart (hence the name) and is unique in shape (see fig. 2.3) with four fatty acid chains instead of two. The headgroup shows a shape similar to two connected phosphatidyglycerol headgroups: two phosphatic acid moieties joint by a glycerol backbone. Because of the small headgroup, cardiolipin has a specific conical structure. The headgroup carries two negative charges at physiological pH [56]. Different species express cardiolipin with different chain composition - e.g. human cardiolipin has a majority of di-unsaturated 18:2 chains [57] - but generally a high degree of unsaturation can be found. Depending on the degree of unsaturation the phase behaviour varies widely. While natural CL mixtures with high unsaturation are in the fluid phase at room temperature, synthetic saturated CLs have gel/fluid phase transitions above 50 °C. Due to the strong negative charge, this transition temperature is very sensitive to the presence of divalent cations [58]. The unusual structure leads to further interesting properties, which will be introduced below.

Cardiolipin occurs mainly in the inner mitochondrial membrane of eukaryotes or the plasma membrane of some bacteria at high fractions of up to 20 % [59]. Its biological function is a topic of high interest, as it seems to be involved in many processes. Deficiency of cardiolipin is related to several diseases like Barth syndrome [60] or heart failure [61], while on a structural level as a membrane component cardiolipin influences the behaviour of lipid bilayers. Due to the cone shape, CL alone has a tendency to form non-lamellar phases [62] and naturally arranges in micro domains of high negative curvature [63]. When combined with other lipids, CL's effect on membrane structure is not yet completely resolved. Stabilizing effects of CL on PC membranes have been reported [58, 64], however, Unsay et al. reported a decrease in mechanical stability upon addition of CL [65]. Zeczycki et al. suggested a dependence on the original packing of the membrane: when added to loosely packed membranes CL increases membrane packing, but when added to densely packed membranes the packing is decreased [66]. Equally, increase of bilayer thickness has been reported upon addition of tetra-myristoyl CL (TMCL) to dimyristoyl phosphocholine (DMPC) membranes [67], while it was also shown that addition of tethra-oleoyl CL (TOCL) to DOPC membranes reduces the overall bilayer thickness [68] while increasing the thickness of the chain region. Due to these ambiguities CL membranes remain an interesting model system to investigate.

Another motivation to investigate CL membranes is its interaction with many membrane proteins. It binds to a number of mitochondrial membrane proteins, but also extramitochondrial and extracellular proteins [69]. It selectively binds to aquaporin and increases its stability [46], cytochrome c oxidase has a 50 % reduced function without CL [70] or even looses enzymatic activity [71], and CL promotes clustering of membrane proteins e.g. in the respiratory supercomplex [72]. Gupta et al. have shown interaction with the membrane protein NhaA [73], which will be expanded in section 2.6. These interactions between CL and proteins are assumed to weaken at low levels of unsaturation [74]. Following that, a model membrane with high fractions of cardiolipin could be an attractive platform for protein incorporation studies, including NhaA.

2.3 DLP tethered lipid bilayers

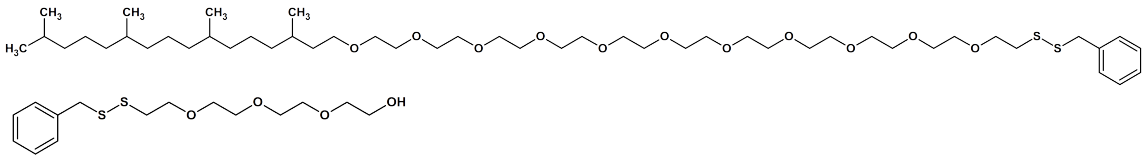

Figure 2.4: Chemical structure of DLP tether molecules (top) and additional surface covering molecules (bottom).

The so called DLP tethers (historically derived from double length phytanyl) have been one of the first tBLM systems and were developed by Cornell and co-workers in the 90s using benzyl disulfide undeca-ethylene glycol phytanyl molecules as tether molecules (see fig.2.4, top)[7]. They are stBLMs with a varying fraction of tether molecules which span the lower leaflet. This system combines a phytanyl chain as the membrane anchoring part with a PEG spacer and a disulfide group to form sulfur bonds to a gold surface. An attached benzene ring increases the surface space occupied by the molecule. The length of the PEG chain is variable, however a length of 11 units has shown to be a good compromise between stability, fluidity, and electrical properties of the lipid bilayer, while a length of 8 units could be used for cases which require a higher stability. Additional benzyl disulfide tetra-ethylene glycol molecules cover the surface to control the amount of tether molecules in the inner leaflet (fig.2.4,bottom), in order to ensure a certain water fraction in the sub-membrane space. They consist of a disulfide group to bind to the gold surface and a short PEG chain of 4 monomers. Similar to the tether molecules, a benzene ring increases the surface space occupied. The two molecules can be mixed at different proportions to create more or less sparsely tethered membranes. Most frequently tether concentrations of 10 mol% (named T10 in the following) or 40 mol% (named T40) have been used, which refers to a 10:90 or 40:60 molecular ratio of tether molecules and lateral spacer molecules respectively.

DLP tethered membranes have been studied extensively in the last 20 years, however the vast majority has been functional studies or indirect structural studies using electrophysiological methods. It has been shown that DLP tBLMs show similar thicknesses and electro-

chemical behaviour as SLBs [75] and thus are suitable for model membrane studies. The exact structure of the spacer moiety has been adapted to prevent ester hydrolysis in order to provide higher stability [76].

Using EIS (see 3.2) an array of properties of the DLP tBLMs themselves has been investigated in the past, like the influence of tether density on the electrical sealing properties and resistance to electroporation of the membrane [77]. The density of tethers is one of the most influencing factors of a stBLM and as such it also leads to more or less stable tBLMs. The whole range of different tether concentrations reaching from 1 % DLP to 100 % DLP, has been studied, always showing high temporal stability. Even 1 % tethered tBLMs have shown electrical stability over one month[40], however, they tend to develop defects over time. 10 % tethered membranes show a much higher stability, while still showing lipid fluidity in the bilayer and leaving enough space between the anchor molecules for protein incorporation studies ([40]). While 100 % tethered membranes naturally lead to the highest stability, such membranes are closer to a lipid monolayer supported by a polymer layer than a lipid bilayer and as such have very different properties. It has to be noted that the mentioned tether concentrations always referred to the ratio between tether molecules and lateral spacer molecules. The actual surface coverage of the different molecules (and thus the amount of tether molecules inserting into the bilayer) is difficult to determine and may differ from this value.

The original motivation for this tether system has been the creation of a model membrane system which supplies an ionic reservoir below the membrane that can be used to study ion transport processes across the membrane for bio-sensing devices. This ion reservoir has been subject of several studies which showed strong dependence of the ion mobility and dielectric constant on the length of the spacer moiety and the tether density [75]. Similar for all tested combination was a behaviour more typical of a hydrated gel, than an actual water compartment below the membrane [30]. By making use of this ion reservoir, the incorporation and activity of several ion transport proteins have been shown (e.g. Valinomycin [75], Gramicidin A [76] or Bacteriorhodopsin [8]). The general use of tBLMs for protein incorporation studies will be further described in 2.5.

As with all lipid membranes the choice of lipids defines the bilayer properties. One of the main uses for DLP tBLMs so far has been the measurement of protein activity, therefore the lipids which were mainly used in these studies were tailored accordingly. For that reason a mixture of diphytanyl ether phosphatidylcholine (DPEPC) and glycero diphytanyl ether (GDPE) at a ratio of 70:30 has been used frequently. While the bilayers formed from this mixture behave differently to more commonly found lipids, they show higher stability and electrical sealing, which is needed for the protein studies [8]. In addition to these rather unusual lipids, more common lipids like phosphadidylcholines (e.g.[36]) and phosphatidylethanolamines (e.g. [8]) have formed stable bilayers. Addition of fractions of cholesterol to such membranes leads to thickening of the membrane, like for untethered membranes [54].

All the properties described above have been interpretations of electrophysiological measurements. Studies using information from additional experimental or computational techniques have only started to be published in the last few years. Coarse grained molecular dynamics simulations showed that tether density influences membrane thickness, lipid diffusion, defect density, free energy of lipid flip-flop and membrane dielectric permittivity [78]. Neutron reflectometry experiments have been used recently to gain structural information about DLP tBLMs on the nanoscale. Cranfield et al. [36] investigated the effect of pH on 100 % tethered DLP tBLMs consisting of DPEPC lipids. Within our group a characterization of T10 and T40 DLP tBLMs has been performed with a simple DMPC composition [79] as well as an OprF protein incorporation study into such a T10 tBLM [80]. These have been the only pieces of information so far on actual dimensions of the sub-membrane space and the tBLMs. Recently, a QCM-D study has been published, which showed an increased rigidity of the tBLM at higher tether fractions [81]. While the electrophysiological studies explored a range of different lipid compositions, even employing bacterial lipids from E. coli or yeast [78], structural studies were limited to the most simple lipid composition. Information on how the lipid composition affects the dimension and water content of the sub-membrane space, as well as its effect on the bilayer dimensions itself, are still lacking. Exploring DLP tBLMs of different lipid composition can thus yield valuable insight into the interaction between lipids and tether molecules.

2.3.1 DLP tethered lipid bilayer production

DLP tBLMs were investigated by NR, EIS and QCM-D in this project. For each of them slightly varying preparation protocols are used which are presented below. The following procedures are the standard procedures used for all samples of the respective experimental technique. If there are deviations for single samples they will be mentioned in the description of the respective measurements. DLP tBLMs are always produced by the rapid solvent exchange method as described in 2.1.1. In fact, they were the experimental system on which this method was developed [7].

For **NR experiments** the DLP tBLMs were formed on 8×5 cm^2 substrates which are suitable for the solid liquid cells available at the D17 and FIGARO instruments at the ILL (see section 3.1.3). The basic blocks were either silicon that was cut and polished along the 111 plane or sapphire blocks. These were coated with a thermally evaporated gold layer of approximately 200 Å thickness. A 50 Å interlayer of titanium was used to promote adhesion of the gold. Before tBLM preparation the substrates were cleaned according to the protocols given in A.3

Benzyl disulfide undeca-ethylene glycol phytanyl molecules (tether molecules) and benzyl disulfide tetra-ethylene glycol molecules (surface blocker) were purchased dissolved in ethanol from SDx tethered membranes (Roseville, Au), and were used either at a concentration of 400 μM or 200 μM.
Depending on the desired tether concentration (always either T10 or T40), tether molecules and lateral spacer molecules were mixed to the desired proportions. The cleaned substrate

block was immersed into the tether solution for at least one hour and then gently rinsed with ethanol. Subsequently the functionalized block was mounted into the NR cell.

For tBLM formation a 3.4 mM solution of the desired lipid mixture was pumped into the cell and incubated for 2 minutes. Afterwards the cell was flushed with a buffer solution, which led to the formation of the tBLM. Usually, the lipids were dissolved in ethanol. When ethanol was not sufficient to dissolve the lipid mixtures, fractions of methanol or chloroform were added, which will be mentioned in the description of each sample. The default buffer was a 10 mM HEPES solution with either 150 mM NaCL or 150 mM KCl.

The substrates for **EIS experiments** were purchased from SDx tethered membranes (Roseville, Au) as pre-coated gold electrodes that are suitable for the tethaPod device as described in 3.2. In general, the sample preparation for EIS measurements followed the procedure described in [82]. The T10 tether layer was already present on the surface, so that the only necessary step was a rinsing with ethanol. After mounting the substrate into the EIS cartridges (see 3.2) 8 μL of 3.4 mM lipid solution in ethanol were added to the 2.1 mm^2 electrode surface by pipette. After 2 minutes of incubation the surface was flushed with 300 μL of buffer solution to form the tBLM. The buffer solutions were the same as for the NR samples.

QCM-D experiments were carried out on gold coated QCM-D crystals purchased from Biolin Scientific (Gothenburg, SE). As one aim of these experiments was the investigation of the tether layer formation process, the cleaned (see appendix A.3), uncoated gold chips were mounted into the QCM-D chambers. Following that a 370 μM ethanol solution of the tether molecules at the desired tether to lateral spacer ratio was injected into the cell to form the tethering monolayer. Subsequent rinsing with ethanol removed all unbound tether molecules. The lipid bilayer was formed by injecting a 3.4 mM lipid solution in ethanol to the chamber and incubating it for 2 minutes. Flushing the cell with buffer led to self assembly of the lipid molecules to form a tBLM.

2.4 DSPE-PEG-NHS (DPN) tethered lipid bilayers

Thiol bound DLP tBLMs with PEG spacers showed a low water content in the sub-membrane space in the past [79]. Other tBLM systems, however, can have much higher hydration below the membrane. To study the importance of this specific structural property, the investigation of a type of tBLM that is connected to a silane functionalized silicon surface by 1,2-distearoyl-sn-glycero-3-phosphoethanolamine-N-[succinimidyl(polyethylene glycol)] (DSPE-PEG-NHS or even shorter DPN) molecules was initiated. Fig. 2.5 shows the structure of these tether molecules.

This type of membrane shows potential because of two main properties. Previous measurements within our group on this type of membranes showed a very high water content in the sub-membrane space of over 80 % while retaining the same substrate-membrane separation [84]. These first measurements were performed on tBLMs consisting of POPC. Expanding this to more complex lipid mixtures containing CL can give valuable information on the

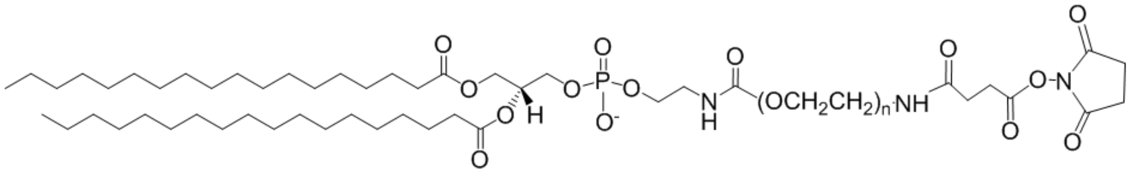

Figure 2.5: Chemical structure of DSPE-PEG-NHS tether molecules [83].

significance of the water content in the sub-membrane space. In the context of membrane protein incorporation a sufficiently high water content in the sub-membrane space is crucial to retain protein function. The second intriguing property arises from the fact that this type of tether connects the membrane to a silicon surface. This eliminates the strong scattering signal of gold from the measured data and thus facilitates analysis of NR data tremendously. Electrophysiological studies can still be performed on such systems if the silicon substrate is e.g. boron doped to a sufficiently high extent [20].

In the past, several tBLM systems with a related structure have been investigated. When connecting structures to a silicon surface, silanization is an common way to achieve a surface functionalization. Depending on the exact type of surface there are several ways to do this, but they mostly result in a surface with exposed amine groups. These amine groups offer the possibility to attach different kinds of molecules using amine-reactive crosslinker chemistry. The chemical compound used to produce such a surface with accessible amine groups in this thesis was (3-aminopropyl)triethoxysilane (APTES) as explained in more detail in the following section 2.4.1. By exchanging the NHS group of the tether molecule, the spacer part can be connected to the amine group.

The spacer unit for this tether architecture is a long PEG chain of 45 units. This flexible chain can offer high mobility within the tethered lipid bilayer. Due to the length of the PEG spacer, the tBLM is less confined, which can lead to a rougher bilayer with more defects, but can also induce higher solvent content in the sub-membrane space [29]. The membrane anchoring component of this system is a DSPE lipid which is directly connected to the PEG chain.

Similar tethering systems have used a triethoxysilane group already connected to the PEG spacer for surface functionalization [23] or used a bottom up approach by grafting every part of the tether molecules separately to the surface in the past. Hertrich el al. used an octenyltrichlorosilane surface functionalization, followed by a multi-step procedure, to create similar PEG-DSPE tBLMs on silicon surfaces [21]. An inverse approach was followed by Rossi et al. who incorporated complete DSPE-PEG-NHS tether molecules into lipid vesicles which were then fused on a amine functionalized gold surface [32, 85]. Both methods lead to complete tBLM formation.

In this thesis a bottom up approach comparable to the one followed in [21] was used, however using a procedure that requires less individual steps. The surface was first functionalized with an APTES layer. Following that the complete DSPE-PEG-NHS tether molecules were

grafted to the surface. On this tether molecule layer, the lipid bilayer was formed using the rapid solvent exchange method 2.1.1.

2.4.1 DPN tethered lipid bilayer production

DPN tBLMs have been investigated before, as introduced above. These studies used a vesicle fusion process that incorporated the tether molecules into the vesicles and spread these combined vesicles onto an amine functionalized surface (e.g. [43]). The approach used in this thesis uses a bottom up construction approach which has not been used before to our knowledge. The tether molecules are grafted to a functionalized surface in a first step, followed by bilayer formation using rapid solvent exchange. This will lead to differing properties than tBLMs prepared with the same tether architecture but by the vesicle fusion method. One key difference is that with the method used here, no tether molecules will be present in the outer bilayer leaflet, which is a disadvantage of the vesicle fusion method.

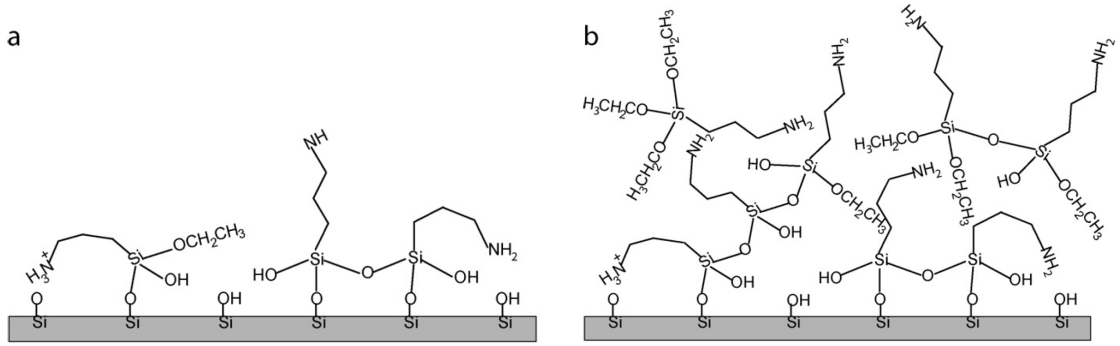

Figure 2.6: a.) The possible structure of an APTES monolayer with the amine groups facing upwards. b.) Unorganized APTES binding to the surface. Taken from [86]

Formation of DPN tBLMs requires a procedure consisting of several steps compared to the simple one-step method for the DLP-tBLMs. Before grafting the tether molecules to the silicon surface, it needs to be functionalized with the silane linker APTES. Coating a surface with a uniform monolayer of APTES is a difficult task which still has not been completely understood (e.g. it is under debate whether APTES forms siloxane bonds or hydrogen bonds to the surface [87]). One has to make sure that actually only one layer of APTES is present on the surface, otherwise an unorganized structure with no clear orientation of the molecules can be formed as shown in fig. 2.6b. With such a random orientation the amine groups are not accessible for molecules above the surface, which makes the functionalization redundant. Preventing this kind of aggregation has been the aim of considerable effort in the past (e.g. [87, 86, 88]). The absence of water has shown to be beneficial for homogeneous monolayer formation [88]. Thus, performing the APTES deposition step in anhydrous conditions is necessary. We used anhydrous toluene and argon atmosphere for this procedure. Furthermore the thickness of the APTES layer has to be controlled to prevent multilayer formation. A monolayer of APTES should have a film thickness of roughly 5 to 15 Å. Higher layer thicknesses indicate an unordered structure

like sketched in fig. 2.6b. Removal of these additional layers can be achieved by mild ultra-sonication. As the monolayer forms stronger bonds to the surface than the loosely attached molecules, the sonication leaves the lowest monolayer intact. APTES layers with larger thickness of up to 10nm can still lead to well formed tBLMs because even in layers with randomly oriented molecules a part of them shows an outwards facing amine group. Such bilayers are tethered to a much lower degree. Finally, curing of the monolayer at elevated temperatures increases the stability significantly [89]. It was found that the curing process leads to more siloxane bonds to the surface per molecule.

The grafting process of the DPN tether molecules is executed in one reaction. The tether molecules which were purchased from Nanocs (New York, USA) are spread onto the surface in dimethylformamide (DMF). This causes the formation of stable amide bonds to the surface by exchange of the NHS group.

The tBLM formation itself can be carried out using the rapid solvent exchange method described in section 2.1.1.
All these considerations led to the following protocol for DPN tBLM formation for NR experiments:

- Cleaned silicon blocks (see appendix A.3) were immersed in anhydrous toluene containing 0.1 %(v/v) APTES under argon atmosphere over night.
- After removal from the toluene-APTES solution, the samples were ultra-sonicated in fresh toluene for 10 minutes, followed by ultra-sonication in ethanol for 10 minutes. Ultra-sonication for such short times removes excess APTES from the surface without damaging the monolayer bound to the silicon.
- Curing took place in an oven at 120 °C for 1 hour directly after sonication.
- Afterwards the samples were sonicated again in ethanol for 10 minutes.
- A small volume of dimethylformamide solution containing 1 mg/ml of DSPE-PEG-NHS tether molecules was deposited onto the surface and incubated over night. This causes the NHS cross linking reaction with the exposed amine groups.
- The substrates were rinsed with ethanol to remove tether molecules that did not bind to the amine groups of the APTES layer. At this stage the samples could be stored until they were used for experiments.
- For bilayer preparation the substrate was placed in the solid/liquid NR cell and a 5 mg/ml lipid solution in ethanol was added to the chamber for 10 minutes.
- The sample chamber was flushed with buffer solution to form the tBLM via rapid solvent exchange.

2.5 Membrane protein incorporation into tBLMs

Membrane proteins are a class of proteins which is very difficult to study. Many characterization methods like NMR spectroscopy or light scattering rely on the protein of interest to be dissolved in water. Due to their nature, membrane proteins often have a hydrophobic part, which leads to insolubility in water and, even if they are soluble in water, they often loose their function. Using detergents to solubilize the proteins in water leads to temporal suppression of protein activity as well. For that reason, membrane protein studies require a lipid membrane environment. As with all biological systems, they can be studied in their natural cell environment, however, the abundance of different components makes identification of single effects difficult. Studying membrane proteins embedded in simplified model systems makes it possible to study the effect of different components independent of each other. However, the study of membrane proteins in model membrane systems poses its own challenges.

As already introduced in 2.1, tBLMs are an attractive model membrane system, especially with respect to membrane protein incorporation, because of their higher stability. The use of detergents is the most common way to solubilize membrane proteins, thus the protein incorporation process (see 2.6.2) causes contact of the tBLM with these detergents. When proteins are transferred from detergent to the tBLM, protein activity is often recovered. Due to anchoring to the surface, tBLMs are less damaged by such a process than e.g. SLBs. The increased stability also removes time constraints and enables long term studies. The ion transport peptide valinomycin has been incorporated into tBLMs after as long as one month, while retaining its function [17]. While this study has been performed on tBLMs with a completely tethered lower leaflet - which offers a stability that stBLMs do not possess - stBLMs show an increased temporal stability as well and thus offer the possibility to perform protein studies on longer timescales than with other model membrane systems.

Another advantage of tBLMs is the water filled sub-membrane space of tBLMs, and this is probably the most exploited property for membrane protein studies. A large amount of studies have been performed on ion transport proteins incorporated into tBLMs, by making use of the ion reservoir supplied by the sub-membrane space. In conjunction with the common gold substrate they can be used for electrochemical characterization of the protein activity, as described in section 3.2.2. Most studies of this kind were little more than proofs of concept, showing that it is possible to incorporate membrane proteins into tBLMs and measure their activity (e.g. [90, 28, 91, 43, 49]). These usually used simple and well studied proteins like aquaporin [90] or cytochromes [23] as exemplary and easy to use membrane proteins. However, others were aimed towards applications like e.g. biosensors, as well as fundamental studies on the behaviour of ion transporters or how the structure of tBLMs affects the function of incorporated proteins and vice versa. Using electrochemical methods the effect of varying transmembrane potentials on the protein sarcolipin activity has been investigated [92]. A study on the ion channel α-hemolysin revealed its position within a tBLM and described changes in the lipid headgroup area upon protein incorporation [9]. Even structural properties like the angular orientation of a protein within the bilayer could

be resolved in tBLMs [93]. Naumann et al. [94] studied the incorporation of H^+-ATP synthase into tBLMs with different fractions of tethers in the lower leaflet. While they were able to incorporate the protein into a tBLM with completely tethered inner leaflet, the protein function was lost. However when using a sparsely tethered lower leaflet of the same type, the protein stayed functionally active.

Lipid-protein interaction affects tBLM systems like other model membrane systems, while adding the additional influence of the anchoring part of the tethers. While the interaction of tether molecules and protein inside of tBLMs has never been investigated (to my knowledge), there have been protein incorporation studies into tBLMs of different lipid composition. From SLB studies and computer simulations, interactions between proteins and lipids have been identified as an important factor in protein function. In nature every type of cell membrane has a characteristic lipid composition and this composition has co-evolved together with the corresponding protein components. Therefore, certain types of lipids are associated with the function of membrane proteins. In general, every property of a lipid influences protein incorporation. Some properties have an indirect effect by e.g. influencing the curvature of a membrane which in turn affects protein incorporation. Others are directly linked to protein interaction, like the charge of the lipid. The aforementioned strong interaction of CL with proteins is at least partly believed to be due to the two negative charges in the headgroup. Lipids with a high degree of unsaturation have shown a beneficial effect on protein incorporation. This has been investigated for the case of cardiolipin, which showed a looser association with membrane proteins when reducing the amount of double bonds ([74]). Many of the lipids used in tBLM studies are used for functional reasons, not to mimic a natural environment. Especially phytanoyl chains, which increase the already enhanced stability of tBLMs even more, are used widely. There are multiple successful protein incorporation studies with this kind of lipids (e.g. [95, 92, 96]), but some studies which observed inactive proteins or lower activity than predicted suggest that unnatural lipid composition may be the cause([91]). While this does not compromise studies with these lipids in general, it serves as a motivation to investigate proteins in tBLMs of different lipid composition.

2.6 NhaA

Sodium-proton antiporters are a class of proteins which have first been described in 1974 by West and Mitchell [97]. They are involved in pH, salt and volume homeostasis across the cytoplasmic membrane of cells. One of the most extensively studied sodium-proton antiporters is the sodium-proton antiporter A (NhaA) from E. coli. First described, overexpressed and purified by Taglicht et al. in 1991[98], this protein is responsible for the adaptation to high salinity and and growth at alkaline pH [99]. While being E. coli exclusive, NhaA has orthologues in different biological kingdoms, including humans [100].

The monomer structure of NhaA has first been described from a down regulated pH 4 crystal by x-ray crystallography in 2005 [101] (see fig. 2.7). It consists of 12 transmembrane α-helices with the N- and C-terminus exposed to the cytoplasm. This side shows a rough

structure with loops and helices protruding into the cytoplasm for a short distance. The periplasmic side is flat, consisting of structured loops and a double stranded β-hairpin[102]. The whole protein has a size of 42 kDa and consists of 388 amino-acid residues. It spans an area of 40×45 Å^2 in the membrane with a thickness of 50 Å [101], which is slightly thicker than many phospholipid membranes. NhaA usually occurs as a dimer (see [103] for a structural characterization of the dimer). Even though the monomer is fully functional ([101]), the dimer keeps functioning under extreme stress conditions, while the monomer has a strongly reduced function [104]. This dimer structure of NhaA shows a higher stability in the presence of the lipid cardiolipin [73].

NhaA transforms an H^+ gradient to a Na^+ gradient [102] (or vice versa) with a stoichiometry of two protons against one sodium ion, making the protein electrogenic, which is unique amongst its homologues, all of which have a symmetric stoichiometry. This ion transport property is strongly pH dependent. Up to a pH of 6.5 NhaA is inactive, but between 6.5 and 8.5 its activity rises by several orders of magnitude to a maximum turnover rate on the order of 10^5/min [105, 98]. The half maximum is reached at cytoplasmic pH. The switch from the inactive to the active state is accompanied by a conformation change [106]. While the exact mechanism of pH activation is still subject of debate, MD simulations suggest that the pH difference causes a net charge switch in the opening tunnel through the protein [107]. NhaA's antiport function is highly symmetrical with Na^+ and H^+ competing for the same binding site [108, 105]. To a lower extent, NhaA is also capable of transporting Li^+ ions instead of Na^+ ions. It can be completely suppressed by the inhibitor 2-aminoperimidine which binds competitively with Na^+ and H^+ to the protein's binding site [109]. Several mutants of this protein have been produced in the past. One of those is completely inactive, while retaining most of the protein structure. This mutant - called NhaA* in the following - is produced by substituting two nucleotides, as described in [110].

2.6.1 NhaA Production

The NhaA used in this project has been overexpressed and purified in the SyNaBi group by Jean-Pierre Alcaraz following a protocol already applied in [112] and [113]. For this, a 22 amino acid histidine tag was added to the N terminal to allow purification with a nickel column.

For overexpression, the NhaA protein gene was introduced into the E. coli strain C43 using the plasmid vector pET15b (Novagen). The process is based on a protocol from Kubicek et al. [114] which was adapted and optimised. The cells were cultivated in LB medium containing ampicillin at 37 °C until OD600 reached 0.4. 200 μM IPTG (Isopropyl β-D-1-thiogalactopyranoside) was added to the culture medium to induce overexpression of NhaA gene, followed by further cultivation for four hours. The cells were centrifuged at 8000 rpm for 5 minutes to form pellets, which could then be stored at -80 °C.

The following two-step purification process was carried out in the absence of NaCl. A binding buffer containing 20 mM TRIS, 500 mM KCl, 10 mM imidazole and 12.6 % (w/v) glycerol was used to incubate the pellets with lysozyme and benzonase nuclease for 30

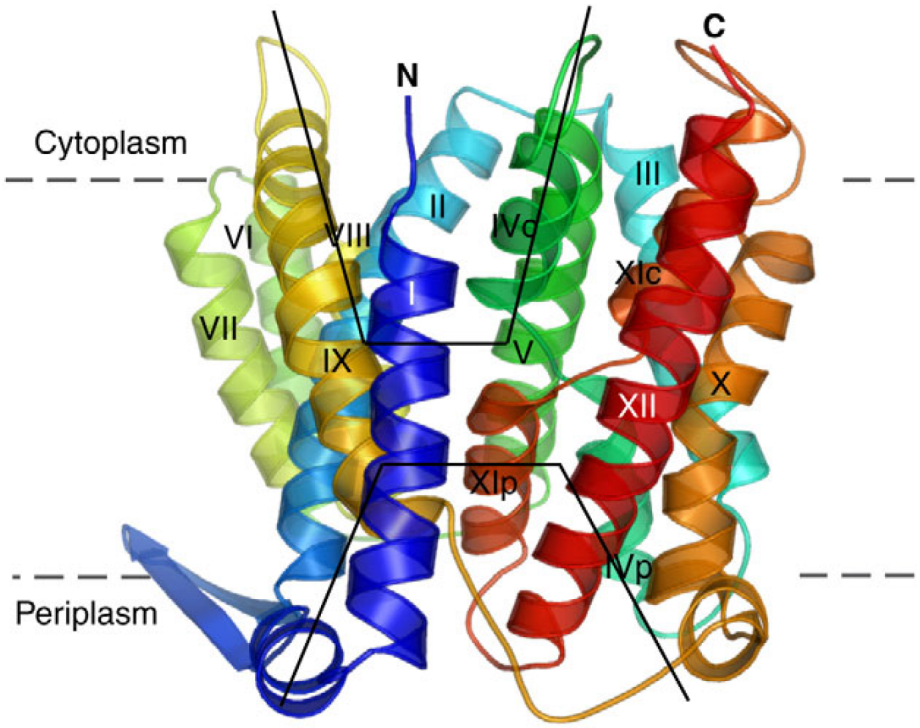

Figure 2.7: Cartoon of the X-ray crystallographic structure of NhaA. The black lines indicate the opening funnels. Taken from [111].

minutes. The incubated cells were then disrupted in a French pressure cell followed by centrifugation at 14000 rpm for 20 min to separate unbroken cells. Subsequent ultra-centrifugation at 36000 rpm for two hours separated the membrane fraction from soluble components, which was resuspended in binding buffer with additional 20 mM DDM. This mixture was incubated over night in a rotator to dissolve the protein with DDM. DDM is a relatively gentle, non-ionic detergent, which helps in retaining function of proteins [115].

The actual purification procedure makes use of an immobilized metal affinity chromatography column (Ni-NTA agarose, Qiagen). The column was first equilibrated with binding buffer and then the membrane fraction was incubated for two hours. This caused the His-tag of NhaA to bind to the column. After rinsing with washing buffer (20 mM TRIS, 500 mM KCl, 40 mM imidazole), the purified NhaA was recovered in elution buffer of 20 mM TRIS, 500 mM KCl, 300 mM imidazole, 12.6 %(w/v) glycerol and 225 μM DDM. This resulted in a final concentration of NhaA of around 0.1 to 0.5 mg/ml. The elution buffer components have not been further separated and NhaA has thus been used in a diluted version of the elution buffer. The inactive NhaA mutant was also introduced into the pET15b vector and overexpression and purification followed the same protocol.

2.6.2 Incorporation Methods

The incorporation of membrane proteins into lipid bilayers and especially into planer systems like tBLM is a difficult task. Moving a hydrophobic structure out of a hydrophobic environment into another one through an aqueous space requires some energy, while the fragility of membrane proteins forbids the use of too much force. Many different protocols have been developed to overcome this hurdle and they require a considerable amount of adaptation for each new protein system and even experimental setup. In the following I will present the two incorporation methods which are used in this project: Detergent mediated incorporation and liposome assisted incorporation.

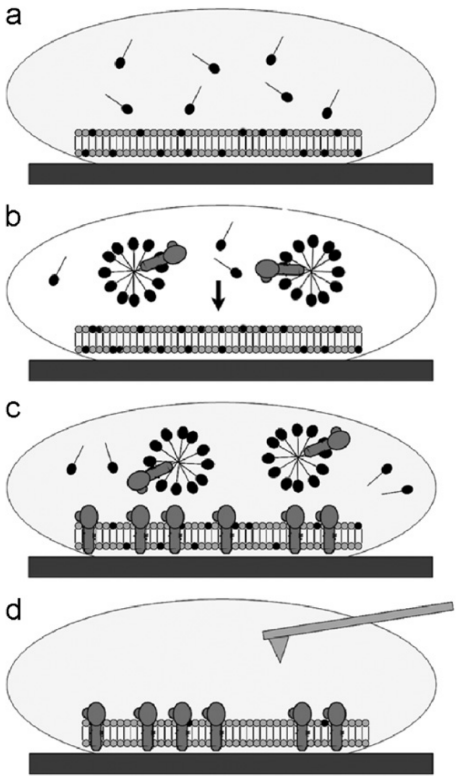

Figure 2.8: Detergent mediated protein incorporation. Taken from [116].

Detergent mediated incorporation

Detergent mediated incorporation is the simplest way of protein incorporation, an illustration of which is shown in fig. 2.8. Membrane proteins are usually not soluble in water. Thus in the purification process they are often enclosed in small detergent micelles which allow a certain solubility in water. Many different detergents with different properties have been used for protein purification [115]. As mentioned in 2.6.1, DDM is used as a detergent during NhaA purification. The incorporation process requires a transfer from these detergent micelles to the lipid bilayer. In the simplest case, addition of the detergent micelles to

the bilayer is enough to trigger the transfer, but more commonly a small additional concentration of detergent is used to cause slight disruptions in the membrane. Either this small amount of detergent is first added to the bilayer to cause disruptions, followed by addition of the protein in detergent micelles, or the protein in micelles and the additional detergent are added in one step. This facilitates protein incorporation by providing attachment points for the protein-detergent micelles. As usually the lipid bilayer is an energetically more favourable environment for the protein than the detergent micelles, this is sufficient to cause a transfer of the protein from the detergent micelles to the tBLM. Extensive rinsing causes the removal of detergent remaining in the solution. The exact concentration of additional detergent depends on the type of protein, detergent, lipid bilayer and many other factors. A detergent concentration of 20 % of the critical micelle concentration has shown good results for different systems [8]. Part of the detergent can also transfer to the membrane which is unavoidable, however this is usually a negligibly small amount.

The detergent mediated incorporation in this project was carried out according to the following protocol. Note that the detergent was added together with the protein in one step:

- A tBLM was produced according to the procedure described in section 2.3.1.
- The protein in elution buffer was diluted with buffer solution to a DDM concentration of 24 mM, which corresponds to 20 % of the critical micelle concentration. This resulted in final protein concentrations of approximately 0.05 mg/ml to 0.2 mg/ml.
- An appropriate volume (2 ml for neutron experiments, 50 μl for EIS experiments) of the mixture was added to the sample chamber and incubated for 30 minutes.
- The unbound components were flushed away with large amounts of buffer solution.

Liposome incorporation

For the liposome incorporation method the proteins first have to be transferred from the detergent to liposomes, which are then fused to the lipid bilayer. This results in the transfer of the protein molecules to the bilayer as part of the proteoliposomes. For easier attachment of the liposomes to the bilayer detergent at 20 % of the CMC is added, which creates disruptions in the bilayer structure, similar to detergent mediated incorporation. This method is a gentler approach, because damage induced in the bilayer by the detergent can be repaired by the lipid material supplied through the liposomes [117]. However, as the transfer rate to the membrane is usually quite low, this method requires a larger amount of protein. For this method, the creation of liposomes and the transfer of protein to the liposomes are additional necessary steps. Similar to planar bilayer preparation, there are many different methods for many different lipid-protein combinations. I will present the proteoliposome production protocol that has been used in this project in the following. Related protocols have already been successfully used to transfer NhaA from detergent to liposomes [118].

- The desired lipids were dissolvent in organic solvent in a small vial, either ethanol or chloroform, depending on the lipids.
- The vial was exposed to a gentle stream of nitrogen until all solvent was evaporated.
- For complete removal of all solvent residues the vial was placed in a vacuum oven for one hour. This resulted in a lipid film at the bottom of the vial.
- This film was resuspended in buffer solution, followed by tip sonication for 3×30 seconds or until the solution was mostly clear and no film remained at the sides of the vial. At this stage the lipids form vesicles of different sizes, which depends strongly on the type of lipids.
- To reduce vesicle size the solution was extruded ten times with a pore size of 400 nm.
- The protein in elution buffer with NhaA was added in an amount which resulted in a final DDM concentration of 24 μM, which corresponds to 20 % of the CMC
- The mixture was extruded ten more times with a pore size of 100 nm, which on one hand reduced the liposomes to a size suitable for fusion with bilayers and on the other hand resulted - together with the lowered detergent concentration - in transfer of NhaA from the detergent micelles to the liposomes.
- An appropriate volume (2 ml for neutron experiments, 50 μl for EIS experiments) of the mixture was added to the sample chamber at a lipid concentration of 5 mg/ml and incubated for 30 minutes, similar to detergent mediated incorporation.
- Subsequent rinsing with copious amount of buffer removed all unfused liposomes and detergent from the sample chamber.

Identically to the detergent mediated incorporation, this method can leave small amounts of detergent in the membrane.

Chapter 3

Methods

3.1 Neutron reflectometry

3.1.1 Basics of NR

The main experimental method in this project is neutron reflectometry (NR). Reflection of neutrons from a surface has first been observed in 1946 by Fermi and Zinn [119], not long after the experimental discovery of the neutron by James Chadwick in 1932 [120]. Neutron reflectometry is a technique that enables the measurement of thickness and composition of planar structures with high resolution. Due to a wavelength comparable to molecular distances, length scales from 10^{-10} to 10^{-7} meters can be probed. While the general principles of NR are similar to other optical methods, neutrons exhibit some specific properties, which give rise to several interesting applications. Neutrons do not possess a charge, which means that interaction between neutrons and matter mainly occurs at the nucleus. As a result, the interaction between neutrons and many materials is weak compared to probes that interact with the electron cloud, which leads to a large penetration depth. This makes neutrons a useful tool to study internal structures in general and buried interfaces in the case of NR. A low interaction between neutrons and their usually low energy decrease the damage induced in samples by a neutron beam. For that reason, NR is much less destructive than the comparable x-ray reflectometry. As neutrons bear a spin, they interact with magnetic fields, as well as magnetic moments of atoms, which is a property often exploited in the study of magnetic materials.

Since neutrons mainly interact with the nuclei, they are very sensitive to the elemental and isotopic composition of matter. A measure of the scattering power of a material, i.e. how strongly different elements interact with neutrons, is the so called scattering length which can have a positive or negative value. Unlike the interaction between X-rays and matter, the scattering length does not increase linearly with atomic number, but is seemingly randomly distributed across the periodic table. Fig. 3.1 shows the scattering lengths for a part of the periodic table. In the range of light elements a large fluctuation of the scattering length

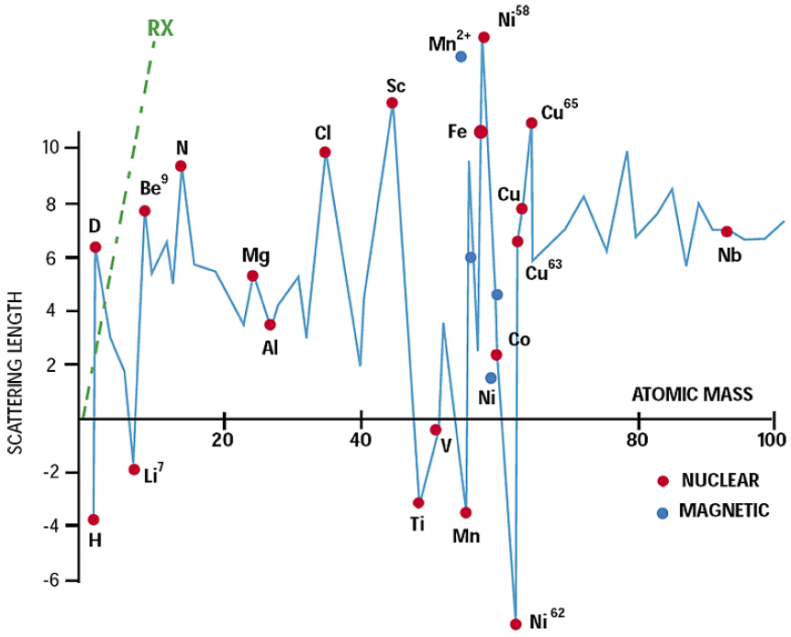

Figure 3.1: Isotopic distribution of neutron scattering length in femtometer. The green line labelled RX indicates the scattering lengths for x-rays of the different elements for comparison.Taken from [121].

is observed, which leads to a sensitivity to light elements, which are prevalent in biological systems, that other probes do not offer. In reflectometry the density of scattering length in a given material is the property of importance, as this distinguishes different materials from each other. This scattering length density Nb (or SLD) is defined as:

$$Nb = \sum_j b_j \rho_j, \tag{3.1}$$

where b_j is the coherent scattering length of a nucleus and ρ_j is the atom density of the respective nucleus. As the scattering length of nuclei can be positive or negative, the SLD of materials can be positive or negative as well. An example for this is the difference between hydrogen and deuterium. While hydrogen is one of the few elements with a negative scattering length, the scattering length of a deuteron is relatively high. This property is often exploited in neutron scattering using the so called contrast variation method, that takes advantage of the fact that neutrons interact differently with elements having a different isotopic composition. Substitution of a hydrogen atom by a deuteron in a compound can induce large changes in the SLD of the sample, while having only minor effects on the system structure and properties. This way the degree of interaction of a sample with neutrons can be manipulated and more importantly for NR measurements, different parts of a sample can be highlighted or rendered invisible. This can be used for example to identify the position of certain compounds in a sample by only replacing the hydrogen atoms of this compound

with deuterium. In biological and soft matter samples in solution this can be used to replace the solvent with deuterated solvent and this way to address the phase problem in scattering. While no direct analytic relationship between reflectivity curves and nano-structure can be found using this so called solvent exchange method, models representing the sample system have to be able to represent the signal measured in H_2O as well as the signal measured in D_2O or mixtures of D_2O and H_2O, by only changing the parameter describing the solvent. This way, meaningful interpretation of NR curves is possible.

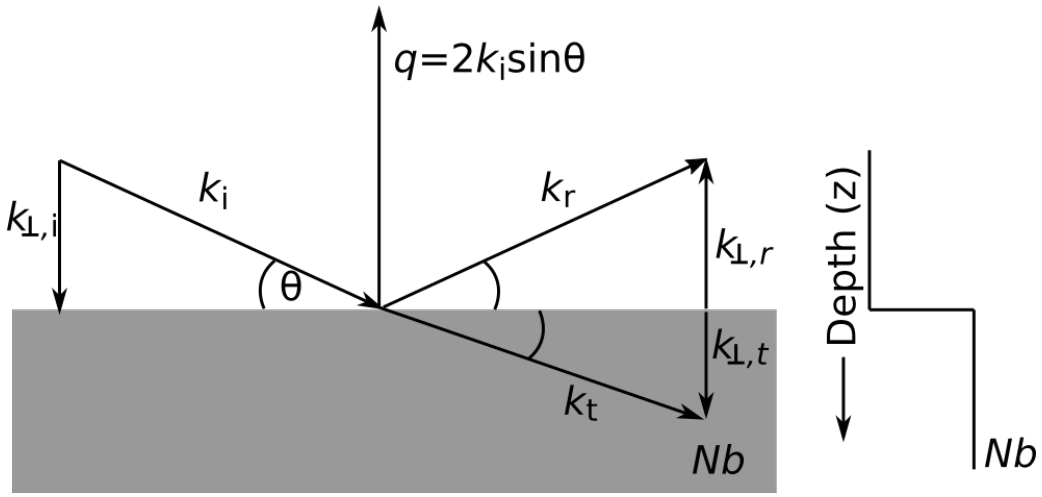

Figure 3.2: Reflection from an interface.

In NR a beam of neutrons with an energy E impinges on a surface at an angle θ and is scattered. A sketch of such a geometry is shown in fig. 3.2. This scattering can be divided into different components which differ depending on the type of interaction with the sample and its structure. For NR, elastic scattering is assumed, thus no energy is transferred in the scattering process. In the following, only specular reflectivity will be treated, which describes reflection under the same angle as the incident beam. This occurs for sample systems which show no structure variation in lateral direction. This way the momentum transfer is only perpendicular to the substrate and all information obtained is averaged over the surface illuminated by the beam. Finally, neutron absorption is neglected, because the absorption cross section of most materials, especially those occurring in biological matter, is very small. The following basics of NR are mainly based on concepts presented in [122, 123, 124, 125, 126, 127].

As a particle with a mass m_n, a wavelength λ can be assigned to a neutron according to the de Broglie equation:

$$\lambda = \frac{h}{m_n v}, \tag{3.2}$$

where v is the velocity of the neutrons. As an entity with particle and wave properties, most of the interaction between neutrons and matter can be described using quantum mechanics as well as classical optics [125]. As a wave, a neutron can be described by the wavelength

dependent wave vector $k = 2\pi/\lambda$. When impinging from air on a flat surface of an infinitely deep material that shows no lateral structure, the neutron wave interacts with a constant potential V of:

$$V = \frac{2\pi\hbar^2}{m_n} Nb. \tag{3.3}$$

Nb is the above defined coherent scattering length density, which depends on the materials elemental composition. The kinetic energy of a neutron is given by:

$$E = \frac{\hbar^2 k^2}{2m_n}. \tag{3.4}$$

When approaching a surface as described by the potential above, momentum transfer between neutron and surface occurs only in the z direction perpendicular to the surface. The perpendicular component of the incoming wave vector is given by:

$$k_{\perp,i} = k_i \ \sin\theta = \frac{2\pi}{\lambda} \sin\theta. \tag{3.5}$$

In neutron scattering a description of the reflectivity in dependence of the momentum transfer $q = 2k \sin\theta$ is often useful, as it takes wavelength and angular dependencies into account, which is needed for e.g. the time of flight technique described further below. If the wave vector component of the kinetic energy of the neutron perpendicular to the surface is smaller than the potential V, then its energy is not enough to overcome the potential barrier, which leads to the total reflection of the wave. The surface normal energy component is given analogously to the perpendicular wave vector as:

$$E_\perp = \frac{2\hbar^2\pi^2}{m_n\lambda^2} \sin^2\theta. \tag{3.6}$$

Following that, a critical angle of total reflection θ_c can be defined, which is reached when the kinetic energy equals the potential:

$$\frac{2\pi\hbar^2}{m_n} Nb = \frac{\hbar^2 k_{\perp,c}^2}{2m_n} = \frac{2\hbar^2\pi^2}{m_n\lambda^2} \sin^2\theta_c. \tag{3.7}$$

This leads to a critical angle and momentum transfer of:

$$\sin\theta_c = \sqrt{\frac{\lambda^2 Nb}{\pi}} \ \text{ and } \ q_c = \sqrt{16\pi Nb}. \tag{3.8}$$

When the SLD shows negative values, no total reflection can occur from vacuum or air. The experimental determination of this critical angle between a medium and air (or two media, if the difference in Nb is taken into account instead of the absolute value) is a precise method to obtain detailed information on the scattering length density and thus composition of materials. If the energy component perpendicular to the surface of the neutron wave is higher than the potential, reflection or transmission may occur. The energy

of the transmitted beam will then correspond to the energy of the incident beam minus the potential. For the normal component of the energy this can be expressed as:

$$\frac{\hbar^2 k_{\perp,t}^2}{2m_n} = \frac{\hbar^2 k_{\perp,i}^2}{2m_n} - \frac{2\pi\hbar^2}{m_n} Nb, \tag{3.9}$$

leading to a transmitted wave vector of:

$$k_{\perp,t}^2 = k_{\perp,i}^2 - 4\pi Nb. \tag{3.10}$$

The transmitted wave undergoes refraction, as the energy is reduced due to the potential. Thus, just like in classical optics, a neutron index of refraction can be defined as the ratio between the wave vectors in two media.

$$n^2 = \frac{k_t^2}{k_i^2} = \frac{k_{\parallel,i}^2 + (k_i^2 - 4\pi Nb)}{k_i^2} = 1 - \frac{4\pi}{k_i^2} Nb = 1 - \frac{\lambda^2}{\pi} Nb. \tag{3.11}$$

For most materials Nb is very small, which leads to n values close to one and allows an approximation as:

$$n \approx 1 - \frac{\lambda^2}{\pi} Nb. \tag{3.12}$$

This index of refraction is slightly below one for positive Nb values which many materials possess. For these cases the beam is refracted towards smaller angles at the interface, so that external reflection occurs frequently.
With these tools neutron interaction can be described in an optical way, which means that behaviour like e.g. Snells law is applicable to neutron scattering.

Reflectivity from an interface

The interaction with a smooth interface can be divided into reflection and transmission. The reflection component is described by the reflection coefficient or reflectance r:

$$r = \frac{k_{\perp,i} - k_{\perp,t}}{k_{\perp,i} + k_{\perp,t}}. \tag{3.13}$$

The transmission coefficient is given by:

$$t = \frac{2k_{\perp,i}}{k_{\perp,i} + k_{\perp,t}}. \tag{3.14}$$

From this the reflectivity R can be derived using eqs. 3.8 and 3.10:

$$R = rr^* = \left(\frac{k_{\perp,i} - (k_{\perp,i}^2 - k_c^2)^{1/2}}{k_{\perp,i} + (k_{\perp,i}^2 - k_c^2)^{1/2}} \right)^2 = \left(\frac{q - (q^2 - q_c^2)^{1/2}}{q + (q^2 - q_c^2)^{1/2}} \right)^2. \tag{3.15}$$

with k_c as the critical wave vector. For values of $q \gg q_c$ and $k_{\perp,i} \gg k_c$ the reflectivities can be approximated as:

$$R \approx \frac{16\pi^2}{q^4} Nb^2. \tag{3.16}$$

At these angles multiple scattering is negligible so that the interaction between neutron and matter is considered small. This allows the use of the Born approximation. This Fresnel reflectivity formula for a perfectly smooth interface leads to a decay in reflectivity according to q^{-4} when far away from the critical angle.

Reflectivity from layers

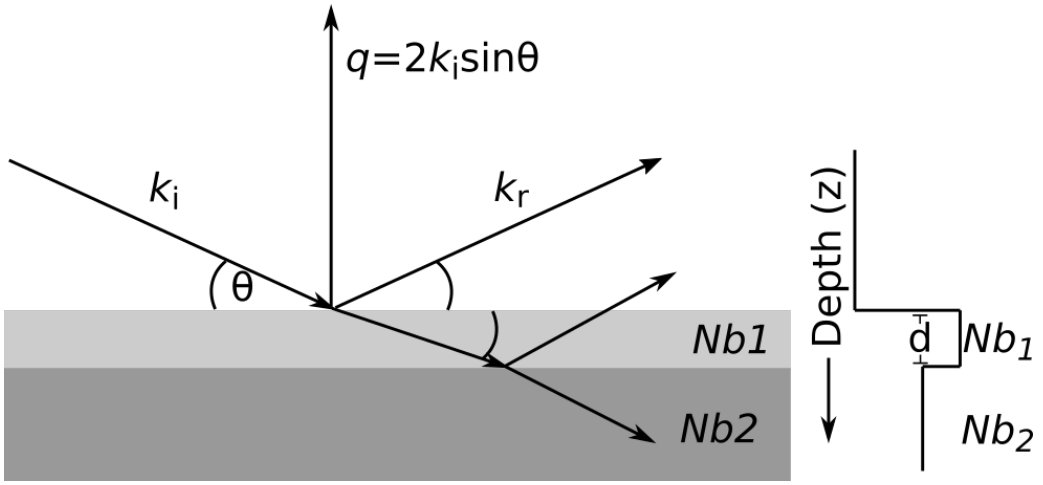

Figure 3.3: Reflection from one layer.

If the slightly more complex situation of reflection on one layer of thickness d on a substrate is considered, reflection and transmission can occur at each of the two the interfaces. This situation is depicted in fig. 3.3. As shown above, each interface on its own can be described by reflection coefficients, in this case $r_{0,1}$ for the interface between medium zero and one and $r_{1,2}$ for the interface between the first and second medium. A combined reflectivity coefficient is determined as:

$$r = \frac{r_{0,1} + r_{1,2} e^{2ik_{\perp,1}d}}{1 + r_{0,1} r_{1,2} e^{2ik_{\perp,1}d}}. \tag{3.17}$$

Similar to the case of one interface, the reflectivity can thus be calculated as:

$$R = \frac{r_{0,1}^2 + r_{1,2}^2 + 2r_{0,1}r_{1,2}\cos(2k_{\perp,1}d)}{1 + r_{0,1}^2 r_{1,2}^2 + 2r_{0,1}r_{1,2}\cos(2k_{\perp,1}d)}. \tag{3.18}$$

This reflectivity shows an oscillation behaviour due to the cosine, which is directly related to the thickness d of the layer by:

$$d \propto \frac{\pi}{\Delta k_{\perp,0}} = \frac{2\pi}{\Delta q}, \tag{3.19}$$

with $\Delta k_{\perp,0}$ and Δq being the distance between two minima of the oscillations. In experimentally obtained reflectivity curves these so called Kiessig fringes allow the precise determination of layer thicknesses.

This calculation can be performed for any number of layers, however for larger numbers several methods have been established, mainly Parratt's recursive algorithm [128] and Abèle's optical matrix method. In the optical matrix method described by Born and Wolf [129], which is used in this thesis, a characteristic matrix M for reflection and transmission is defined for each interface:

$$M_i = \begin{bmatrix} \cos(k_i d_i) & -\sin(k_i d_i / k_i) \\ k_i \sin(k_i d_i) & \cos(k_i d_i) \end{bmatrix}. \tag{3.20}$$

The multiplication of these matrices for each layer in a system leads to the the total reflectivity curve for this series of layers with known properties.

Using this method, different combinations of layers can lead to the same reflectivity profile, which is an effect of the well known phase problem caused by the fact that only intensities can be experimentally accessed, but not the phase. As introduced above, one of the strategies to obtain unambiguous results using this method is the contrast variation method, if the necessary previous information about the sample is available.

In reality no interface is perfectly smooth. Surfaces show a roughness, which affects the scattering signal. In general, roughness causes a faster decline of reflectivity with momentum transfer than the q^{-4} dependency described by the Fresnel reflectivity shown above. In data modelling there are different ways to approach this situation, namely ways to mathematically model roughness. After Névot & Croce [130] this can be modelled as an error function $\mathrm{erf}(z/\sqrt{\sigma})$ with σ being a measure of the roughness of the system. This corresponds to a multiplication of the reflectivity with a Gaussian function, similar to the multiplication with a Debye-Waller factor for a crystal. This is the method employed in the Motofit software. It has to be noted that the two cases of roughness as a sharp but irregular interface and as interdiffusion with a gradual merging of the two layers cannot be distinguished from each other, as long as the structure size is below the coherence length of the neutrons. This is sketched in fig. 3.4.

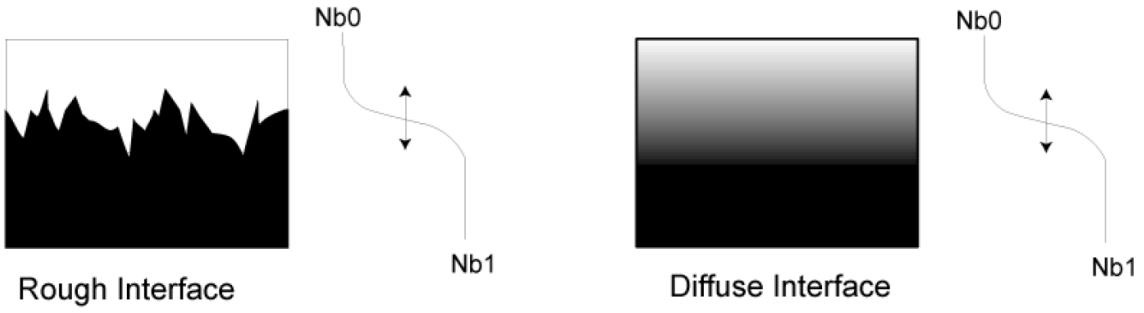

Figure 3.4: Two surface profiles, that lead to the same SLD profile. Taken from [125].

3.1.2 Experimental NR

In a NR experiment the specular reflected intensity R is measured as a fraction of the incoming intensity R_i in dependence of the momentum transfer:

$$\frac{R}{R_i}(q).$$

This is done for a q-range as large as possible to maximize information gain. Because q depends on wavelength as well as incident angle (see eq. 3.5), different methods to vary q are available. In NR two methods are used: monochromatic reflectometry and time of flight (TOF) reflectometry. In monochromatic mode the incident angle is varied and the reflected intensity recorded for each incident angle, leading to a reflectivity profile. The time of flight mode makes use of the properties of neutrons as a particle with mass. Neutrons with different wavelength have a different velocity according to de Broglie 3.2. Interaction of neutrons with different wavelength with the sample at the same angle leads to different momentum transfer q, and thus a wavelength range results in a q range, just like variation of the incident angle. In a reactor source, neutrons of different wavelength and thus different velocity are produced. For the cold neutrons used at the ILL reflectometers, this covers a range of roughly 1-30 Å. Consider a pulse of neutrons with different velocity, which all started from a source at the same time, impinging on a surface. The neutrons are reflected and due to their different velocity arrive at a detector at different times. With knowledge of the flight path, the wavelength of the neutrons can be determined from the time they arrive at the detector. With a detector with time resolution, the neutrons can thus be sorted according to wavelength and, following that, momentum transfer upon interaction with the sample. Using this technique, a reflectivity profile can be obtained from neutrons impinging on the surface under the same angle. To cover a larger range in q-space, multiple angles are often measured and combined to one reflectivity profile. To determine a common starting time of all neutrons in a pulse, choppers are used, which cut a continuous beam into short pulses. The duration of these pulses is one of the resolution limitations of NR. Further geometrical limitations arise from the divergence of the neutron beam.

Scattering background that is not caused by the specular reflection limits the usable q range in an experiment. For this reason, on one hand the background is determined and subtracted from the specular intensity. On the other hand, sources of background scattering are minimized. Water causes a high incoherent background signal and shows a relatively low transmission, thus the incident beam is usually transmitted through the sample substrate. The substrate materials used in this thesis (silicon and sapphire) show a low absorption and incoherent scattering cross section.

3.1.3 Experimental NR setups

NR experiments presented in this thesis were carried out on three neutron reflectometers: D17 and FIGARO at the ILL (Grenoble, France) and SURF at ISIS (Didcot, UK).

D17 has a horizontal scattering geometry and was used in TOF mode [124, 131]. A sketch of the instrument setup is shown in fig. 3.5. The constant neutron flux from the reactor

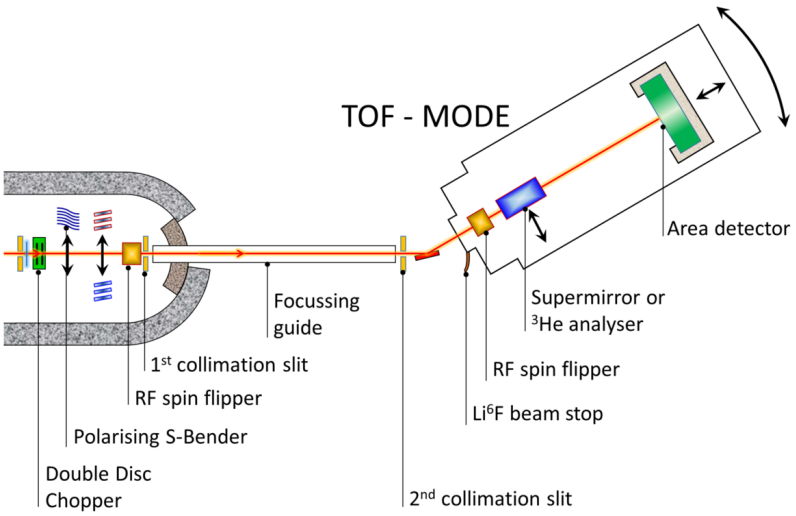

Figure 3.5: Sketch of the reflectometer D17 [131].

is cut into pulses by a set of two choppers. Scattering patterns are recorded by a 250×480 mm^2 2D ILL monoblock tube detector filled with ^{3}He gas. The instrument was operated at a resolution of 1.6 or 2 %, depending on the experiment, with slit settings illuminating around 70 % of the sample. All samples were characterized at two different angles to increase the available q-range. Silicon substrates were measured either at 0.8 and 3.0° or 0.8 and 3.3°. For sapphire substrates, either 0.8 and 3.0° or 0.4 and 2.8° were chosen. A wavelength range from 2 to 30 Å was used. This way a q-range was covered that started at 0.009 Å^{-1} for silicon samples and 0.003 Å^{-1} for sapphire samples. At values around 0.2 Å^{-1} the signal starts to be dominated by the sample background, which is - in the case of tBLMs - mainly caused by incoherent scattering from the solvent reservoir.

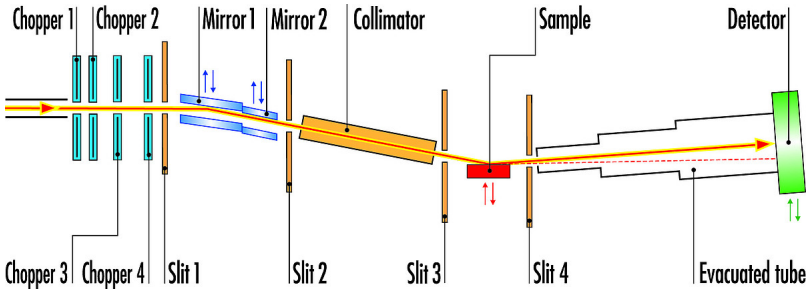

Figure 3.6: Sketch of the reflectometer FIGARO [132].

The TOF reflectometer FIGARO has a vertical scattering geometry [133]. Fig. 3.6 shows a schematic view of the instrument. It was used in the reflection up geometry, meaning that the lipid bilayers were positioned below the substrate. Like on D17, choppers divide the constant beam into pulses for TOF mode. FIGARO is equipped with a 2D 500×150 mm^2 ^{3}He tubular aluminium monoblock detector. Experiments were performed with a 7

% $\Delta\lambda/\lambda$ resolution. Each sample was measured at two different incident angles of 0.8° and 3.2°. With a wavelength range of 2-20 Å, this led to a covered q-range starting at 0.009 $Å^{-1}$ up to around 0.2 $Å^{-1}$ at which point the sample background dominates the signal.

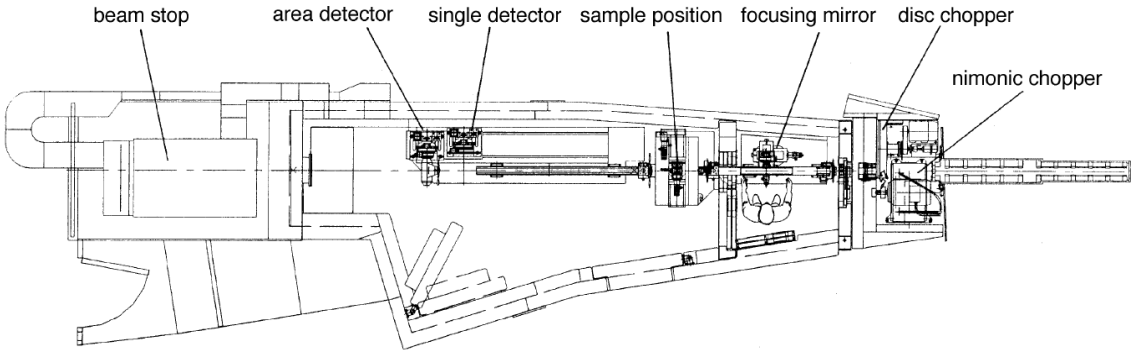

Figure 3.7: Sketch of the SURF reflectometer [134].

Different to D17 and FIGARO, the SURF reflectometer at ISIS receives neutrons from a spallation source, not a reactor. It has a vertical scattering geometry and operates in TOF mode. Fig. 3.7 shows a top view sketch of the instrument setup. Choppers refine the neutron pulses to remove fast neutrons and gamma rays. A 1D shielded ^{3}He gas detector is used to record the reflectivity curves. Samples were characterized at the three angles 0.35°, 0.65° and 1.5°. A wavelength range from 1-7 Å with a resolution of 4.5 % $\Delta\lambda/\lambda$ was used. The usable q space ranges from 0.012 $Å^{-1}$ to roughly 0.15 $Å^{-1}$.

In all experiments solid/liquid sample cells that were developed at the ILL were used. In this setup the substrate block is sandwiched between an aluminium plate and a PEEK (polyether ether ketone) trough containing the liquid solution in contact with the sample formed on the surface of the solid substrate. The sample cell holds a volume of approximately 2 ml and is connected to tubes for solvent inlet and outlet. A computer controlled HPLC pump (Smartline pump 1000) is used for automated solvent exchange. The cell temperature is controlled by a water circuit in the cell holder. Substrate blocks of 10 mm or 15 mm thickness for silicon and 15 mm thickness for sapphire were used. The neutron beam penetrates through the substrate block and is reflected at the inner side of the substrate on which the tBLMs is formed.

In all experiments, the direct beam through the sample substrates was measured with the settings for each used angle, in order to normalize the reflected intensity to the incoming beam. Each sample substrate was characterized at one or two contrasts before deposition of the tBLMs. For titanium and gold coated substrates this served to determine the respective layer thicknesses. For substrates used in DPN tBLM measurements the silicon blocks with the APTES and tether molecules layer were investigated. While one or two contrasts are not sufficient to find an unambiguous interpretation of the data, these measurements serve as a cross check for data analysis of the final tBLMs. Subsequently, each sample was characterized in different mixtures of D_2O and H_2O, to use the contrast variation method.

For most samples, four different contrasts were measured due to the high complexity of the system. Pure D_2O and H_2O were used and two mixtures with SLDs equal to the SLD of silicon (38 % D_2O, 62 % H_2O, called SiMW in the following) and gold (73 % D_2O, 27 % H_2O, abbreviated as AuMW) for samples on gold coated substrates, or SiMW and SiO_2's SLD (58 % D_2O, 42 % H_2O, abbreviated as OxMW) for samples formed on substrates without a gold coating. Counting times for each contrast were adjusted according to the sample system to allow for satisfactory statistics of the NR curves.

3.1.4 Data analysis and modelling

Data reduction for experiments at D17 or FIGARO was performed using the COSMOS software which is accessible from the lamp software package [135]. The specular peak intensity is integrated from detector lines of constant wavelength in order to obtain a reflectivity profile value in dependence of q. Normalization and attenuation factors are calculated from the direct beam measurements mentioned above and from a reflected beam measurement that includes an area of total reflection. Thus attenuation by the sample substrate as well as attenuators used for detector protection is taken into account. A scale factor between the different angles, also determined from the different attenuation needed for the settings of first and second angle, is applied and ensures overlapping of the data measured at the two incident angles. The background signal induced by instrument components, the substrate and the incoherent scattering from the solvent limits the accessible q-range. A background correction is performed by subtracting the average detector values close to the specular peak from the measured specular peak intensity, thus giving access to higher q features. Data obtained from the SURF reflectometer was reduced in a similar fashion using the Mantid framework [136]. However due to the single 1D detector no background subtraction was performed and a slightly lower usable q-range was achieved.

Data analysis was performed using the Motofit plug-in for Igor Pro for all samples that exhibited a uniform structure [137]. The software refnx was used for samples that needed a multi-region approach, as will be explained further below [138]. For selected samples the data analysis was performed with both programs to check the consistency of results between programs. The sample systems were modelled as a series of homogeneous slabs. Each slab was described by the four parameters thickness, SLD, roughness and solvent percentage or hydration in the layer. These four parameters per slab were optimised in the fitting procedure to find the best model representation of the reflectivity curves. Depending on the sample system a varying number of slabs was needed as will be further expanded in the detailed model description below. The solvent content was modelled as a replacement of a fraction of the slab's SLD with the SLD of the respective contrast's solvent. As all samples were characterized at multiple different contrasts, the slab model had to lead to an accurate representation of the reflectivity curves for each contrast without altering this solvent content. This way, contribution of solvent and non aqueous components could be disentangled. Roughness was implemented as an error function for each slab as described by Névot & Croce [130]. Using Abèle's optical matrix method [139] to calculate reflectivity profiles corresponding to these parameters, they were used to determine which set of

parameters yields the best agreement with the experimentally obtained NR curves. As a measure for the goodness of the fit, the χ^2 quantity is used to determine the deviation of the fitted curves from the data set:

$$\chi^2 = \sum_{n=1}^{L} \frac{1}{L-P} \left(\frac{R_{\mathrm{meas},n} - R_{\mathrm{fit},n}}{\sigma_{\mathrm{error},n}} \right)^2 ,$$

with $R_{\mathrm{meas},n}$ and $R_{\mathrm{fit},n}$ being the measured and fitted reflectivity of the nth data point, L the number of data points, P the number of fit parameters and $\sigma_{error,n}$ the standard error of the nth data point. During the fitting process this quantity is minimized by a genetic algorithm using the differential evolution technique [140]. This type of algorithm has the advantage, that it is capable of finding global minima instead of converging towards local minima like e.g. the Levenberg-Marquardt algorithm [141, 142]. The fitting procedure results in a set of sample parameters, for which an error corresponding to 5 % $\Delta\chi^2/\chi^2$ is specified.

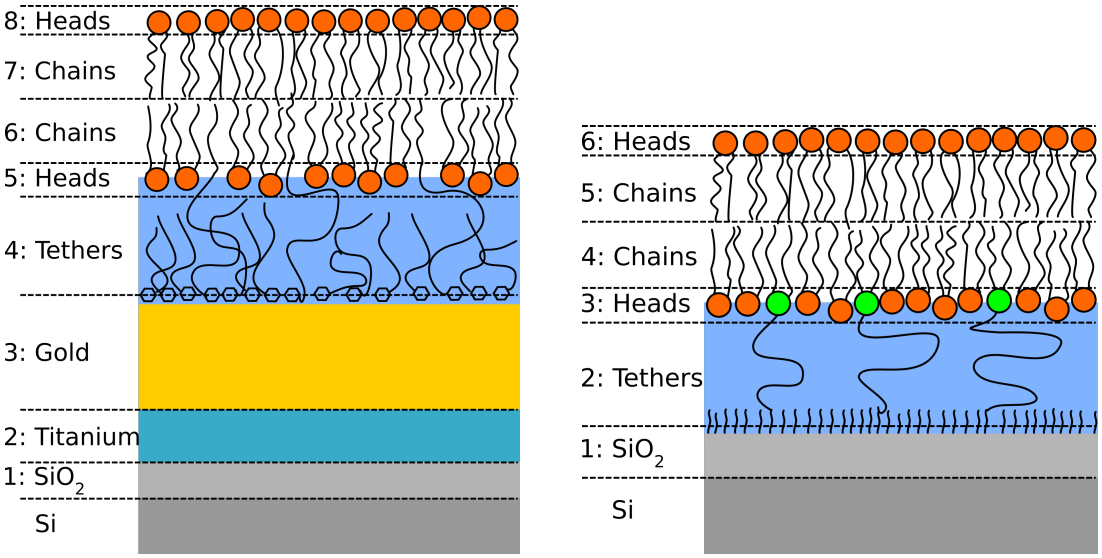

(a) DLP tBLMs **(b)** DPN tBLMs

Figure 3.8: Slab model used for representation of DLP and DPN tBLM structure.

The slab models that were used for data modelling of DLP and DPN tBLMs are shown in fig. 3.8. Lipid bilayers can generally be divided into four different regions of different average SLD. Both, the inner and outer leaflet are represented by a hydrophilic headgroup layer and a hydrophobic chain region. Apart from their difference in physical properties, they are also well distinguishable in neutron scattering experiments as the headgroups usually have SLD values between 2 and 3 $\times 10^{-6}$ Å^{-2}, while the SLD of chain regions is slightly below zero for hydrogenous lipids. Molecules possessing labile hydrogen atoms usually show a change in SLD value when the surrounding solvent is changed, because part of the hydrogen atoms are exchanged by deuterium or vice versa. This was not modelled by changing the SLD

Lipids

	DOPC head	DOPC chains	CL head	CL chains
SLD [10^{-6}Å^{-2}]	1.88	-0.3	2.68	-0.3

Substrate

	PEG	Gold	Titanium	SiO_2	Si	Sapphire
SLD [10^{-6}Å^{-2}]	0.6	4.5	-1.95-2.5	3.47	2.07	5.7

Solvents

	H_2O	SiMW	OxMW	AuMW	D_2O
SLD [10^{-6}Å^{-2}]	-0.56	2.07	3.47	4.5	6.36

NhaA

Solvent	H_2O	SiMW	OxMW	AuMW	D_2O
SLD [10^{-6}Å^{-2}]	1.6	2.1	2.3	2.4	2.75

Table 3.1: SLDs of the materials used in this thesis.

value of lipids at different contrasts, but by letting the solvent content in the respective bilayer slab vary. A certain volume fraction of solvent in a slab causes the same change in total SLD value as different SLD values of the lipid fraction and can therefore model the hydrogen exchange of lipids in this layer. This is why there is always a certain amount of solvent present in the headgroup layers of tBLMs, which does not actually represent defects in the membrane but accounts for these exchangeable hydrogen atoms. This method of modelling exchangeable hydrogen atoms is especially favourable for bilayers composed of different lipid species, as they have different amounts of labile hydrogen atoms. While phosphocholines have no exchangeable hydrogen atoms, CL can show a certain variation in SLD upon solvent exchange due to exchangeable hydrogen. To determine the SLD values of lipids, knowledge of the headgroup and chain region volumes is necessary. This can be obtained by different methods and for many lipids extensive studies have been performed to obtain volumes under different experimental conditions. As they are very specific to the environmental conditions these values are always just an approximation unless exactly the same experiment is conducted, which is seldomly the case, especially for highly variable biological systems. Most of the component volumes for lipids used in this thesis stem from X-ray and neutron scattering studies of vesicles or planar lipid bilayer stacks. Volumes of lipids and thus their SLDs vary with temperature. As all experiments presented here were executed at 21°C, all SLD values are given for that temperature or close to it. Metals show a more regular structure so that the SLD values of substrate components are well tabulated. The SLD values for all components used in this thesis are shown in table 3.1.

In addition to the structure of the lipid bilayer itself, in the case of tBLMs, the substrate and the sub-membrane space must be modelled. The model differs for the two tBLM systems investigated in this study. **DLP tBLMs** are formed on gold coated silicon or sapphire

substrates. Gold does not adhere well to silicon or sapphire, so that an intermediate layer of titanium is necessary. On silicon surfaces an additional native SiO_2 layer is formed. This leads to a three layer model for the substrate on silicon and a 2 layer model on sapphire. Due to this already complex substrate, NR measurements of each bare substrate were performed before tBLM formation. Fits of the tBLMs were then compared to these substrate fits for plausibility. While SLD values of SiO_2 and gold are well characterized and usually do not vary in conditions like those present in these NR experiments, the SLD of titanium can vary due to the unavoidable inclusion of hydrogen atoms that occurs in the titanium deposition process [143]. To account for that, the SLD of titanium was allowed to differ from the nominal value of -1.95·10^{-6} Å^{-2} in all fits towards more negative values, while the other substrate SLDs were kept fixed.

The sub-membrane space is built up of the tether and lateral spacer molecules. The main component of these molecules are PEG chains which either connect the membrane and surface in the case of tether molecules, or fill the sub-membrane space in case of the lateral spacer molecules. The sub-membrane space was thus represented by one layer with the SLD value 0.6·10^{-6} Å^{-2} of PEG. While the benzyl disulfide groups on the surface show a different structure, their SLD lies in between the SLD of 0.6·10^{-6} Å^{-2} of PEG and 4.5·10^{-6} Å^{-2} of gold. Combined with the expected small thickness of below 5 Å, this layer can not be distinguished from the neighbouring layers and will contribute as a roughness factor to the interface. While a homogeneous distribution of PEG in the sub-membrane space is not evident, trying to model it with multiple layers did not increase fit quality.

For the representation of DLP tethered bilayers themselves, a modified model of a lipid bilayer was used. Like a free standing membrane, the bilayer was divided into two leaflets of head and chain region. To account for the unknown amount of tether molecules that insert into the inner leaflet, its parameters were allowed to vary accordingly. The SLD of the slab representing the inner headgroup was not fixed, but allowed to vary between the value of PEG - which accounts for the hydrophilic part of the tether molecules that inserts into the headgroup layer - and the value expected for lipid headgroups of the respective membrane composition. The SLD of the inner chain region was kept fixed. Although the phytanyl chains of the tether molecules insert into this layer, they are indistinguishable from lipid chains. The outer chain region parameters were linked to the inner chain regions, because the chain regions are expected to be largely symmetric. The SLD values of the outer headgroup were fixed for membranes consisting of only one lipid and were allowed to vary between the expected headgroup SLDs of the different lipids for tBLMs consisting of more than one lipid species. This accounts for the fact that, despite knowing the exact lipid composition of the mixture used to produce the tBLMs, the final lipid composition of the bilayer in general and the lipid distribution within the two leaflets in particular is not exactly known. In addition, headgroup and chain region volumes of bilayers formed from lipid mixtures may differ from the volume they have in lipid bilayers consisting only of one lipid type.

All these considerations led to the 8 layer model to represent DLP tBLMs formed on silicon substrates shown in fig 3.8a and a 7 layer model without the SiO_2 layer for DLP tBLMs formed on sapphire substrates.

DPN tBLMs require another model representation. The lipid bilayer itself was modelled in a similar way with four layers representing the headgroups and chain regions of the two leaflets. Different to DLP tether molecules the part of the tether molecule that inserts into the inner leaflet consists of an actual lipid head structure for this molecule. However, parts of the PEG chains are expected to locate close to or in this layer as well, especially because the PE headgroup that is part of the tether molecules is smaller than the PC headgroups that were present in all investigated tBLMs. Thus the SLD of this layer was allowed to vary between the values of PEG and the lipid headgroup as well. The substrate consisted of silicon blocks for this tBLM system, so that only a SiO_2 layer was necessary for modelling the space below the tethers. The sub-membrane space including the tether molecules is of an unknown structure, as a tBLM system of exactly this composition has not been investigated before. However, the formation of APTES layers on planar surfaces has been studied before. When a monolayer of amino silane is formed, an SLD value very close to PEG is expected, which makes this layer indistinguishable from PEG. The silane groups themselves on the other hand show an SLD comparable to SiO_2. In case of formation of an unordered layer as described in section 2.4 the resulting SLD may vary but is expected to range between the SLD values of PEG and SiO_2. This leads to it being indistinguishable from the neighbouring layers and possibly contributing to a higher roughness of the interface between these slabs. As a majority of the sub-membrane space is composed of PEG molecules, it was modelled as one layer with the SLD of PEG. Similar to DLP tBLMs, a uniform distribution of PEG in the sub-membrane space can not be expected, but introduction of further layers did not increase fit quality. Thus most DPN tBLMs were modelled with the 6 layer model shown in fig. 3.8b.

This model assumes a laterally uniform distribution of the tBLM on the surface. Some DPN tBLMs however required a modelling that assumed the formation of a tBLM on part of the substrate, with significant areas on the substrate being only covered by a tether molecule layer and no lipid bilayer above. Although small diffuse imperfections within the bilayer and extended areas with no membrane both cause an increased presence of solvent molecules, they must be treated differently in modelling the reflectivity profile. Small diffuse imperfections are generally below the coherence length of the neutrons ($\sim \mu$m) [144]. Their contribution to the scattering will be given as an incoherent sum of coherently scattered events whose presence can be accounted for by varying the properties of the relevant slabs in the model describing the system. Defects of larger area, like macroscopic regions of the substrate not covered by the membrane, will reflect the neutrons independently from the area covered with the membrane. The total reflectivity in this case will be given by the sum of the reflectivities of the two regions weighted by the relative fraction of the two area

$$R(q) = A_1 R_1(q) + (1 - A_1) R_2(q), \tag{3.21}$$

where R_1 is the reflectivity of the area of the substrate of areal fraction A_1 where the lipid membrane is present, and R_2 is the reflectivity of the substrate region of areal fraction $(1 - A_1)$ where the lipid membrane is absent. Hereafter, I will refer to *mixed area model* when multiple regions must be considered to model the data. Alternatively, I will refer to *single area model* when the surface of the substrate is covered by a uniform membrane that does not present macroscopical defects. Such a mixed area model was used for DPN tBLMs by modelling part of the surface as described above, and a second region as only covered by a SiO_2 layer and a tether layer. This tether layer takes into account the presence of the lipid molecules attached to the end of the PEG chains and thus was modelled with an SLD similar to PEG, which was allowed to vary. For the analysis of these samples the refnx software was used, which allows to model such mixed area structures. The mathematical treatment by refnx is similar to that of Motofit: the Abèles method is used to calculate the reflectivity from a slab model and a genetic algorithm is used to minimize the χ^2 value to find the best fitting representation of the measured data [138].

For the modelling of NhaA incorporation into tBLMs a model was used that assumes the replacement of a fraction of the lipid bilayer slab volumes with protein. The SLD of NhaA was estimated from the amino acid sequence using the ISIS protein scattering length density calculator [145]. As NhaA can be modelled as approximately cylinder shaped, the fraction that is replaced was forced to be equal in every membrane layer. In the fitting procedure this was implemented by introducing an additional protein fraction parameter ϕ_{prot}. The SLD of each lipid bilayer slab was thus replaced by an SLD of:

$$Nb_{\text{slab}} = \phi_{\text{prot}} \cdot Nb_{\text{prot}} + (1 - \phi_{\text{prot}}) \cdot Nb_{\text{mem}}, \tag{3.22}$$

with Nb_{mem} being the SLD of the respective lipid bilayer slab and Nb_{prot} being the SLD of the protein. Protein SLD was fixed in the fitting procedure, but has different values depending on the surrounding solvent, as part of the hydrogen atoms in the protein structure are exchangeable. This protein fraction serves as a simplified estimation of the protein content. Protein parts protruding from the membrane and the histidine tag were not modelled as separate layer as they are assumed to contribute to the model as an extension of the the outer headgroup layer of the tBLM.

3.2 Electrochemical impedance spectroscopy

Electrochemical impedance spectroscopy (EIS) is an experimental technique in which a sample system of interest is perturbed with an electric AC signal of small magnitude while monitoring the system's reaction. By scanning a range of excitation signal frequencies and observing the system's response for each frequency, it is possible to derive the impedance of the system, which carries information on the electrophysiological properties of the investigated sample. EIS always observes the system in a steady state and is an ideal tool for lipid membrane studies, because it can e.g. give information on ion transduction across the membrane as well as derive membrane thickness from its capacitance. As many membrane proteins transport ions across the membrane, EIS is especially interesting for the characterization of ion channel protein activity. This has seen great interest in the past, especially

in combination with tBLMs, as it opens possibilities for a new range of stable biosensor devices. EIS utilizes an electric field to probe the system of interest and is thus a non-invasive and label-free characterization method. However, the placement of electrodes on both sides of the lipid bilayer is necessary, which poses a series of experimental challenges. In the following, I will give an overview of the principles of EIS and how it is applied to the study of tBLMs. Data modelling will be described as well as the used instrumentation.

3.2.1 Basics of EIS

The aim of EIS is the interpretation of the measured impedance at different frequencies of sample systems. Impedance can be described as a more general reaction to an applied electric signal than a resistor. The latter can only describe a very limited amount of systems. The resistance R according to Ohm's law, is the ability of a material or structure to resist the flow of electric current and is defined as:

$$R = \frac{U}{I}, \tag{3.23}$$

where I is the current and U is the applied electric potential. This relation holds true as long as no time dependence exists. If an alternating potential is used to excite the system, the concept of resistance has to be expanded. When a potential of sinusoid shape is applied to a system, the response is sinusoidal as well, but may be shifted in time. This assumes a linear relation between potential and current, which is a basic assumption of EIS. While most systems exhibit non-linear behaviour, for very small potentials, like those used in EIS, a pseudo linear behaviour is shown. Thus all following considerations are done for linear systems. An AC excitation signal $U(t)$ is described by $U(t) = U_0 \sin(\omega t)$, where U_0 is the amplitude of the signal, t is the time and ω is the angular frequency related to the frequency f by $\omega = 2\pi f$. The resulting current flowing through the system $I(t) = I_0 \sin(\omega t + \phi)$ shows the same time dependence shifted by a phase ϕ. Depending on the system this phase can be ahead of the potential or behind. Analogous to Ohm's law the frequency and time-dependent impedance Z can be defined as:

$$Z = \frac{U(t)}{I(t)} = \frac{U_0 \sin(\omega t)}{I_0 \sin(\omega t + \phi)} = Z_0 \frac{\sin(\omega t)}{\sin(\omega t + \phi)}, \tag{3.24}$$

where Z_0 is the amplitude of the impedance. Using Euler's formula this can be expressed as a complex quantity:

$$Z = Z_0 e^{i\phi} = Z_0(\cos\phi + i\ \sin\phi). \tag{3.25}$$

Therefore, the impedance can be expressed as a vector in the complex plane that is defined by impedance magnitude Z_0 and the phase angle ϕ. Alternatively it can be expressed as the real part Re Z and the imaginary part Im Z of the complex impedance.

In an EIS experiment, Z is measured for a range of frequencies. To depict this complex value, different ways of representation have been established over for different fields of application. Two frequently used ways to depict Z are the Nyquist and Bode plots. In a Nyquist plot, the imaginary part of the impedance on the y-axis is plotted against the

real part of the impedance on the x-axis. Each data point on this plot corresponds to one measured frequency. While the curve shape of a Nyquist plot can give information on the measured system, the frequency information is obscured, as it is impossible to determine which data point corresponds to which frequency. The Bode representation includes this frequency information. In a Bode plot, the magnitude of the impedance is shown against the frequency on one y-axis, while a second y-axis shows the phase shift in dependence of the frequency. Just like the Nyquist plot, focal points like minima or the limit of impedance towards zero frequency can give rough estimations of the properties of the investigated system, if enough information about the sample system is available. Usually, Bode and Nyquist plots are presented together to give a comprehensive picture of a system's impedance response [146].

	Impedance	Phase angle [°]
Resistor	R	0
Capacitor	$1/i\omega C$	90
Constant phase element	$1/(i\omega)^{\alpha}Q$	0-90

Table 3.2: Impedance and phase angles for equivalent circuit components used in this thesis. The impedance of a capacitor is defined by its capacity C and the angular frequency ω. A constant phase element's impedance shows an additional exponent α with a value between 0 and 1.

Comparable to NR measurements, the resulting EIS curves do not give immediate detailed information on sample properties, but are model based. A form of simplified model representation of the sample system can be used to reproduce the curve shape, thus give information according to the model chosen. In EIS this can be done by using equivalent electrical circuits, a representation in which the electrical properties of the system are substituted by electronic elements like resistors, capacitors, or inductors. These are combined according to rules analogous to those applicable to resistors to define the value of the complex impedance. Equivalent circuits as non-physical models can be composed of real existing electronic components, but also of theoretical elements, which induce a certain shape of the impedance and can be used to describe certain processes like diffusion. It is important to keep in mind that these theoretical elements, though very useful, do not exist in reality. Moreover, the equivalent circuits often have no physical meaning but represent the general curve shape well. So just like for NR data modelling, prior knowledge about the sample system is necessary to obtain physically meaningful information. In this way a simplified picture of the complex behaviour of real systems can be drawn by relating different electrical circuit elements to certain parts or properties of the sample. This aspect will be further expanded for lipid bilayers in the following section. The impedance behaviour of the different equivalent circuit components that are relevant for this thesis is shown in tab. 3.2. While resistor and capacitor are standard electronic components - the resistor with a purely real valued impedance and the capacitor with a purely imaginary impedance - a constant phase element is a theoretical element. Its impedance can show resistive properties if the exponent α is close to zero, as the influence of frequency is eliminated. If α is exactly one it

shows purely capacitive behaviour. The value of the exponent α determines the phase shift. Constant phase elements can be used to model features like heterogeneous electrode surfaces [147] or frequency dissipation [148]. Equivalent circuits are only one way of interpretation for EIS data and a full mechanistic analysis may provide more detailed information [149]. For the systems studied in this thesis project, equivalent circuits were used as they present a simple way to use a sufficiently complex model to obtain basic information like resistance and capacitance from a very complex sample system like tBLMs.

3.2.2 EIS of tBLMs and data analysis

Lipid bilayers on planar supports are systems often investigated by EIS. EIS allows to determine electronic equivalent parameters, which can be related to various electrophysiological properties of membranes. As an electrochemical method EIS is sensitive to ion movement, thus properties like ion permeability can be investigated, as well as also structural properties like the membrane thickness can be indirectly derived from impedance measurements. EIS has been used in the past to determine the intrinsic properties of lipid bilayers, and how ion transport proteins behave when inserted into membranes.

The simplest equivalent circuit representation for a free-standing perfect lipid bilayer is a resistor and a capacitor in series. The resistor represents the ion flow resistance of the solvent while the capacitor describes the lipid bilayer itself. A perfect bilayer does not transduce any ions across the hydrophobic bilayer core, and thus acts as a dielectric. This can be described as a classical parallel plate capacitor of capacitance C:

$$C = \epsilon\epsilon_0 \frac{A}{d}, \tag{3.26}$$

where ϵ and ϵ_0 are the relative permittivities of the membrane and the free space respectively, d is the hydrophobic membrane thickness and A is the surface area. However, such a simplistic representation fails in reality, as every bilayer is permeable to ions, that are present in the surrounding solution to a certain degree. This increases the resistive properties of the lipid bilayer [150]. Usually, lipid bilayers feature a certain amount of small defects, which allows additional ions to diffuse through the membrane. This creates a further ohmic flow across the bilayer, which adds to its resistive behaviour. Taking this into account, a lipid bilayer is described by a resistor and a capacitor in parallel with a resistor describing the solution resistance in series. Such a simplified model circuit has been successfully used in the past to describe the behaviour of free-standing or solid supported membranes (e.g.[151]). By using eq. 3.26 the thickness of bilayers can be estimated from the obtained capacitance. In fact measurements of the membrane capacitance have been the first experimental estimation of the bilayer thickness [152], which - despite being misinterpreted at that time - confirmed that a membrane actually consists of only a bilayer of lipid molecules. Further increase of equivalent circuit complexity is necessary to increase the accuracy and physical relevance of model circuits for lipid bilayers. Based on this basic RC circuit, different extensions have been proposed to describe different additional aspects. Many are simply analogue equivalent circuits and do not present any physical model for

the equivalent circuit elements [149]. To perform EIS measurements of membranes, electrodes are required to apply an AC potential across the membrane. Depending on the type of electrode, additional capacitive and resistive behaviour occurs at the interface between electrode and electrolyte [153]. In the case of gold electrodes, as those used in this thesis, no chemical reaction occurs for small applied potentials of below 100 mV, which means that no current crosses the electrode-electrolyte interface, so that they can be approximated as ideal polarizable electrodes. Their behaviour can be described by an additional capacitor in the equivalent circuit, while no resistor is necessary. If charge transfer from the electrode to the electrolyte occurred, an additional resistor parallel to the electrode capacitor would be necessary. Such equivalent circuits are the basic standard circuit for the representation of free-standing or solid-supported membranes [25].

When describing tBLMs, further adjustments of the equivalent circuit may be needed. This depends strongly on the tether architecture and the equivalent circuits for different tether systems may vary drastically and have so in literature. The sub-membrane space is a small confined region with a limited ion reservoir. At high tether density, it usually has very low water content and shows hydrogel like behaviour with drastically reduced ion mobility and lower dielectric constant [30]. Thus the description of the sub-membrane space in terms of equivalent circuit elements is highly complex. Defects in the lipid bilayer have an important influence as their structure and density affect the electric field distribution throughout the tBLM drastically [154]. Significant effort has been put into describing the effects of defects theoretically (e.g.[39, 155, 154]). Their nature determines the implementation into the equivalent circuit. Electrolyte filled pores which allow flow of ions can usually be described by an ohmic resistance which can be included in the membrane resistance parameter. In addition to them contributing to the electric properties of the bilayer itself, defects influence the electric field distribution in the sub-membrane space. Because of the confined space and reduced ion mobility in the sub-membrane space, equipotentiality between all points below and above the membrane can no longer be assumed, especially considering the accumulation of ions due to the polarizable electrode [156]. This leads to an electric field component parallel to the electrode surface, as sketched in fig. 3.9b, that depends both on the structure of the defects and that of the sub-membrane space. Representing the sub-membrane space by a constant phase element in series with the resistance of the membrane/defects allows to account for these different situations. For few isolated effects, an exponent α_{sub} of the constant phase element of around 0.5 has been observed, which increases towards $\alpha_{\mathrm{sub}} = 1$ with increasing defect density [25, 157]. The magnitude of Q_{sub} presents a description of the electrical conductivity of the sub-membrane space [39].

Following these considerations, the equivalent circuit shown in fig. 3.9a was used to model the DLP tBLMs in this thesis. R_{sol} describes the solution resistance. Its value is much lower than the resistance of the bilayer and affects the modelling only to a minor degree. The bilayer itself is represented by a constant phase element $\mathrm{CPE}_{\mathrm{mem}}$, representing the non-conductive regions of the bilayer. This quantity includes contributions from the Helmholtz layer at the electrode surface. The heterogeneity of the substrate determines how far the exponent α_{mem} diverges from one. Usually, its values are close enough to one to show

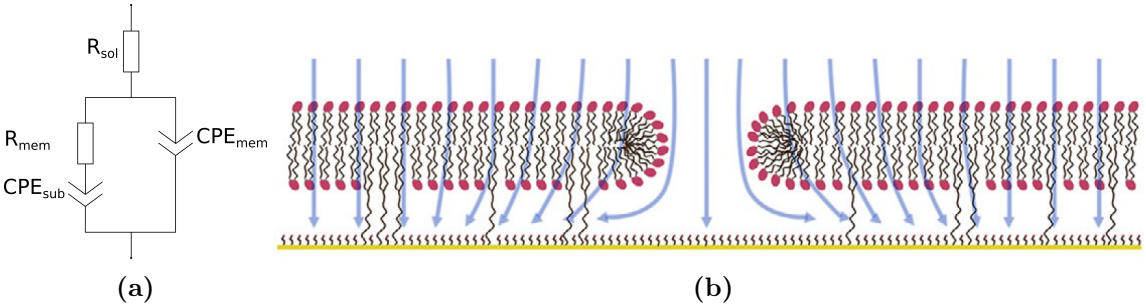

Figure 3.9: a.) Equivalent circuit used for modelling of DLP tBLMs. b.) Sketch of the electric field distribution in a tBLM containing defects [156].

mainly capacitive behaviour, so that it will be referred to as the membrane capacitance in the results chapter 4. Parallel to the constant phase element representing the membrane, a resistor R_{mem} and a constant phase element CPE_{sub} in series model the electric field through membrane defects. The resistor depicts the resistive ion flow through the bilayer while the constant phase element describes the behaviour of the sub-membrane space. Due to the electric field line components parallel to the surface, this constant phase element is not in series with CPE_{mem}. For this equivalent circuit, the individual component impedances add up to:

$$Z_{\mathrm{tBLM}} = Z(R_{\mathrm{sol}}) + \left(\frac{1}{Z(Q_{\mathrm{mem}})} + \frac{1}{Z(R_{\mathrm{mem}}) + Z(Q_{\mathrm{sub}})} \right)^{-1}. \tag{3.27}$$

Taking the impedance definition for different circuit elements given in tab. 3.2 into account this leads to:

$$Z_{\mathrm{tBLM}} = R_{\mathrm{sol}} + \frac{1 + R_{\mathrm{mem}} Q_{\mathrm{sub}} (i\omega)^{\alpha_{\mathrm{sub}}}}{Q_{\mathrm{sub}} (i\omega)^{\alpha_{\mathrm{sub}}} + Q_{\mathrm{mem}} (i\omega)^{\alpha_{\mathrm{mem}}} (1 + R_{\mathrm{mem}} Q_{\mathrm{sub}} (i\omega)^{\alpha_{\mathrm{sub}}})}. \tag{3.28}$$

This model was used in a fitting process to determine the electrophysiological properties of DLP tBLMs. The Ellis2 software extension for Igor Pro was used for this data analysis [158]. Ellis2 applies the differential evolution genetic algorithm that is also used in the Motofit software for NR analysis [140]. Similarly, it offers the advantage of converging towards global minima instead of local minima. While EIS circuits are much less complex than NR models due to the significantly lower amount of parameters, the small solution space means exploration of the whole solution space can be ensured by a fast and robust algorithm. χ^2 was used as the quantity to minimize as a measure for the goodness of the fits.

Ion transport protein activity measurements by EIS

The activity of ion transport proteins can be investigated by electrochemical impedance spectroscopy. Many ion transport proteins cause additional ion transduction across the membrane that behaves electrochemically similar to pores and defects. The equivalent circuit representation for such lipid bilayers with incorporated ion transporter does not

necessarily differ significantly from the equivalent circuit describing tBLMs. Often the protein's activity can simply be modelled as an increase in defect density that is represented by the membrane resistance parameter decreasing in value. To be able to identify the effect of ion transport by a protein, the surrounding membrane must be highly sealing. In a leaky membrane, the effect of the protein on membrane resistance would be on the same order of magnitude as the membrane resistance itself and thus indistinguishable. Different transporters may behave differently in electrical equivalent terms, but mostly resistive property changes have been used and observed (e.g. [9, 22]). Even when results indicated a non-ohmic behaviour of protein activity, the resistor representation was used as an approximation [95]. From the first developments of tBLM systems on, they were proposed for and applied to protein incorporation studies. In the first description of DLP tBLMs, Cornell et al. used them to demonstrate a biosensor concept based on the activity of the incorporated ion channel protein gramicidin, which is known to cause changes in electrophysiological behaviour [7]. Similar studies of gramicidin channels have been conducted on solid-supported bilayers. However, for these bilayers an expansion of the electric equivalent circuit similar to the description of the sub-membrane space was necessary to describe ion channel behaviour [151]. When the activity of an ion transport protein can be described as a change in membrane resistance, protein activity studies often revealed significant membrane resistance changes up to one order of magnitude, showing that this technique is very sensitive to protein activity (e.g. [159, 9]).

Experimental EIS setup

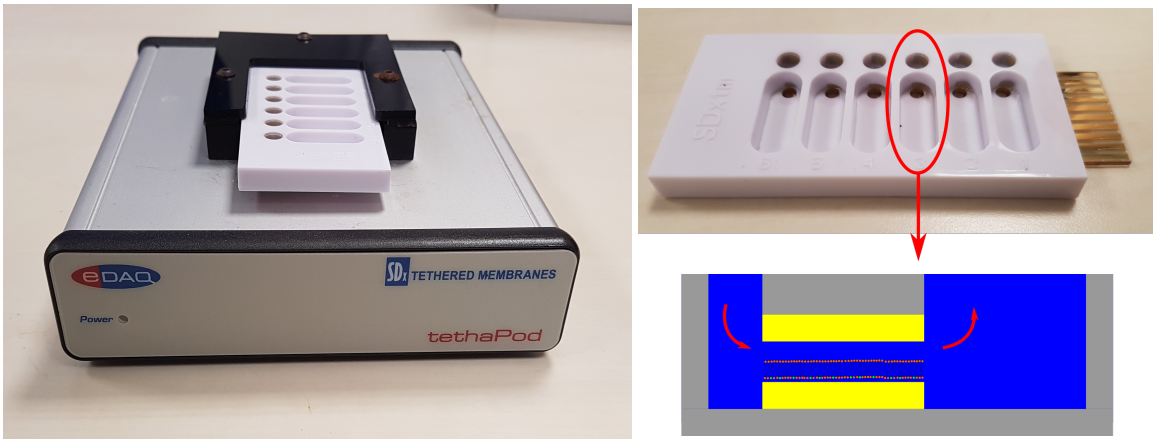

Figure 3.10: The tethaPod EIS instrument and sample cell cartridges.

EIS measurements were performed on a tethaPod instrument by SDx Tethered Membranes (Roseville, Au). Fig. 3.10 shows the instrument and the sample cell system exhibiting a two electrode geometry. The tethaPod allows for six parallel measurements on different channels. A six-well cartridge as shown in fig. 3.10 is used to produce DLP tBLMs via fast solvent exchange. The electrodes are purchased pre-coated with a T10 mixture of DLP tether molecules. In short, for membrane formation a drop of 8 μl lipids in ethanol is added

to the left inlet of the cell, which is rinsed with buffer after two minutes of incubation. This leads to self assembly of the lipids into DLP tBLMs via rapid solvent exchange as described in section 2.3.1. The experiments were conducted under varying conditions. Usually an excitation voltage amplitude of 50 mV was used with a bias potential of 0 V, unless otherwise stated in the description of the specific measurement. Real and imaginary part of the resulting complex signal were recorded for frequency ranges of usually 0.1 Hz to 1200 Hz.

3.3 Quartz crystal microbalance with dissipation monitoring (QCM-D)

QCM-D is an experimental technique that allows quantification of mass adsorbed to a surface with extremely high precision. It exploits the change in frequency that is induced when an additional mass is adsorbed on a crystal that is oscillating close to its resonant frequency. This technique was first employed and theoretically described by Günter Sauerbrey in 1959 [160]. When it was shown that this technique can also be applied in aqueous environments [161], it became an attractive method to investigate biological adsorption processes like protein or polymer adsorption [162, 163], cell adhesion [164], and lipid bilayer formation [41]. By observing additional parameters like the dissipation or resistance of the quartz crystal, information on the viscoelastic properties of the adsorbed mass can be obtained. In case of QCM-D the decay of the crystal oscillation after excitation is used to determine the rigidity of the adsorbed mass.

The crystals used for QCM-D experiments are usually piezoelectric quartz crystals, that can be driven to oscillate by applying an alternating electric signal, which causes shear waves to propagate through the crystal and - at the right frequencies - resonant oscillations. These quartz crystals can be coated with different material according to the experimental requirements. By monitoring the changes in frequency, the adsorbed mass Δm can be deduced according to the Sauerbrey equation:

$$\Delta m = \frac{t_q \rho_q}{f_0} = -\frac{C}{n} \cdot \Delta f, \tag{3.29}$$

where t_q denotes the thickness of the quartz crystal, ρ_q is its density, f_0 is the resonance frequency of the quartz and n the overtone number. The parameters that are constant for a specific crystal can be combined to the sensitivity constant C. For the quartz crystals of a 5 Mhz resonant frequency that were used in the experiments in this thesis, C takes a value of -17.7 Hz ng/cm^2 [165]. The Sauerbrey equation holds true for rigid adsorbed masses, an even distribution of the adsorbed mass on the crystal and a small mass adsorption compared to the crystal mass (or small frequency change compared to resonance frequency). For a homogeneous material of mass m with known density ρ and a covered surface area F the layer thickness can be estimated as $t = m/F\rho$ [160].

Biological mass is often not rigid and contains significant fractions of water. For such materials, the Sauerbrey equation does not hold any more. Measuring the decay of the

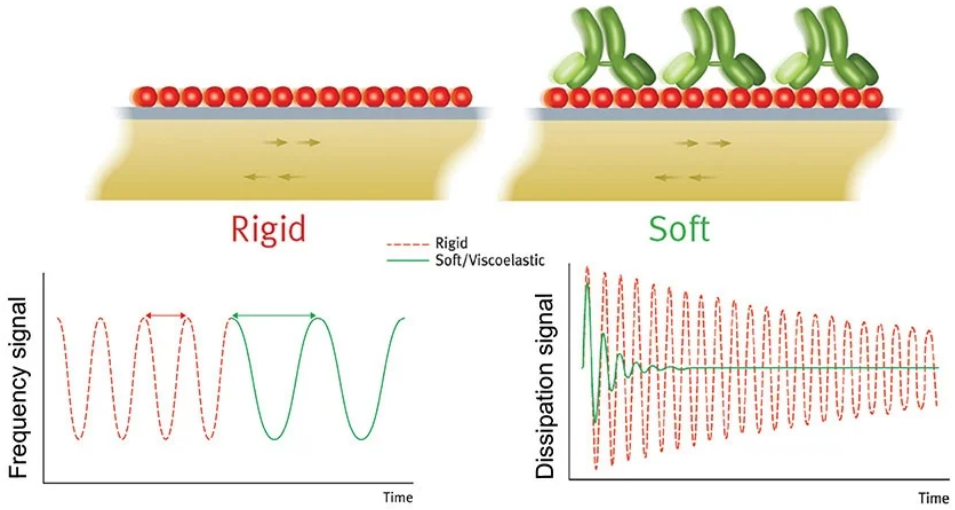

Figure 3.11: Operating principle of the QCM-D technique. Bottom left: Frequency change induced by adsorption of mass onto the QCM crystal. Bottom right: Change in dissipation induced by an adsorbed rigid mass (red curve) compared to a viscoelastic mass (green curve). Taken from www.biolinscientific.com

quartz crystal oscillation when stopping the excitation is a way to determine whether the adsorbed mass shows viscoelastic properties. Since viscoelastic materials cause energy loss due to dissipation, the dampening occurs much faster for soft materials, as sketched in fig.3.11. The oscillation amplitude $A(t)$ decays over a characteristic time τ depending on the properties of the material. The dampening of the sinus functions follows an exponential decay:

$$A(t) = A_0 e^{-t/\tau} \sin(2\pi f t + \alpha). \tag{3.30}$$

Fitting an experimentally recorded decay with such a dampened sinusoidal function allows to obtain the resonant frequency and the so called dissipation factor, a dimensionless parameter D [166]:

$$D = \frac{1}{\pi f \tau} = \frac{E_{\text{Dissipated}}}{2\pi E_{\text{Stored}}}. \tag{3.31}$$

It describes the dissipated energy in relation to the total energy per oscillation. By using Maxwell or Kelvin/Voigt models for viscoelastic solids, precise descriptions of the adsorbed mass can be obtained for soft, water containing materials. Monitoring the dissipation factor changes and frequency changes simultaneously, gives information on mass and viscoelastic properties. By observing multiple harmonics of both the frequency and the dissipation, the sensitivity of the experiments can be further increased. Higher orders are adsorbed faster in the material and thus travel less far, therefore they are more sensitive to material close to the surface.

As it allows to follow the adsorption of vesicles to a surface and their subsequent fusion, QCM-D has been used extensively in the past for formation studies of solid supported bilayers (e.g. [167, 50, 168]). Vesicles, as a structure containing large amounts of water, induce large changes in dissipation, while a lipid bilayer is relatively rigid, which makes the transition from adsorbed vesicles to a planar lipid bilayer easy to follow. For tBLM systems, QCM-D studies are more difficult to exploit due to the often very complex formation processes. Many tether layer formations require aggressive solvents, multiple instruments or take place over time scales which are unrealistic to follow. But QCM-D is still a valuable tool to follow partial processes of tBLM formation. In tBLM systems that rely on vesicle fusion the membrane formation step itself can be observed [90]. For other systems like the DLP tBLMs used in this thesis the tether adsorption to the surface can be characterized. While the use of different solvents during the process prohibits the calculation of direct mass changes between all single steps, differences between preparation steps that were executed in the same solvent can be compared.

The QCM-D instrument used for experiments in this thesis was a QSense Analyzer E4 from Biolin Scientific. It can measure four samples chambers in parallel and is equipped with an IPC 4 channel pump from Ismatec to allow automatic exchange of solvents. The pumping speed was kept at 150 μl/min to prevent disruption of the sample due to solvent turbulences. For bilayer formation by rapid solvent exchange the pumping speed was set to the maximum available speed of roughly 900 μl/min. Heating elements were used to control the sample temperature, which was kept at 21 °C for all experiments in this thesis. Since part of the DLP tBLM formation process has to be carried out in ethanol, samples in which this step was to be investigated had the baseline measured in ethanol to enable determination of the adsorbed mass. Experiments in which the final adsorbed mass of the lipid bilayer was of interest had the baseline measured in buffer solution.

Chapter 4

Results

4.1 DLP tBLMs

4.1.1 Electrophysiological characterization of DLP-tBLMs

EIS provides measurements of the properties of lipid membranes described in terms of electrical circuit components as introduced in section 3.2. To this end, DLP tBLMs with different lipid compositions were investigated by EIS with the main focus being on membranes that contain CL. These experiments serve on one hand to characterize the influence of CL on the structure of tBLMs as compared to the influence of other lipids. On the other hand, these measurements serve as an assay to determine the suitability of tBLMs containing CL for protein incorporation. For this, tBLMs with low defect densities are needed to measure protein-induced ion transport. The corresponding electrophysiological properties of such tBLMs are high membrane resistances (see section 3.2.2). Furthermore, the EIS measurements serve as a pre-selection for subsequent and more extensive NR experiments.

All the results from EIS experiments were obtained using the tethaPod system introduced in section 3.2.2. The tBLMs were formed using the rapid solvent exchange method on a 2.1 mm^2 gold surface pre-coated with a T10 tether layer. All experiments were carried out at room temperature. Either TRIS or HEPES buffer were used. All mentioned lipid ratios are denoted as mol% ratios.
The equivalent circuit introduced in section 3.2.2 was used to model all the data. Solvent resistance was kept fixed, as it plays a minor role in the modelling, because it is several orders of magnitude lower than the membrane resistance. For all experiments, the exponent of the constant phase element representing the lipid bilayer showed values close to one, which means that the behaviour of the tBLM was close to an ideal capacitor.

The tBLMs were comprised predominantly of DOPC. Low amounts of CL and cholesterol were added to assess their effects on the electrophysiological properties of the tBLM. The novelty of these experiments is to compare the effect of CL on the properties of tBLMs to cholesterol. Similar behaviour and effects on bilayer properties have been reported in

literature for both cholesterol and CL. They have been assumed to be positioned below the headgroup region of PC lipids, showing a position of their headgroup near the glycerol-carbonyl region of the other lipids. Both cholesterol and CL have been reported to thicken and stiffen the membrane, thus decreasing its permeability [53, 67].

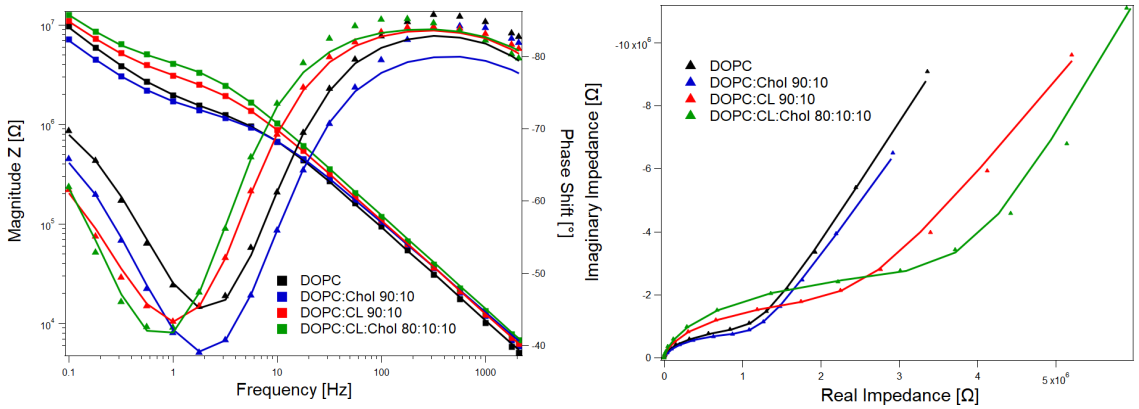

	DOPC	DOPC:Chol 90:10	DOPC:CL 90:10	DOPC:Chol:CL 80:10:10
Q_{mem} [μF/cm^2]	1.2 ± 0.3	1.3 ± 0.3	1.0 ± 0.2	0.9 ± 0.2
α_{mem}	0.94 ± 0.01	0.91 ± 0.01	0.94 ± 0.01	0.94 ± 0.02
R_{mem} [k$\Omega \cdot$ cm^2]	33 ± 6	30 ± 2	65 ± 6	103 ± 28
Q_{sub} [μF/cm^2]	6.7 ± 1.3	9.5 ± 2.0	6.2 ± 1.2	5.6 ± 1.1
α_{sub}	0.83 ± 0.07	0.80 ± 0.03	0.79 ± 0.04	0.85 ± 0.01

Figure 4.1: Results obtained from EIS measurements of DOPC DLP tBLMs with small fractions of CL and/or Chol. Top left: Bode plot, top right: Nyquist plot, bottom: Fit parameters normalized by area of the equivalent circuit used to model the data.

Fig. 4.1 shows EIS curves in Bode and Nyquist representation as well as the corresponding equivalent circuit parameters for DLP tBLMs of different compositions. A general indicator for well-formed bilayers is the frequency value of the minimum in the phase shift in the Bode plots. All the tBLMs showed a minimum around 1 Hz, which is characteristic for these DLP tBLMs [36] with a phase shift value around 40°. Fig. 4.2 summarizes the membrane resistance and capacitance of the bilayers obtained from modelling the data with the equivalent circuit. These values are normalized by the membrane area for better comparability with findings in literature. For the resistance this means multiplication by the area, while the capacitance is divided by the area. As the exponent α is close to one, the constant phase element can be considered as close to a capacitive behaviour, and will be described as such in the following discussion. Starting from a basis of pure DOPC, the membrane showed a resistance of 33 kΩcm^2 and a capacitance of 1.2 μF/cm^2. These values are in accordance with what is reported in literature [77]. A 10 % addition of cholesterol only affected the membrane resistance and capacitance to an extent which is similar to the variation between samples (see further below). 10 % of CL however caused an increase in membrane resistance by 100 %, while the membrane capacitance decreased

only by 20 %, which is comparable to the size of the errors. Combining both CL and cholesterol in an 80 % DOPC 10 % CL and 10 % Chol membrane yielded an even further increased membrane resistance to be threefold that of 100 % DOPC tBLMs. In this case, the membrane capacitance decreased by 33 % compared to the 100 % DOPC sample.

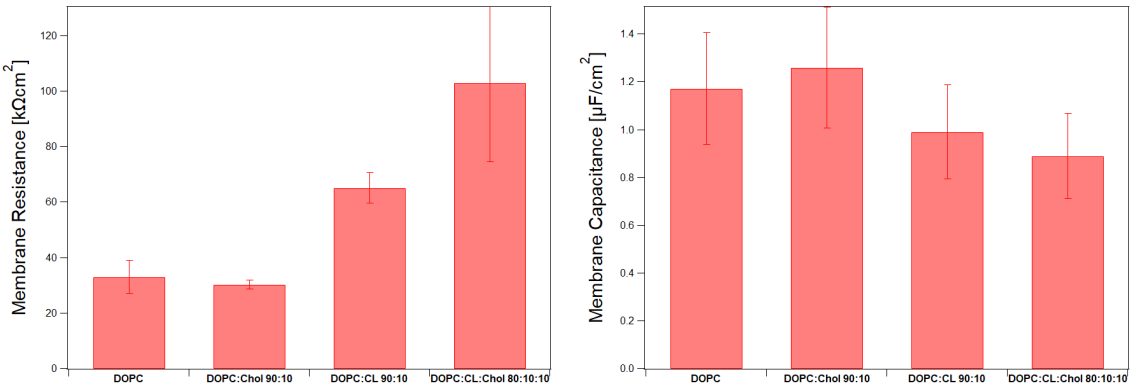

Figure 4.2: Membrane resistance (left) and capacitance (right) of DOPC DLP tBLMs with small fractions of CL and/or Chol.

A low fraction of CL thus had a greater effect on membrane parameters than cholesterol, possibly at least in part due to its higher molecular mass. Chol has a molecular mass of 387 g/mol while CL's molecular mass is around 1400 g/mol (depending on the fatty acid chain distribution). This led to a much higher weight fraction for the CL samples when compared to Chol samples with the same molar ratio. Combining both CL and cholesterol in a membrane increased the membrane resistance more than the simple addition of the separate effects of both (and also more than 20 % of CL alone, as shown below). The capacitance of all mixtures remained in a range that is characteristic for DLP tBLMs. The minor decreases for the tBLMs with CL alone or CL plus cholesterol also suggest a slightly ticker membrane, since the capacitance is inversely related to the hydrophobic thickness of the membrane, however, this increase is not very significant.

Following this intriguing effect of CL, DOPC tBLMs with increasing fractions of CL were investigated. The results of such measurements are shown in fig. 4.3 together with the parameters obtained from modelling the curves with the equivalent circuit method described in 3.2.2. In comparison to pure DOPC membranes, CL contents of 20 %, 50 %, and 80 % were examined. All of the CL concentrations resulted in curve shapes that indicate well-formed tBLMs. The tBLMs that contained 50 % and 80 % CL were tightly sealed, as indicated by a frequency of the minimum in the phase curve around 0.5 Hz. Fig. 4.4 shows the area-normalized membrane resistance and capacitance obtained from the modelling. The tBLMs containing 20 % CL showed a moderate increase in membrane resistance of around 30 %, which is comparable to the 10 % CL sample mentioned previously. The membrane capacitance was not affected. A higher CL content of 50 % caused a drastic increase in membrane resistance to almost 400 % of the DOPC resistance while the membrane capacit-

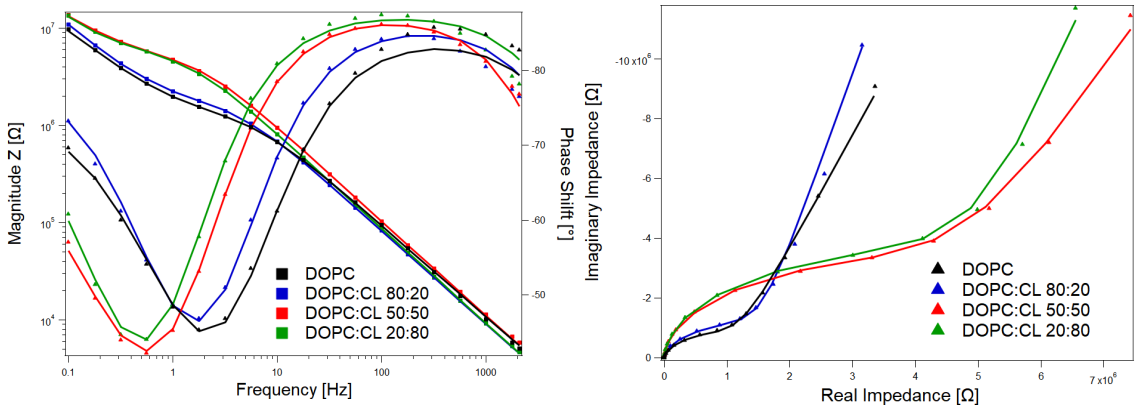

	DOPC	DOPC:CL 80:20	DOPC:CL 50:50	DOPC:CL 20:80
Q_{mem} [μF/cm^2]	1.2 ± 0.2	1.2 ± 0.2	0.9 ± 0.2	1.0 ± 0.2
α_{mem}	0.94 ± 0.01	0.96 ± 0.01	0.97 ± 0.01	0.98 ± 0.02
R_{mem} [k$\Omega \cdot$ cm^2]	33 ± 6	45 ± 10	122 ± 13	137 ± 28
Q_{sub} [μF/cm^2]	6.7 ± 1.3	5.7 ± 1.1	5.6 ± 1.1	5.6 ± 1.1
α_{sub}	0.83 ± 0.07	0.88 ± 0.05	0.80 ± 0.06	0.87 ± 0.07

Figure 4.3: Results obtained from EIS measurements of DLP tBLMs with varying amount of CL. Top left: Bode plot, top right: Nyquist plot, bottom: Fit parameters normalized by area of the equivalent circuit used to model the data.

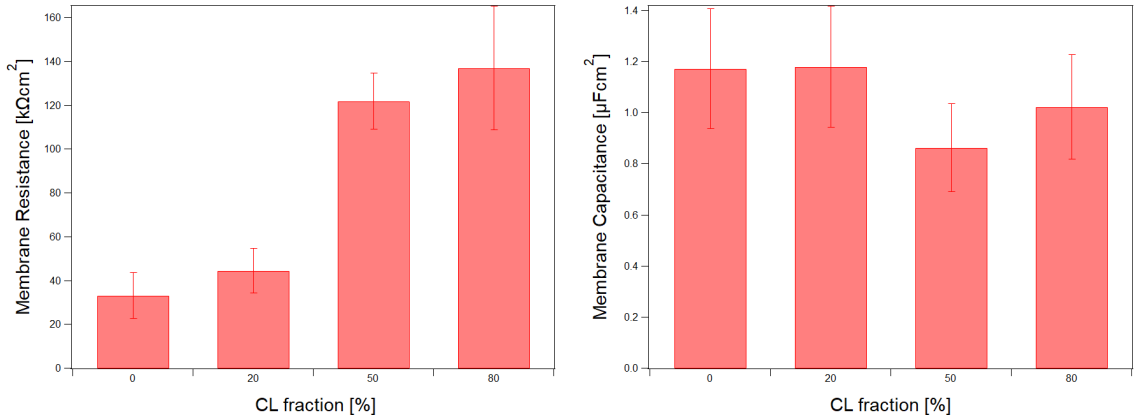

Figure 4.4: Membrane resistance (left) and capacitance (right) of DOPC DLP tBLMs with varying fractions of CL.

ance dropped to ca. 70 %. Increasing the CL concentration to 80 % caused a further small increase in membrane resistance with a capacitance of roughly 80 %. While the smaller differences between 50 % and 80 % CL might still be attributed to variations in sample preparation, the differences between 0 % or 20 % and the higher fractions of CL are striking. It is clearly visible that membranes with large fractions of CL formed tBLMs with

sealing properties much higher than DOPC tBLMs. The membranes with large fractions of CL showed a slightly lower membrane capacitance, which corresponds to an increased hydrophobic membrane thickness. However, these effects are much less pronounced than the changes in membrane resistance.

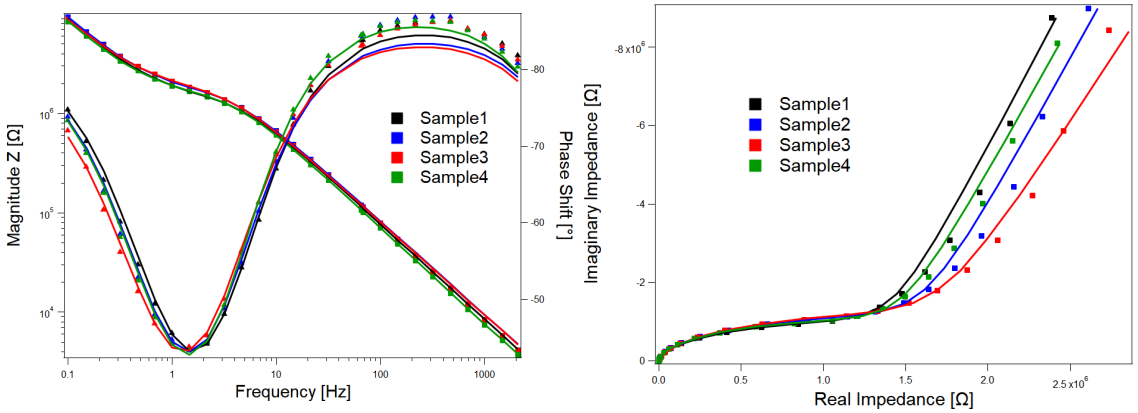

Sample No.	1	2	3	4
Q_{mem} [μF/cm^2]	1.3 ± 0.3	1.3 ± 0.3	1.4 ± 0.3	1.3 ± 0.3
α_{mem}	0.96 ± 0.01	0.95 ± 0.01	0.94 ± 0.01	0.97 ± 0.01
R_{mem} [k$\Omega \cdot$ cm^2]	40 ± 4	45 ± 5	48 ± 6	40 ± 4
Q_{sub} [μF/cm^2]	7.1 ± 1.4	6.8 ± 1.4	7.3 ± 1.5	7.8 ± 1.6
α_{sub}	0.92 ± 0.02	0.91 ± 0.02	0.90 ± 0.02	0.91 ± 0.03

Figure 4.5: Four DOPC:CL 50:50 tBLMs prepared at the same time under the same conditions. Top left: Bode plot, top right: Nyquist plot, bottom: Fit parameters normalized by area of the equivalent circuit used to model the data.

The experiments discussed above indicated bilayer parameter changes due to lipid composition. Lipid bilayer production in general and tBLM production especially are complex processes that can lead to differences in bilayer structure due to small alterations in sample preparation or even statistical variation. To assess the significance of the results presented above and to determine the reproducibility of the rapid solvent exchange protocol for the type of bilayers used here, EIS measurements of four DOPC:CL 50:50 samples prepared in the same conditions were performed and are shown fig. 4.5. Note that these measurements were carried out in a different buffer solution, which leads to different membrane parameters than the DOPC:CL 50:50 sample presented above. The membrane capacitance showed no significant variation between all four samples. The membrane resistance varied by roughly 25 %, which can be considered as a kind of resolution limit for these EIS measurements.

All four samples showed well-formed membranes, indicated by a phase minimum around 1 Hz. However, occasionally there were bilayers not forming correctly when using the fast solvent exchange method. These tBLMs usually exhibited a frequency greater than 10 Hz for the phase minimum, which suggests a very low membrane coverage of the surface. Such samples were discarded in the analysis, as they occur independently of lipid composition.

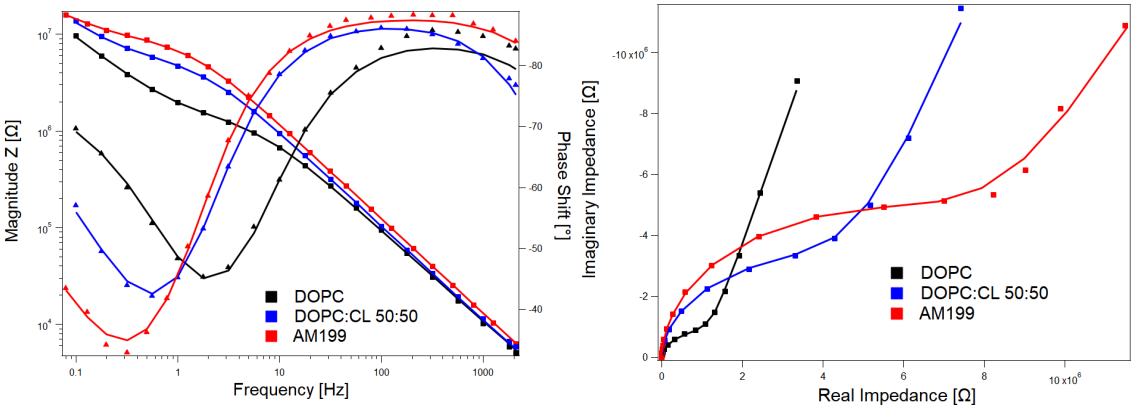

	DOPC	DOPC:CL 50:50	AM199
Q_{mem} [μF/cm^2]	1.2 ± 0.2	0.9 ± 0.2	0.7 ± 0.1
α_{mem}	0.94 ± 0.01	0.97 ± 0.01	0.98 ± 0.01
R_{mem} [k$\Omega \cdot$ cm^2]	33 ± 6	122 ± 13	186 ± 3
Q_{sub} [μF/cm^2]	6.7 ± 1.3	5.6 ± 1.1	6.8 ± 1.4
α_{sub}	0.83 ± 0.07	0.80 ± 0.06	0.73 ± 0.01

Figure 4.6: AM199 membrane compared to a DOPC and DOPC:CL 50:50 membrane. Top left: Bode plot, top right: Nyquist plot, bottom: Fit parameters normalized by area of the equivalent circuit used to model the data.

Many of the tBLM systems used in literature make use of lipids with phytanyl chains since these form highly covering bilayers. This thesis focussed on more biologically relevant lipid compositions, and it is important to compare the results obtained here to DLP tBLMs containing phytanyl lipids. Fig. 4.6 shows EIS measurements of an AM199 lipid composition compared to the DOPC and DOPC:CL 50:50 compositions discussed above. AM199 is a 70 mol%:30 mol% mixture of DPEPC and GDPE which has been used frequently in conjunction with DLP tethers [8]. The frequency at the phase minimum is always well below 1 Hz for AM199 tBLMs, which is confirmed by the measurement of around 0.5 Hz shown in the Bode plot in fig. 4.6. Although the membrane capacitance was only slightly decreased when compared with a DOPC:CL 50:50 tBLM, the membrane resistance was much higher for AM199. DOPC:CL 50:50 already showed a difference of almost 300 % in membrane resistance when compared to DOPC, and AM199 showed an even higher resistance of roughly 600 % compared to the resistance of DOPC.

Summary

It has been demonstrated that DOPC DLP tBLMs with high fractions of CL can be formed using the rapid solvent exchange method. They have electrophysiological properties comparable to other phospholipid tBLMs, but show much higher membrane resistances. Although cholesterol is similar to CL in terms of its effect on membrane structure, cholesterol has less impact on the electrophysiological parameters of the membrane. This could be in part due to the molecular mass difference between cholesterol and CL. Interestingly, a

combined CL:Chol membrane had a resistance comparable to a tBLM with 50 % of CL. As cholesterol is known to have detrimental effects on bilayers at larger fractions, higher cholesterol content has not been further investigated. To keep the model membrane systems as simple as possible, ternary mixtures with larger fractions of both CL and cholesterol were also not studied, despite showing interesting properties. All investigated mixtures showed membrane resistances that were still far below those found for phytanyl chains containing tBLMs. Although this can be a limitation for protein incorporation studies, the similarity of those mixtures to biological phospholipid membranes provides a more physiologically relevant environment.

The variation between different samples of the same composition was relatively large, so that small differences in properties, such as those observed between samples with 0 % and 10 % of CL or cholesterol, have to be considered with appropriate reservations. The characteristics of the sub-membrane space were not discussed for the different samples, since the model equivalent circuit is not very sensitive to it. Furthermore, the sub-membrane space is not assumed to change significantly with lipid composition.

4.1.2 Nanostructural characterization of DLP tBLMs containing CL

As introduced before, lipid bilayers containing CL show interesting properties. CL-protein interaction can remarkably affect the structure-function relationship between lipid bilayer and protein due to CL's unique structure and properties. It is therefore important to investigate more stable tBLM systems composed of CL, as they can be an attractive platform for protein incorporation studies. I hereafter present a series of NR experiments to characterize the nanostructure of tBLMs with different CL content. Previous EIS measurements were used to drive the research and identification of promising lipid mixtures that were subsequently studied with the more complex NR technique. The individual measurements will be presented below, followed by a short summary.

DOPC is widely used to form planar membranes due to its cylindrical shape and lipid bilayers composed of this lipid are well characterized. It is natural to choose DOPC bilayers as a reference so that any deviation from it can be ascribed to the contribution of CL. With this in mind, we investigated the nanostructure of DOPC tBLMs with increasing amounts of CL (10 %, 50 % and 80 %). Since all relative compositions are denoted in molar percent, the actual volume representation of CL in a resulting bilayer is significantly higher because CL's area per molecule is almost twice a big as the one of DOPC. In addition to varying CL content, NR experiments with different concentration of tether molecules were performed, as this parameter in conjunction with the lipid composition is the major structural contributions to bilayer properties.

All experiments were performed at 21°C, a temperature at which both DOPC and CL are in the fluid phase. The CL used here consisted mainly of linoleic acid chains and other polyunsaturated fatty acids, so that the degree of unsaturation of all the resulting bilayers is relatively high. Hence, we assume the tBLMs of a mixture of DOPC and CL to be in the fluid phase as well

In the analysis of the NR data, all DLP tBLMs were modelled as a series of successive slabs. A minimum of 5 slabs was needed to represent the tBLM as described in detail in section 3.1.4. In addition, two or three extra slabs were used to model the sapphire or silicon substrates respectively. Sapphire substrates were represented by a layer of titanium and a gold layer on top, while silicon substrates required a silicon oxide layer below the titanium layer. These substrates were always measured and modelled separately, and the resulting parameters were used to constrain the parameters in the analysis of the tBLM measurements. For the substrate analysis, the SLD of the titanium layer was allowed to vary towards higher negative values. This accounts for hydrogen inclusion which will inevitably occur in the coating process [143]. While the substrates contributed strongly to the overall reflectivity signal, reflectivity curves of bare substrates and substrates with tBLMs were still sufficiently different to justify meaningful interpretation of the scattering data. Fig. 4.7 shows an exemplary NR curve of a DLP tBLM on a gold surface compared to the signal of the bare substrate.

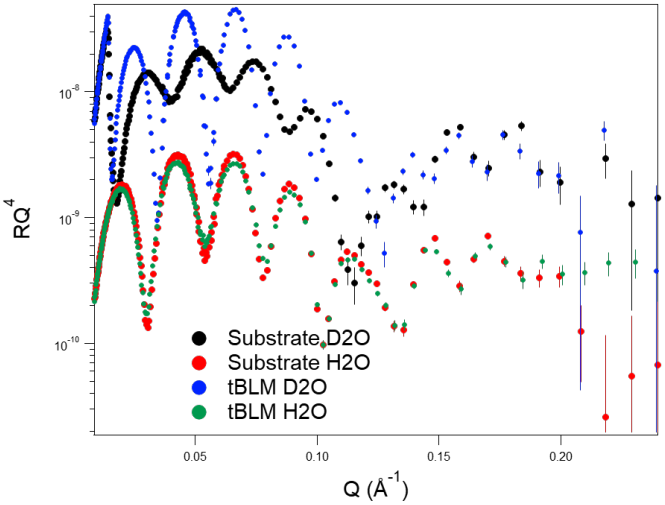

Figure 4.7: NR curves of a bare, gold coated silicon substrate compared to the same substrate after formation of a DLP tBLM.

The model representation for the tBLMs specifically consisted of one layer representing the sub-membrane space, the inner headgroup of the lipid bilayer, two layers for the two chain regions of inner and outer leaflet and finally the outer headgroup layer. The choice of representing the sub-membrane space as one layer was made following the conception that the PEG part is flexible and can span the sub-membrane space homogeneously. Introducing an additional layer to model this region did not increase the fit quality. The benzyl disulfide group can not be distinguished from the gold or PEG layers - especially at high roughness - because its SLD value lies in between the values of gold and PEG and was thus not modelled as a separate slab as well.

The SLD of the inner headgroups were allowed to vary as an unknown fraction of tethering molecules inserts into the bilayer. PEG has an SLD value of 0.6 $\cdot 10^{-6}$ Å^{-2}, which causes a

decrease in the headgroup SLD when present at significant concentration. The parameters corresponding to the lipid chains of the two leaflets (thickness, SLD, and water content) were linked since it is reasonable to assume that the water is distributed approximately evenly in the chain regions of the bilayer.

The solvent content in the inner chain region can serve as a rough estimation of the membrane coverage, since a perfect membrane would not contain any water molecules in the hydrophobic tails of the lipids. Solvent molecules in the chain region can be the result of small and diffuse imperfections within the bilayer. However, the modelled water content in the chain region generally overestimates the real amount of water in the inner chain region (i.e. it underestimates the coverage), since by using a slab model, a rough surface is approximated by a slab. Roughness and undulation of the lipid membrane lead to partial overlapping in the same slab of the chain regions and the neighbouring layers which contain a larger fraction of solvent. Therefore, some water molecules belonging to adjacent (and more hydrated) slabs might be counted as hydration of the tails. This is especially the case for tBLMs, because the tether layer induces a slightly higher roughness when compared to SLBs. The membrane roughness can also be affected by extended regions where no membrane is present. Given the large surface area of the samples used in NR (5 x 8 cm^2), this can sometimes be observed. These cases require the use of a mixed area model for data analysis. Further details on the data analysis process are described in section 3.1.4.

Hereafter the following notation to identify the studied samples will be used:

$$\text{lipid}_1 : \text{lipid}_2 \; mf_1 : mf_2 \; tr, \tag{4.1}$$

where lipid_1 and lipid_2 refer to the used lipids with mf_1 and mf_2 denoting their respective mole percentage in the sample. The molar fraction of tethering molecules to spacers is given by tr and in this work it will be T10 and T40 to denote a mole percentage of 10:90 and 40:60 respectively.

DOPC:CL 90:10 T40

Fig. 4.8 shows the reflectivity and SLD curves obtained from the best fits of a NR measurement of a tBLM prepared from a 90:10 mol%:mol% mixture of DOPC and CL on a T40 tether layer on a gold coated sapphire substrate. The model parameters are shown in the table below the graphs. Like most samples it was measured in four different contrasts. The measurements were performed on the reflectometer D17. The tBLM was produced by first coating the substrate with a tether layer through immersion in an ethanol solution containing the tethers for one hour, followed by bilayer formation using the rapid solvent exchange method 2.3.1. Measurements were carried out in the standard buffer of 10 mM HEPES with 150 mM KCl present at a physiological pH of 7.4.

The sample was modelled as described above, i.e. four slabs describing the lipid bilayer on top of the PEG layer that is tethered to the substrate. This sample showed a coverage of 80 % in the inner leaflet. The apparent larger difference in SLD in the chain regions between the different contrasts is influenced by the roughness of the tBLM system as described

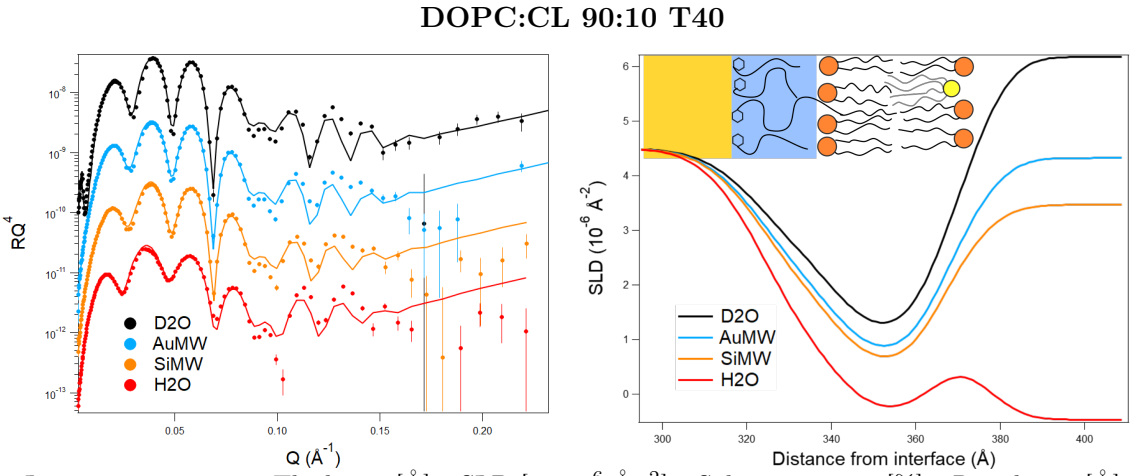

Layer	Thickness [Å]	SLD [$\times 10^{-6}$ Å^{-2}]	Solvent content [%]	Roughness [Å]
Titanium	66 ± 1	-2.4 ± 0.1	0	16 ± 1
Gold	259 ± 1	4.5	0	14 ± 1
Tethers	12 ± 2	0.6	27 ± 10	12 ± 2
Inner Headgroup	5 ± 2	0.8 ± 1.0	25 ± 20	7 ± 3
Inner chain region	12 ± 1	-0.3	22 ± 4	7 ± 3
Outer chain region	12 ± 1	-0.3	22 ± 4	7 ± 3
Outer Headgroup	11 ± 3	2.0 ± 0.8	45 ± 15	7 ± 3

Figure 4.8: NR measurement of a DOPC:CL 90:10 T40 membrane on gold coated sapphire. Top left: Neutron reflectivity curve, top right: The corresponding SLD profile, bottom: Structural parameters obtained from the NR curves.

above. A single area model was sufficient to describe the reflectivity profile, indicating that no macroscopical defects were present in the membrane.

The sub-membrane space, consisting of the PEG part of the tether molecules and solvent, had a thickness of 12±2 Å and contained 27±10 % of solvent, which supplies the expected ion reservoir. This conflicts with the assumption of earlier publications that estimated the sub-membrane space to be roughly 40 Åthick [76]. In these publications the PEG molecules were assumed to be relatively extended. However as PEG molecules form a flexible chain it is more likely that they coil and form a sub-membrane space much thinner than their molecular length. The low thickness of the tether layer shown here supports this assumption and is in agreement with previous results found from our group [79].

The analysis showed that the inner headgroup had a thickness of around 5±2 Å, which is within the range found in literature [169]. Interestingly, the SLD of the inner headgroup was lower than normally expected for lipids such as DOPC or CL and closer to the value expected for PEG. This suggests that a large proportion of the slab representing the inner headgroup in the model was actually composed of PEG. This is not surprising, considering that the tether molecules were present on a significant fraction of the surface and that the

approximately 35 Å long PEG chains were confined in a sub-membrane region as thin as 12±2 Å.

The chain regions of the tBLM are visibly compressed with respect to analogue lipid bilayer systems, as the analysis showed a thickness of around 12±1 Å per chain compared with ticker 14-15 Å found in literature for similar lipids [169] or similar tethers [80].

The outer headgroup was relatively thick compared to the inner headgroup layer and lay over the range observed in literature for this parameter [68]. At the same time the outer headgroup layer showed a SLD only slightly above the value of DOPC, compatible with the presence of CL in a fraction of 10 %. CL is known to position below the headgroups of PC lipids [67]. A headgroup region of DOPC with small fractions of CL should thus show a thicker headgroup thickness due to the offset of the two lipid heads.

DOPC:CL 50:50 T40

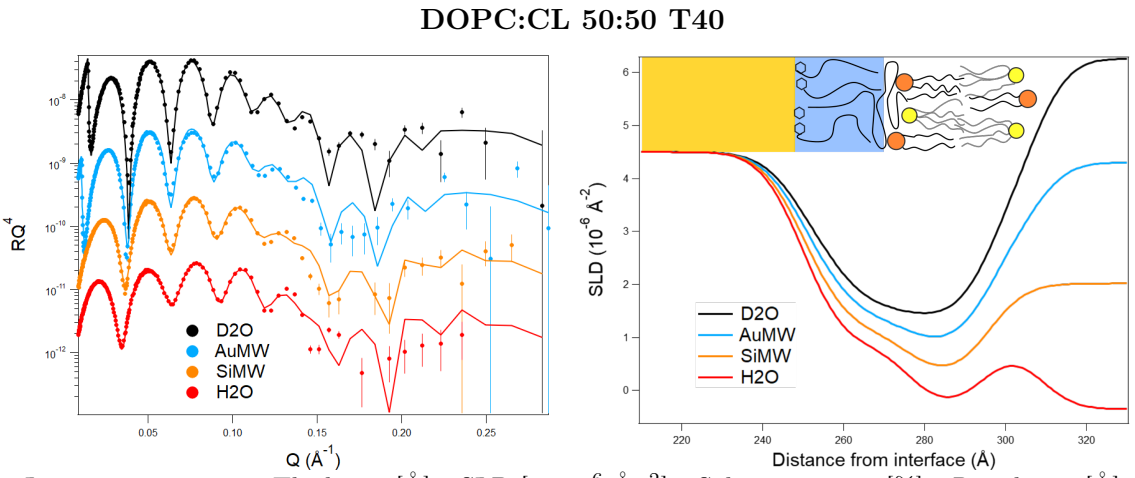

Layer	Thickness [Å]	SLD [$\times 10^{-6}$ Å^{-2}]	Solvent content [%]	Roughness [Å]
SiO_2	9 ± 2	3.47	0	3 ± 3
Titanium	38 ± 1	-2.0 ± 0.1	0	8 ± 1
Gold	204 ± 1	4.5	0	5 ± 1
Tethers	10 ± 1	0.6	25 ± 10	9 ± 2
Inner Headgroup	15 ± 1	1.0 ± 0.3	10 ± 4	7 ± 1
Inner chain region	10 ± 1	-0.3	26 ± 4	7 ± 1
Outer chain region	10 ± 1	-0.3	26 ± 4	7 ± 1
Outer Headgroup	12 ± 2	1.9 ± 0.5	41 ± 9	7 ± 1

Figure 4.9: NR measurements of a DOPC:CL 50:50 T40 membrane on gold coated silicon. Top left: Neutron reflectivity curves, top right: The corresponding SLD profiles, bottom: Structural parameters obtained from the NR curves.

Fig. 4.9 shows a DOPC:CL 50:50 tBLM on a gold coated silicon substrate. The deposition procedure followed the same principles as before by first coating the substrate using an ethanol mixture of 40:60 tether:lateral spacer molecules for one hour, followed by bilayer

formation via rapid solvent exchange. Standard HEPES buffer solution at pH 7.4 at 21°C was used and the sample was characterized in four different contrasts on D17.

The same model as described above was used to fit the data, with the addition of a native silicon oxide layer which is always present on silicon substrates. All samples described in the following were formed on silicon substrates and include an extra layer corresponding to the native SiO_2 layer in the model. A single area model was enough to appropriately fit the data, suggesting the absence of macroscopical defects in the lipid membrane. The resulting tBLM showed a coverage of around 75 % which is comparable to the sample containing only 10 % CL that was described above. The thickness and hydration of the sub-membrane space of this sample were consistent with the previous case. The chain regions were only 10±1 Å thick which confirms that this is a general tendency for this DLP tBLM system with CL content. The most significant feature of this sample was the thickness associated with the inner headgroup region of around 15±1 Å thickness with a SLD of just $1\pm0.3 \cdot 10^{-6}$ $Å^{-2}$. This thickness was far outside the limits expected for this kind of lipids and, as in the previous sample, it suggests the presence of PEG within the inner headgroup layer in view of the SLD value close to that of PEG. The sample with lower CL content did not show this thick inner headgroup layer, as did a similar DPN tBLM without CL (see sec 4.2.1), thus CL's specific structure may induce this feature. The low solvent content in this region suggests that this structure is densely packed, which prevents hydration of the layer. The outer headgroup was expanded as well, however to a much lower extent. This expanded headgroup could still be explained by the offset in lipid headgroup position between DOPC and CL that was described above. The SLD of $1.9\pm0.5\cdot10^{-6}$ $Å^{-2}$, which was again close to the DOPC SLD, confirms that.

DOPC:CL 20:80 T40

Fig. 4.10 shows a DOPC tBLM containing 80 mol% CL on a gold coated silicon substrate. The deposition procedure followed the same protocols as described before. Likewise, the sample was characterized at four different contrasts at the reflectometer D17. All measurements were carried out at 21°C, at a pH of 7.4 and in 10 mM HEPES buffer containing 150 mM KCl.

The same model as applied to the previous samples was used here. This is interesting, as it shows, that DLP tBLMs can be formed with a lipid composition where cardiolipin predominates, and still show a similar structure to tBLMs with lower CL content.

Similar to the other CL mixtures, this sample showed 70 % coverage of the substrate with a similar sub-membrane space structure. The latter showed consistent features between different samples.

The region that overlaps with the inner headgroup confirmed and even reinforced the trend observed in the DOPC:CL 50:50 T40 sample. The parameter resulting from the fit converged to a slab thicker than that observed in the previous sample with comparable SLD and hydration. The trend suggests that the increasing portion of CL promotes some sort of crowding of the PEG chains into the headgroups, accompanied by the expulsion of water

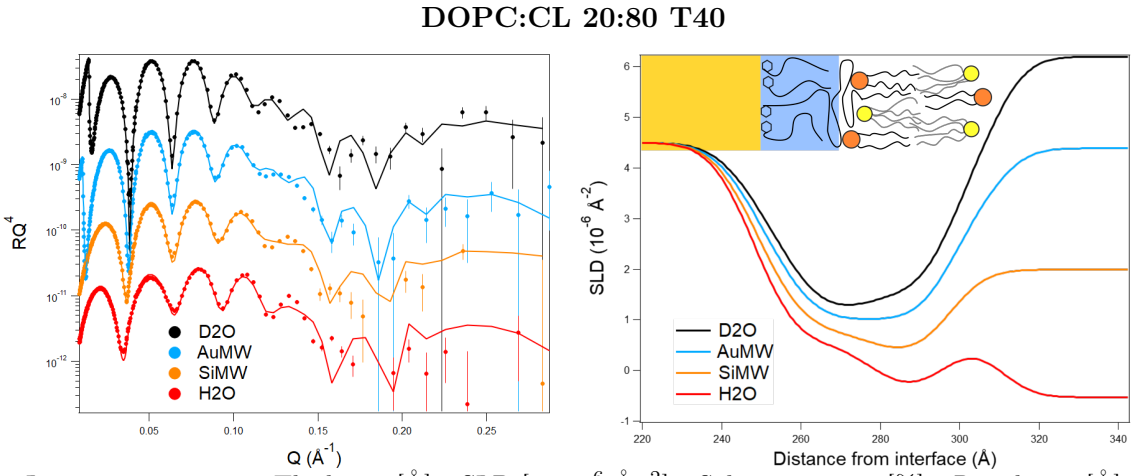

Layer	Thickness [Å]	SLD [$\times 10^{-6}$ Å^{-2}]	Solvent content [%]	Roughness [Å]
SiO_2	9 ± 2	3.47	0	3 ± 3
Titanium	38 ± 1	-2.0 ± 0.1	0	8 ± 1
Gold	201 ± 1	4.5	0	5 ± 1
Tethers	10 ± 1	0.6	28 ±7	9 ± 2
Inner Headgroup	19 ±1	0.6 ± 0.2	10 ± 7	7 ± 1
Inner chain region	10 ± 1	-0.3	28 ± 4	7 ± 1
Outer chain region	10 ± 1	-0.3	28 ± 4	7 ± 1
Outer Headgroup	12 ± 2	1.9 ± 0.4	50 ± 8	7 ± 1

Figure 4.10: NR measurements of a DOPC:CL 20:80 T40 membrane on gold coated silicon. Top left: Neutron reflectivity curves, top right: The corresponding SLD profiles, bottom: Structural parameters obtained from the NR curves.

molecules, which renders the headgroup region less hydrated compared to, for example, a supported or floating lipid bilayer. As in the previous sample, the chain regions were compressed to a thickness of 10±1 Å. The outer headgroup thickness and SLD values of 12±2 Å and 1.9±0.4 $\cdot 10^{-6}$ Å^{-2} respectively show the offset location of DOPC and CL again.

DLP tBLMs with a tether percentage of 10 % with respect to the lateral spacer molecules (T10) were investigated at different CL concentrations to identify whether the surface density of tethers influences their structure significantly. Two CL concentrations were measured with T10 type tethers, DOPC:CL 90:10 which is shown in fig.4.11 and DOPC:CL 50:50, shown in fig. 4.12. These experiments serve on one hand to further characterize the effect of CL content in tBLMs, on the other hand to study the effect of the surface density of tethering molecules on tBLM structure. In general, the density of tethers can affect the freedom of a membrane to fluctuate, its stability, the hydration and the available space in the sub-membrane space. All these features can in turn affect the ability to incorporate a membrane protein and its functionality.

DOPC:CL 90:10 T10

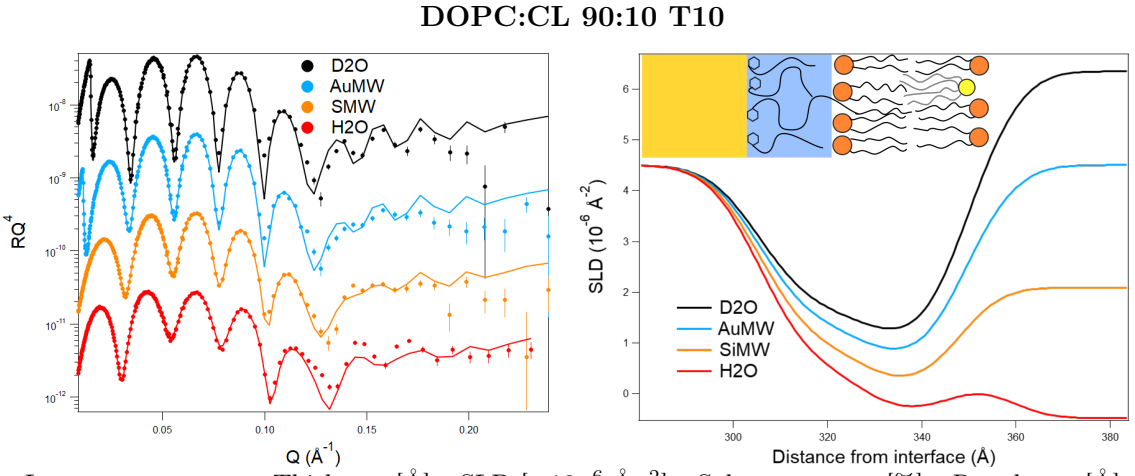

Layer	Thickness [Å]	SLD [$\times 10^{-6}$ Å^{-2}]	Solvent content [%]	Roughness [Å]
SiO_2	16 ± 2	3.47	0	12 ± 2
Titanium	52 ± 1	-2.5 ± 0.1	0	12 ± 1
Gold	239 ± 1	4.5	0	8 ± 1
Tethers	15 ± 1	0.6	17 ± 3	9 ± 1
Inner Headgroup	6 ± 1	0.8 ± 0.4	16 ± 10	7 ± 1
Inner chain region	11 ± 1	-0.3	22 ± 2	7 ± 1
Outer chain region	11 ± 1	-0.3	22 ± 2	7 ± 1
Outer Headgroup	9 ± 2	1.9 ± 0.5	64 ± 7	7 ± 1

Figure 4.11: NR measurements of a DOPC:CL 90:10 T10 membrane on gold coated silicon. Top left: Neutron reflectivity curves, top right: The corresponding SLD profiles, bottom: Structural parameters obtained from the NR curves.

Fig. 4.11 shows the DOPC:CL 90:10 sample with a T10 tether concentration. Sample production was identical to the samples shown before, followed by characterization at four different contrasts on D17. The pH was at a physiological level of 7.4, the temperature was kept at 21°C and the used buffer was 10 mM HEPES with 150 mM salt. T10 samples could be modelled with the same slab model as the T40 samples.

In general this tBLM showed very similar features to the T40 samples shown before. A single area model was used to describe the membrane which covers 80 % of the surface. The thickness of the chain regions of 11±1 Å was similar to what was observed for all other DLP tBLMs. Despite the lower tether fraction on the surface the water content in the sub-membrane space remained at a relatively low level of 17±3 % with a layer thickness of 15±1 Å. This challenges the original design idea that - besides influencing the properties of the inner leaflet less - a lower density of tethering molecules should cause an increase of the sub-membrane space hydration. The inner headgroup shows a thickness of 6±1 Å, which is in accordance to the thickness observed in the DOPC:CL 90:10 T40 sample and with data from literature [169]. Interestingly, even in this case the SLD of this layer converged

to a low value of 0.8±0.4 $\cdot 10^{-6}$ Å^{-2} (i.e. close to the SLD of PEG), comparable to what was observed in the DOPC:CL 90:10 T40 sample. Intuitively, we would have expected this effect to be less pronounced due to the presence of less tethering molecules. Therefore we argue that, similar to what we observed for the T40 samples, a significant amount of PEG is present in the slab representing the inner headgroup. Clearly, more factors than the pure tether concentration in the tether solution used for surface coating play a role in determining the amount of tethers actually inserting into the membrane, or alternatively the amount of PEG in the proximity of the inner headgroup layer does not depend significantly on this parameter. Effectively, as the full length of the tether molecules is much larger than the sub-membrane space, the limited available space can result in a significant presence of coiled PEG chains even for a significantly lower concentration of tethering molecules. Another possibility is that the presence of tether molecules on the surface is higher than expected. In the preparation process the actual concentration of tethers on the surface is not known, only what mixture was used to create it. Indeed, the larger tether molecules might adsorb preferentially to the surface due to stronger van der Waals forces [81]. Thus, even at T10 tether concentration enough tether molecules may be present to occupy a large fraction of the inner headgroup. Furthermore, even if the ratio of tether molecules to lateral spacer molecules on the surface matches that of the solution used in the production process, the coverage may vary due to parameters not controllable in the tether layer deposition process, which may lead to less dependence on the original tether/lateral spacer ratio. Finally, this sample also shows an outer headgroup region which is slightly thicker than comparable SLBs, but to a smaller extent than the T40 samples. This large thickness of the headgroup can also be explained with the offset arrangement of the CL and DOPC heads.

DOPC:CL 50:50 T10

Fig. 4.12 shows a DOPC:CL 50:50 tBLM with a tether density of 10 %. The preparation followed the same protocol as the other samples, while for time reasons this sample has only been characterized at three different contrasts on D17. The experimental conditions were 21°C, a pH of 7.4 and a buffer solution of 10 mM HEPES and 150 mM salt.

Data modelling performed with a single area model resulted in a coverage of 85 %, similar to all other samples. The sub-membrane space was 11±1 Å thick, but shows a higher hydration of 35±9 %. While this supports the idea that a high concentration of lateral spacer molecules increases the water content of the sub-membrane space, the DOPC:CL 90:10 sample showed a lower water content at the same tether concentration. Therefore, this deviation is probably a statistical effect.

Coherent to what was observed observed in the T40 sample of similar composition, the slab describing the inner headgroup region showed a high thickness of 18±2 Å accompanied by an SLD value close to that of PEG. This indicates a significant presence of PEG chains in proximity or within the inner lipid headgroups. Similarly, the outer headgroup layer showed a high thickness which is probably caused by the offset arrangement of the CL and DOPC headgroups.

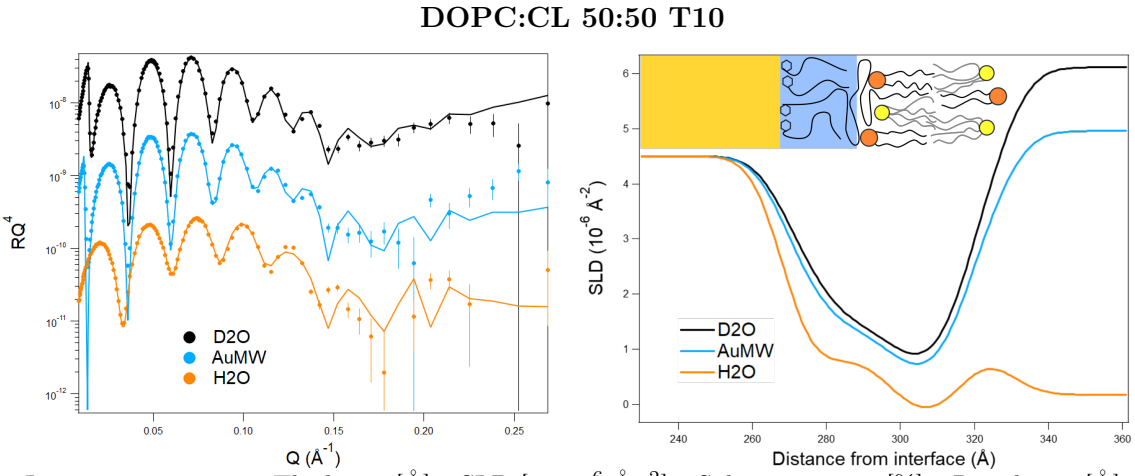

Layer	Thickness [Å]	SLD [$\times 10^{-6}$ Å^{-2}]	Solvent content [%]	Roughness [Å]
SiO_2	15 ± 3	3.47	0	8.9 ± 5
Titanium	37 ± 1	-2.3 ± 0.1	0	9 ± 1
Gold	217 ± 1	4.5	0	7 ± 1
Tethers	11 ± 1	0.6	36 ± 9	7 ± 3
Inner Headgroup	18 ±2	0.9 ± 0.2	10 ± 7	9 ± 2
Inner chain region	10 ± 1	-0.3	16 ± 4	9 ± 2
Outer chain region	10 ± 1	-0.3	16 ± 4	9 ± 2
Outer Headgroup	11 ± 2	1.9 ± 0.6	45 ± 10	9 ± 2

Figure 4.12: NR measurements of a DOPC:CL 50:50 T10 membrane on gold coated silicon. Top left: Neutron reflectivity curves, top right: The corresponding SLD profiles, bottom: Structural parameters obtained from the NR curves.

4.1.3 NhaA incorporation into DLP tBLMs

NR was used to detect and quantify changes in the tBLM following the exposure to the membrane protein NhaA. By appropriate modelling of the reflectivity profile, the effect on the tBLM structure could be probed and the amount of protein incorporated quantified. NhaA incorporation was carried out using the liposome assisted protein incorporation method described in section 2.6.2, in which the protein is first transferred to liposomes which are then introduced to the sample cell together with a low concentration of DDM detergent to induce fusion with the bilayer. After incubation for 30 minutes this caused partial transfer of the protein from the liposomes to the tBLM. Left over unbound liposomes and detergent were flushed out of the chamber with buffer.

Fig. 4.13 shows the NR curves before and after NhaA incorporation for the DOPC:CL 50:50 T40 tBLM described in the previous section 4.1.2. The incorporation process caused visible changes in the reflectivity curves, which will be discussed below.

Data modelling was carried out according to the procedure described in section 3.1.4. In short, the protein was represented as a replacement of a fraction of the lipid bilayer volume

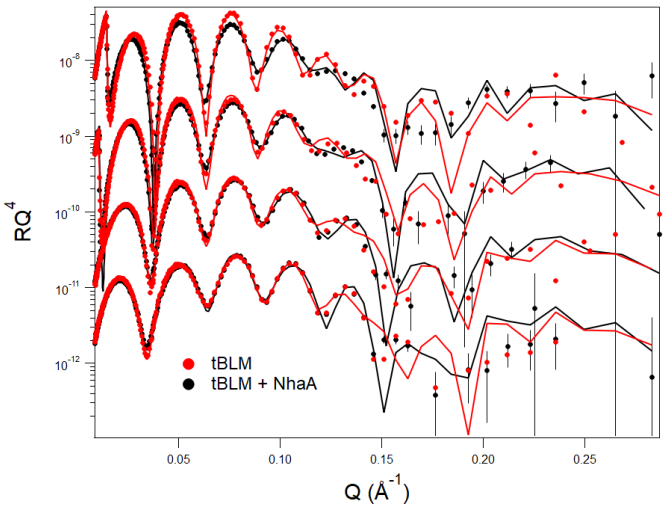

Figure 4.13: NR curves of a DOPC:CL 50:50 DLP tBLM before (black) and after (red) NhaA incorporation.

with an SLD corresponding to the protein. This fraction was forced to be the same in all bilayer slabs, as the NhaA protein shape was roughly approximated as a cylinder. While some protrusions out of the bilayer are expected for parts of the protein, these are assumed to be included in the headgroup layer. The substrate parameters were allowed to vary slightly within the errors determined in the characterization of the tBLM before protein incorporation. Otherwise the tBLM structure was allowed to vary to observe changes induced by protein incorporation.

Fig. 4.14 shows the NR curves with the best fits resulting from the analysis and the corresponding SLD profiles. In the lower part of the figure the model parameters used to obtain these fits are listed. Another way to visualize the results is to translate the SLD profiles obtained at different contrasts to a plot that reports the volume fraction of each component as a function of the z coordinate perpendicular to the interface before and after the protein incorporation. This is plotted in fig. 4.15, along with a comparison of relevant model parameters.

The tBLM with incorporated NhaA showed significant changes in the bilayer properties. First of all, a drastic change in the SLD of the tail regions was noted that passed from a negative value of -0.3$\times 10^{-6}$ Å^{-2} to a value of 1.2$\pm$0.1 $\times 10^{-6}$ Å^{-2}. Having a negative value, the SLD of this region is a very sensitive indicator of protein incorporation, since, depending on the solvent contrast, the SLD of NhaA ranges between 1.6 and 2.75 $\times 10^{-6}$ Å^{-2}. In other words, the tail region has a high contrast with respect to the protein. From our analysis, an incorporation of NhaA that amounts to 49$\pm$5 % of the bilayer volume was observed. In this process the inner headgroup headgroup layer, which before NhaA incorporation showed a high thickness of 15$\pm$1 Å, decreased significantly in thickness to a value of 4$\pm$2 Å. The chain regions on the other hand expanded from 10$\pm$1 Å to 19$\pm$1 Å, while loosing a large

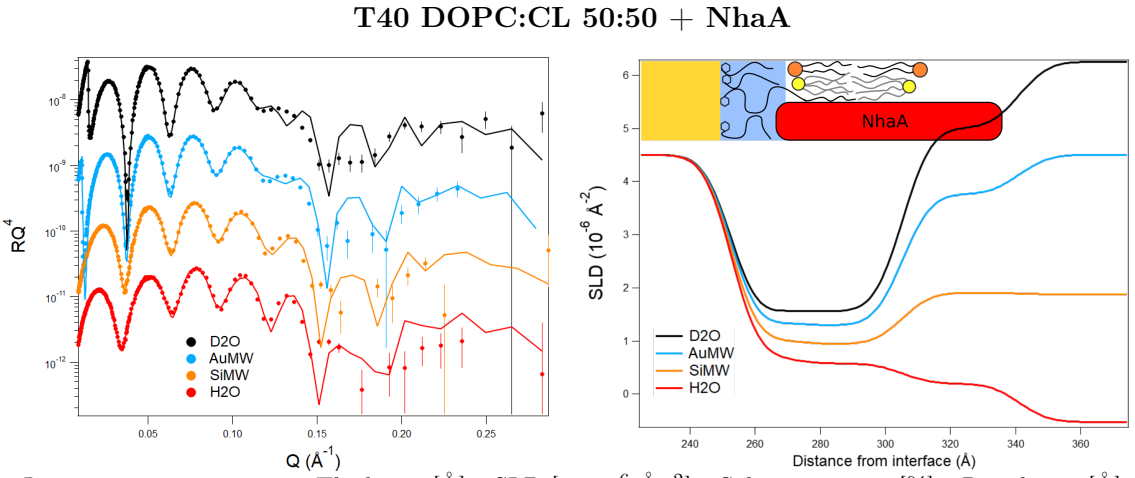

Layer	Thickness [Å]	SLD [$\times 10^{-6}$ Å^{-2}]	Solvent content [%]	Roughness [Å]
SiO_2	10 ± 3	3.47	0	4 ± 5
Titanium	39 ± 1	-2.0 ± 0.1	0	7 ± 1
Gold	204 ± 1	4.5	0	5 ± 1
Tethers	11 ± 2	0.6	10 ± 9	7 ± 2
Inner Headgroup	4 ± 2	1.7 ± 1.2	5 ± 20	7 ± 1
Inner chain region	19 ± 1	1.2 ± 0.1	7 ± 5	7 ± 1
Outer chain region	19 ± 1	1.2 ± 0.1	7 ± 5	7 ± 1
Outer Headgroup	36 ± 5	2.3 ± 1.1	68 ± 5	7 ± 1
Volume fraction protein	0.49 ± 0.05			

Figure 4.14: NR measurements of a DOPC:CL 50:50 T40 membrane with incorporated NhaA on gold coated silicon. Top left: Neutron reflectivity curves, top right: The corresponding SLD profiles, bottom: Structural parameters obtained from the NR curves.

fraction of their solvent content. The outer headgroup showed a similarly strong expansion from 12±2 Å to 36±5 Å, while its solvent content increased from 41±9 % to 68±5 %. These striking changes may be interpreted as follows. The expansion of the chain regions is an expected change, as the thickness of the protein across the membrane of 5 nm is higher than the tBLM thickness. Hence, the overall bilayer thickness increases to accommodate the thicker protein. During the incorporation process the protein may have replaced some lipids of the tBLM but also used the space provided by existing defects in the membrane. Either way, the lower solvent content in the chain regions after the protein incorporation suggests that the incorporation was accompanied by a net reparation effect on the bilayer. This is plausible also in view of the fact that the protein transfer from the liposomes could include transfer of lipids from the liposome to the bilayer, that may fill pre-existing defects in the bilayer. The inner headgroups decrease in thickness may be an effect directly related to the properties of CL DLP tBLMs. When uncoupled from the proteins SLD, this layers SLD value is still very close to the PEG SLD. Thus this layer may be mainly composed of protein and tether molecules with only a minor presence of lipids in general and CL specifically. It was assumed that the presence of CL is the cause of the formation of this

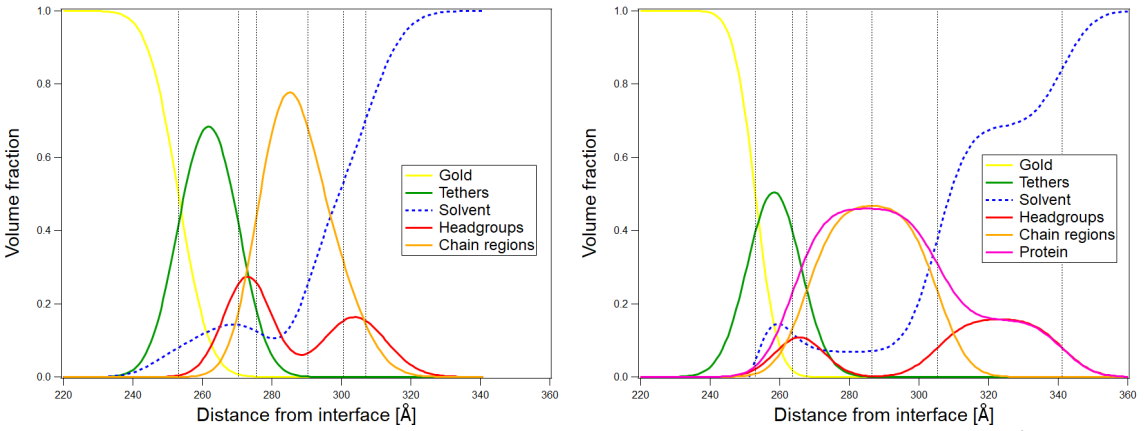

	tBLM			tBLM + NhaA		
	Thickness [Å]	SLD [10^{-6} Å^{-2}]	Solvent [%]	Thickness [Å]	SLD 10^{-6} Å^{-2}	Solvent [%]
Tethers	10± 1	0.6	25 ±10	11 ±2	0.6	10 ±9
Inner headgroup	15 ±1	1.0±0.3	10 ±4	4 ±2	1.7±1.2	5 ± 20
Inner chain region	10 ±1	-0.3	26 ±4	19 ±1	1.2±0.1	7 ±5
Outer chain region	10 ±1	-0.3	26 ±4	19 ±1	1.2±0.1	7 ±5
Outer headgroup	12 ±2	1.9±0.5	41 ±9	36 ±5	2.3±1.1	68 ±5
Volume fraction protein		0			0.49 ± 0.05	

Figure 4.15: Volume fraction distribution of the different system components of a pure DOPC:CL 50:50 DLP tBLM (top left) and the same sample after NhaA incorporation. The table shows a comparison of the fit parameters with and without NhaA.

thick unstructured inner headgroup layer. A decrease of total CL content in this layer should thus lead to a thinner headgroup layer structure, like observed for tBLMs without CL content. The decrease in solvent content of the sub-membrane space may show the movement of PEG that was accumulated below or in the inner headgroup towards a more homogeneous distribution in the sub-membrane space. Sub-structures of the protein which protrude out of the bilayer will also add to this observed lower solvent content. NhaA shows structural loops that protrude from the membrane on the cytoplasmic side. Orientation of NhaA is not controlled in the experiments, so that these groups can protrude from both sides of the tBLM. In addition to the naturally protruding sub-structures of NhaA, the histidine-tag, which remains from protein purification, is a feature that is assumed to protrude from the membrane or lay on top of the bilayer surface. These two components are assumed to cause the extremely thick outer headgroup layer as well. The increased headgroup solvent content supports the assumption, that this layer is partly composed of protein parts protruding out of the membrane with solvent in between. Modelling this as an additional slab did not increase the fit quality significantly, so the layer of lipid headgroups, protein and sub-structures protruding from the membrane with solvent in between is most likely unstructured.

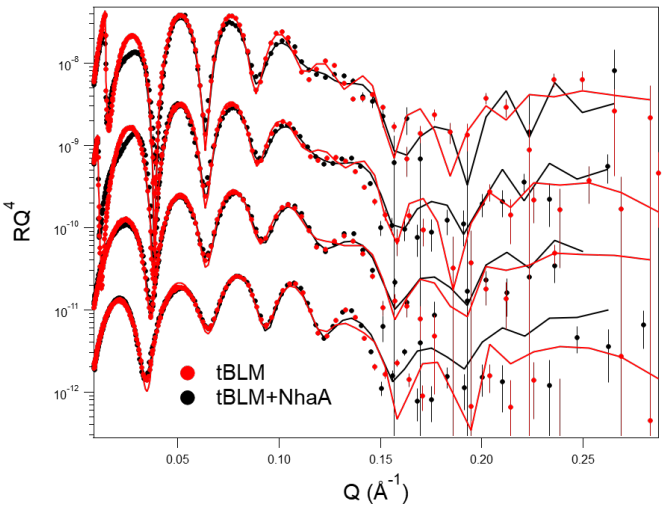

Figure 4.16: NR curves of a DOPC:CL 20:80 DLP tBLM before (black) and after (red) NhaA incorporation.

Fig. 4.16 shows NR curves with best fits of a DOPC:CL 20:80 DLP tBLM before and after NhaA incorporation. Fig. 4.17 shows details of the NR curves with best fits and the corresponding SLD profiles for the tBLM with incorporated NhaA as well as a comparison of the bilayer parameters before and after NhaA incorporation. The protein was incorporated following the same procedure as the previous sample and the same model for protein incorporation was used for data analysis. Likewise, the corresponding pure tBLM structure was described in detail in section 4.1.2 (see fig. 4.10). This sample showed the same tendencies in reflectivity curve shape change upon protein incorporation, but in addition featured an unusual signal in the low q range below 0.03 $Å^{-1}$. This almost linear region in the reflectivity curves of the D2O and AuMW contrasts was attributed to instrumental issues. Thus, the fitting process was only carried out in the q range from 0.03 $Å^{-1}$ to 0.3 $Å^{-1}$. The resulting characterization can therefore only serve as a rough estimation.

In general, the structural changes indicated by the best fits are very similar to the previously described sample. The tether layer shows a decrease in solvent content. The inner headgroup thickness decreases from 19±1 Å to 6±3 Å while the chain regions expand from 10±1 Å to 15±4 Å. Solvent content in this chain region is reduced significantly. Finally, the outer headgroup expands from 12±2 Å to 21±9 Å with a constant solvent content of 50 %. A NhaA volume fraction of 50±5 % was obtained from the analysis. As all changes mirror the changes observed for the DOPC:CL 50:50 tBLM it can be assumed that this interpretation is correct. This shows that NhaA can be incorporated into tBLMs with CL fractions as high as 80 %. Structural changes induced by this incorporation appear to be coherent for different samples.

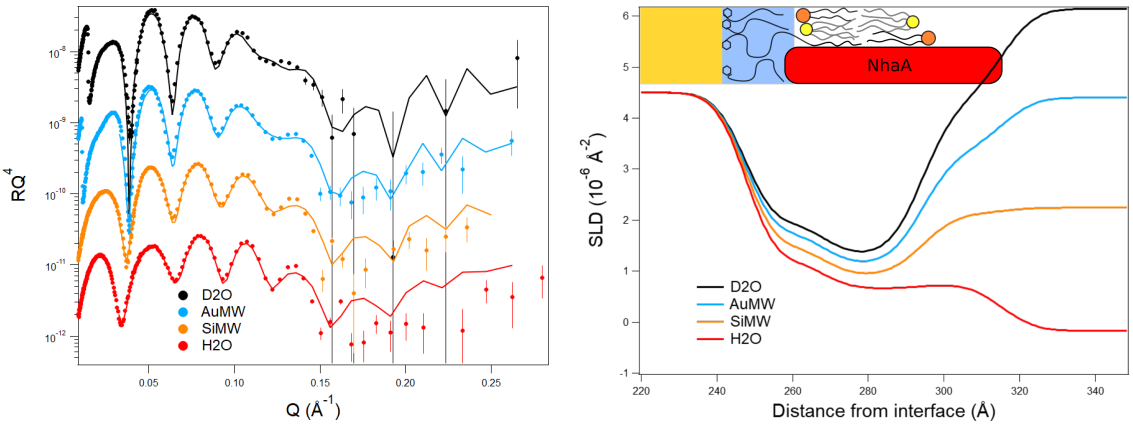

	tBLM			tBLM + NhaA		
	Thickness [Å]	SLD [10^{-6} Å^{-2}]	Solvent [%]	Thickness [Å]	SLD 10^{-6} Å^{-2}	Solvent [%]
Tethers	10±1	0.6	28±7	10±5	0.6	12±14
Inner headgroup	19±1	0.6±0.2	10±7	6±3	2.6±0.5	5±30
Inner chain region	10±1	-0.3	28±4	15±4	1.2±0.3	2±13
Outer chain region	10±1	-0.3	28±4	15±4	1.2±0.3	2±13
Outer headgroup	12±2	1.9±0.4	50±8	21±9	2.3±0.9	52±20
Volume fraction protein		0			0.50 ± 0.05	

Figure 4.17: NR measurements of a DOPC:CL 20:80 T40 membrane with incorporated NhaA on gold coated silicon. Top left: Neutron reflectivity curves, top right: The corresponding SLD profiles. The table shows a comparison of the fit parameters compared to the parameters of the same tBLM before protein incorporation.

4.1.4 Summary

Gold adsorbed tBLMs containing different amounts of CL and different ratios of tether molecules to lateral spacer molecules were studied with NR to elucidate several fundamental aspects of their nanostructure. Tables 4.1 and 4.2 show a comparison of membrane parameters for these two series.

All investigated membranes showed no macroscopic defects, since a single area model could be used to fit the reflectivity profiles. If the solvent content of the chain regions is used to estimate the coverage, all membranes showed a relatively high coverage around 80 %. As explained at the beginning if this section, the modelling can overestimate the amount of water molecules in the chain region due to roughness and undulation of the membrane.

The sub-membrane space layer of all investigated samples was between 10 and 15 Å thick and showed a low solvent content between 15 % and 35 %. Notably, the general thickness of the sub-membrane space was lower compared to the value estimated by the Cornell group, who assumed it to be approximately 4 nm thick [76]. A partial explanation for this discrepancy may be the benzyl disulfide group, which can not be distinguished from

DOPC:CL ratio	90:10		50:50		20:80	
	Thickness [Å]	Solvent [%]	Thickness [Å]	Solvent [%]	Thickness [Å]	Solvent [%]
Tethers	12 ± 2	27 ± 10	10 ± 1	25 ± 10	10 ± 1	28 ± 7
Inner headgroup	5 ± 2	25 ± 20	15 ± 1	10 ± 4	19 ± 1	10 ± 7
Inner chain region	12 ± 1	22 ± 4	10 ± 1	25 ± 4	10 ± 1	28 ± 4
Outer chain region	12 ± 1	22 ± 4	10 ± 1	25 ± 4	10 ± 1	28 ± 4
Outer headgroup	11 ± 3	45 ± 15	12 ± 2	40 ± 9	12 ± 2	50 ± 8

Table 4.1: Membrane parameters for DOPC:CL tBLMs with a tether concentration of 40%.

DOPC:CL ratio	90:10		50:50	
	Thickness [Å]	Solvent [%]	Thickness [Å]	Solvent [%]
Tethers	15 ± 1	17 ± 3	11 ± 1	36 ± 9
Inner headgroup	6 ± 1	16 ± 10	18 ± 2	10 ± 7
Inner chain region	11 ± 1	22 ± 2	10 ± 1	16 ± 4
Outer chain region	11 ± 1	22 ± 2	10 ± 1	16 ± 4
Outer headgroup	9 ± 2	63 ± 7	11 ± 2	45 ± 10

Table 4.2: Membrane parameters for DOPC:CL tBLMs with a tether concentration of 10%.

the neighbouring layers. The SLD of the benzyl disulfide group is in between the SLD of $4.5{\cdot}10^{-6}$ Å^{-2} of gold and the SLD of $0.6{\cdot}10^{-6}$ Å^{-2} of PEG. Thus, this layer may be accounted for in our fits as part of the gold layer as a roughness effect. Keeping that in mind, the actual tether layer may be thicker than our defined "tether" slab. However, the diameter of benzene is only around 2.5 Å. As this structure is the major contribution to the benzyl disulfide volume, this group is unlikely to occupy a layer of more than 5 Å thickness. Even considering this contribution, the value obtained in our analysis is thinner compared to the value estimated by the Cornell group. The low hydration of the sub-membrane region and the fact that part of the PEG chains are crowded in the proximity of or within the inner headgroup, suggest that the PEG chains are not in their more extended conformation.

The tether to lateral spacer ratio did not have a large influence on the thickness and water content of the sub-membrane space, at least in the range investigated in this study (10 % and 40 % molar percent ratio). This does not confirm the assumption, that a larger fraction of lateral spacer molecules leads to a higher hydration of the sub-membrane space. While the highest water content was observed in a T10 sample, the variation between different samples was higher than the differences between tether concentration. This was observed at high and low CL content, suggesting that this feature is not caused by the presence of CL. As a matter of fact, the generally low water content in the sub-membrane space is in agreement with what was found on tBLMs that used the same tethering system and

different lipids [79, 80]. Despite PEG being hydrophilic, tBLMs with short PEG spacers can show very low hydration, down to only 5 % [29]. On the other hand, longer PEG spacers than the 11 monomer chain that was used here can lead to higher water content [33].

The structure of the inner headgroup of the lipid bilayers was significantly affected by the presence of CL. The slab that represents this region in the model was characterized by: (i) a SLD value significantly lower than that of the lipid heads that composed the bilayer, (ii) a thickness that increased with the molar ratio of CL and (iii) a water content lower than what is expected for the headgroup regions of lipid bilayers. This behaviour was observed for both tether to lateral spacer ratios T40 and T10. In particular, both samples containing only 10 % CL had an inner headgroup thickness comparable to DOPC SLBs and a SLD lower than that of the DOPC and CL lipid heads. For higher CL content (50 % and 80 %) the lower SLD of the inner headgroup region was accompanied by a significant increase in its thickness. This trend suggests that CL promoted crowding of the PEG chains of the tether molecules in the proximity and/or within the inner headgroups. As a matter of fact, the presence of PEG would reduce the SLD of the slab, increase its thickness and reduce the hydration by physically expelling water molecules. The low solvent content in the neighbouring sub-membrane space, which could be described as a hydrogel-like structure, may further limit hydration of this layer. This would be in accordance with the decreased capacitance observed in the EIS measurements, shown in section 4.1.1 for tBLMs with high CL content. The capacitance is inversely related to the bilayer thickness. As the overall thickness of tBLMs with high CL fractions increases due to the presence of the thick inner headgroup layer with low solvent content, a decreased capacitance could be expected.

A second prominent property, which all the investigated samples share, is the thin chain region. This feature seems to be independent of tether concentration but is observable whenever CL is present. Since previous experiments on the same tBLM system with different lipids (DMPC [79, 80]) and literature results of CL in vesicle shaped lipid bilayers [68, 67] did not show any thinning of the chain region, we argue that it is connected to the presence of CL within this particular tBLM system. A compressed chain region has been reported before by Cranfield et al. [36] for this tether system with a completely tethered inner leaflet and outer leaflet composed of phytanyl chains containing DPEPC. This might support the idea that this feature is partially induced by the tether architecture. It may be caused for example by extension of the phytanyl chains of the tether molecules into the outer leaflet, which causes a general overlapping of chain regions. The unordered arrangement of lipid heads in the inner headgroup supports this, because following the assumed presence of coiled PEG in this layer, space would be freed in the inner chain region, which may be partly filled with overlapping chains from the outer leaflet.

The outer headgroups seem generally swollen to a differing degree, when compared to SLBs of similar composition. A slight influence of CL concentration can be observed, as samples with 50 % or 80 % CL showed a thicker outer headgroup by 1-2 Å. However, this may well be within the range of statistical variation. Boscia et al. [67] report the position of CL headgroups in a PC bilayer to be slightly below the PC headgroups, similar to cholesterol.

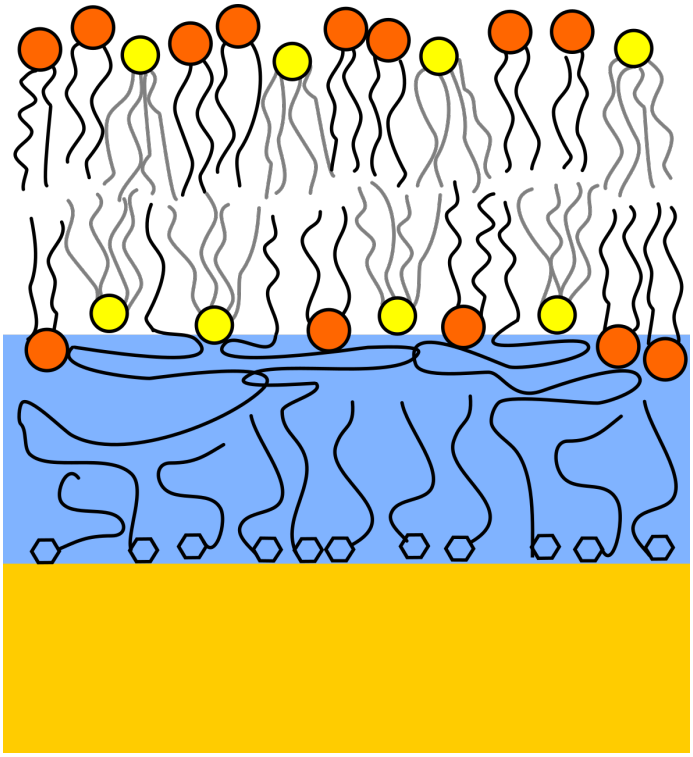

Figure 4.18: Sketch of the structure of DLP tBLMs containing large fractions of CL. Yellow lipids depict CL while orange lipids represent DOPC.

Such a shifted structure could result in a perceived higher headgroup thickness which is already present at low fractions of CL and increases with higher CL content. It would also explain an overlapping of chain regions from outer and inner leaflet. A generally less ordered structure of the outer bilayer leaflet could also contribute to these expanded headgroups. Fig. 4.18 shows a sketch that illustrates the structure of DLP tBLMs with high CL content as interpreted from the NR characterization.

Large fractions of 50 % of NhaA protein could be incorporated into DLP tBLMs that consisted largely of CL. The incorporation left the tBLM structure intact and caused some interesting changes in the dimensions. Generally the tBLMs lipid chain region expanded, likely due to hydrophobic mismatch between the tBLM and the protein. In addition, protein substructures protruding from the bilayer increased the overall bilayer thickness. The solvent content in the chain regions decreased, which is in agreement with the assumption, that liposome incorporation can have a repairing effect on bilayers by supplying additional lipids. Most curiously the thickness of the inner head group layer decreased drastically, which suggests that the PEG, that had accumulated around the inner headgroups, was removed. As a large portion of the tBLM structure was composed of NhaA, the effect of CL, which is assumed to cause this accumulation, may be diminished.

4.1.5 EIS of DLP-tBLMs with incorporated NhaA

NR measurements provided strong evidence that NhaA can be incorporated into DLP tBLMs at high fractions of up to 50 %. To determine whether the protein retains its activity when incorporated into DLP tBLMs, a series of EIS experiments were performed. The NhaA protein has been incorporated into tBLMs of different composition and under varying experimental conditions, for measurements of the electrophysiological behaviour using EIS. EIS can measure the activity of the NhaA protein since its function is to provide electrogenic membrane transport of two H^+ ions in exchange for one Na^+ ion. This electrogenic transport will decrease the membrane resistance as described in more detail in section 3.2.2. The membrane resistance describes the ohmic ion flow through small defects in the membrane. Ion transport by proteins causes an additional ion flow, thus the total ion flow across the membrane is increased which leads to a lower total membrane resistance. These experiments were carried out using the same tethaPod system that was used for the characterization of the tBLMs previously described in this chapter. As all these experiments mainly have an effect on the membrane resistance while other parameters of the equivalent circuit remain constant, the following results will only show the changes in membrane resistance.

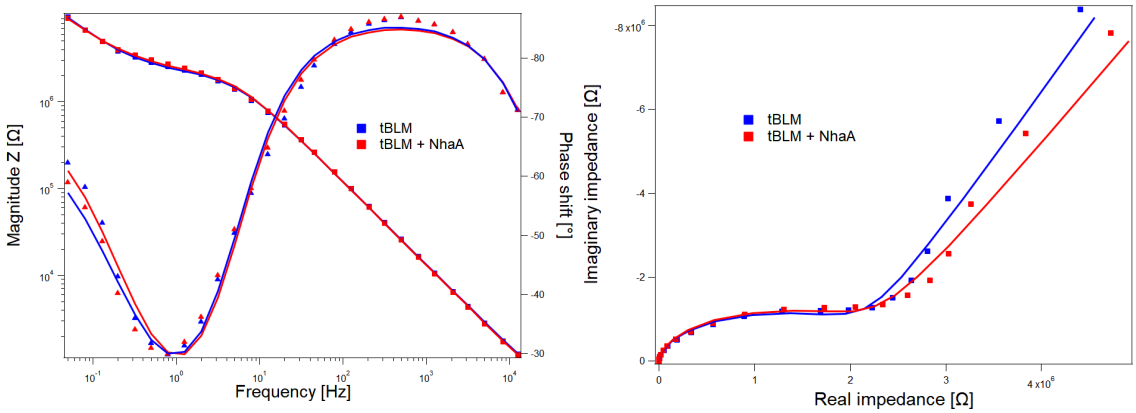

	tBLM	tBLM + NhaA
Q_{mem} [μF/cm^2]	0.8 ±0.2	0.8±0.2
α_{mem}	0.96±0.1	0.96±0.1
R_{mem} [k$\Omega \cdot$ cm^2]	48.2±9.6	50±10
Q_{sub} [μF/cm^2]	13.6±2.7	13.8±2.8
α_{sub}	0.80±0.08	0.77±0.08

Figure 4.19: AM199 tBLM before and after NhaA incorporation. Top left: Bode plot, top right: Nyquist plot, bottom: Fit parameters normalized by area of the equivalent circuit used to model the data.

Fig. 4.19 shows a typical EIS measurement of a tBLM before (blue curves) and after NhaA incorporation (red curves), including Bode and Nyquist plots as well as the parameters obtained from modelling the equivalent circuit. In this case detergent mediated incorpor-

ation was used with an approximated NhaA concentration of 50 μg/ml. After 30 minutes of incubation in the sample cell the unbound NhaA and detergent in the solution were rinsed out of the cell. The sample shows generally very little variation due to the protein incorporation process. Changes in membrane resistance or capacitance are on the same order as changes induced by exchanging the solvent alone. For some samples the membrane resistance decreased due to the incorporation process, however no correlation between this decrease and specific experiment parameters could be found. In general, this conforms with the process of protein replacing part of the bilayer without significantly damaging its structure. Additionally the observation that this whole process does not cause large changes to the bilayer properties serves as an indicator that the presence of low fractions of detergent does not damage the membrane.

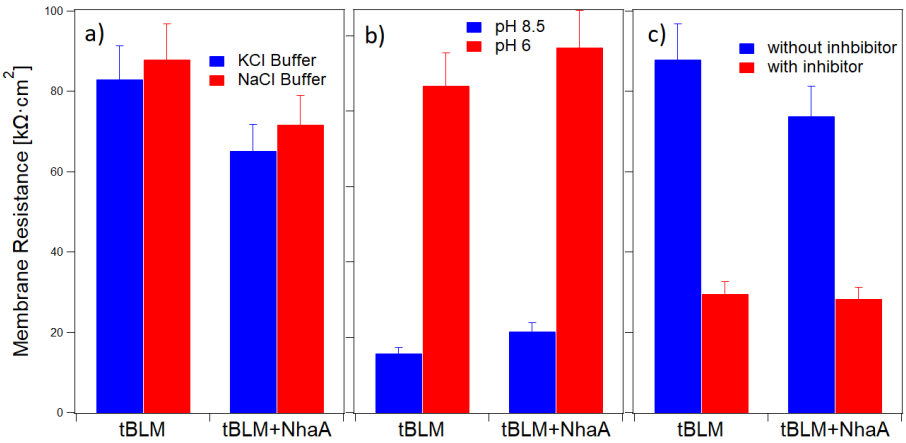

Figure 4.20: Effect of different experimental parameters on the area normalized membrane resistance of tBLMs with and without incorporated NhaA. The tBLMs were composed of AM199.

The activity of the incorporated NhaA was investigated by comparing the behaviour of tBLMs without protein to tBLMs with incorporated NhaA. For those experiments the superfusing solution for the tBLMs was varied by the composition of the ions, the pH or by the presence of an inhibiting compound. Fig. 4.20 shows a selection of measurements that should indicate whether the protein is in an active state or not.
In panel (a) the membrane resistance in the presence of different ions is shown. NhaA is an antiporter that transports preferentially sodium ions (lithium ions to a lesser extent). A solution containing only potassium ions thus prohibits NhaA activity. The membrane resistance for tBLMs with and without incorporated NhaA was compared between buffer solutions containing either a certain concentration of NaCl (red bars) or the same concentration of KCl (blue bars). For a tBLM without NhaA the membrane resistance increases slightly by usually around 5 % to 10 % when switching from KCl buffer to NaCl buffer while keeping constant all other experimental parameters (e.g. pH and temperature). This is most likely caused by structural changes in the sample system induced by different ion types which lead to different ion permeability. Sodium ions are expected to locate prefer-

entially in the headgroup region and this way decrease membrane penetration [170]. When repeating the same experiment for tBLMs with incorporated NhaA, a similar relative increase by 5 % to 10 % in membrane resistance was observed. The incorporation of an active electrogenic protein would be expected to reduce significantly the membrane resistance. Note that the overall membrane resistance of this tBLM + NhaA sample is lower than for the pure tBLM, which is most likely due to the variation between different samples of the same type.

In panel (b) of fig. 4.20 the membrane resistance of tBLMs and tBLMs with incorporated NhaA is compared for different pH conditions. NhaA shows a maximum in activity at a pH of 8.5, while being completely inactive at pH 6. Thus, changing from pH 6 to pH 8.5 and vice versa should be expected to activate or deactivate the protein. When switching from pH 8.5 (blue bars) to pH 6 (red bars) for a tBLM without NhaA, a drastic increase in membrane resistance from roughly 15 to 85 kΩ cm^2 is observed. This dramatic change seems counter-intuitive at first when considering the higher H_3O^+ ion concentration at lower pH. It is however in accordance with literature and has been attributed to the alteration of phosphate hydrogen bonds at different pH, as this increase in membrane resistance is not observed in the absence of a phosphate group [36]. The tBLM with incorporated NhaA shows a similar behaviour, with an increase in membrane resistance from 20 to 95 kΩ cm^2. Again, with an active NhaA a much more pronounced change in membrane resistance would be expected, because the increase in membrane resistance due to lowering the pH should be superimposed on the decrease due to the deactivation of the additional ion transport by NhaA across the bilayer.

Panel (c) of fig. 4.20 shows the effect of the inhibitor 2-aminoperimidine on membrane resistance. This is again another way to render the NhaA protein inactive. When comparing the inhibitor's effect on a tBLM without NhaA to a tBLM with incorporated NhaA, the presence of active NhaA should induce a difference of behaviour. The inhibitor causes a large decrease in membrane resistance from 88 to 30 kΩ cm^2 when introduced to the tBLM without NhaA. This change was reversible by removing the inhibitor from the sample chamber by flushing with buffer, which leads to the assumption that it is caused by changes in membrane conformation rather than damage caused to the bilayer. Repeating the same experiment with a tBLM with incorporated NhaA shows a decrease in membrane resistance from 74 to 28 kΩ cm^2. This change is in the same range as the changes observed for a tBLM without NhaA. With an active NhaA protein incorporated the decrease in membrane resistance should have been counter-balanced by an increase in resistance due to deactivation of the sodium-proton antiport. This could not be observed here.

Further experiments have been performed to investigate possible activity of the NhaA protein. Various experimental conditions have been changed, including different bias voltage or buffer molecules. Furthermore, the behaviour of NhaA has been compared to that of the inactive mutant NhaA*. Both incorporation methods described in section 2.6.2 have been explored to rule out the possibility of unsuccessful incorporation for all of these experiments. While the experiments presented here were performed on tBLMs consisting of AM199 lipids, because electrophysiological experiments show results of higher significance with highly

resistive membranes, other lipid compositions like DOPC:CL mixtures or pure DOPC and POPC membranes have been investigated as well. In none of these experiments was it possible to determine any effect that indicated activity of the NhaA protein. While there are differences between the behaviour of tBLMs and tBLMs with incorporated NhaA they are on the same order as variations between samples or the effect of a simple buffer change.

4.2 DPN tBLMs

4.2.1 Nanostructural characterization of DPN tBLMs containing CL

DSPE-PEG-NHS or DPN tBLMs are a system that differs in several structural aspect from DLP tethers. The part that inserts into the membrane is actually a lipid molecule itself, not a single strained hydrophobic chain as in the DLP tethers. This can affect how other lipids of the bilayer will arrange around it. The PEG chain that links the lipid to the surface grafting group is four times as long as the one of DLP tethers. This clearly has an effect on the properties of the sub-membrane space. Finally, the surface grafting group follows a completely different concept than the disulfide bonds to gold of DLP tBLMs. For DPN tethers, as they are used in this thesis, a crucial step is the surface functionalization via APTES. While tBLMs using DSPE-PEG-NHS molecules have been used in the past as described in section 2.4, the use of an APTES layer as a means to functionalize silicon substrates for DSPE-PEG-NHS molecules to bind is still largely unexplored. First NR experiments that have been performed using this system [84], were utilizing simple POPC lipids to test whether this method can result in tBLMs. Here, NR experiments using different DOPC and CL mixtures are presented to extend the knowledge on this DPN tether system on an APTES functionalized surface on one hand, and to determine how large fractions of CL affect another tBLM system in addition to the DLP tBLMs on the other hand.

The tBLM formation for all presented samples followed the procedure described in detail in section 2.4.1. The buffer solution for all experiments shown was 10 mM HEPES with 150 mM KCl or NaCl. Experiments were carried out at 21°C and data analysis followed the procedure described in section 3.1.4. The standard model utilized in this thesis for this kind of tBLM consists of six layers: a SiO_2 layer, a tether layer with the SLD of PEG, an inner headgroup, the chain regions and finally the outer headgroup.

DOPC

Fig. 4.21 shows the NR curves measured at three contrasts for a DOPC tBLM formed using the DPN tether system. The curves representing the best fits to the data are shown, along with the corresponding SLD profiles. The model parameters are listed in the lower part. This measurement was carried out at the SURF reflectometer at ISIS and the data analysis was performed using the single area slab model described in more detail in section 3.1.4. This suggests that no macroscopical defects were present. The results indicate the formation of a tBLM with a surface coverage of 75 % as derived from the solvent content in the lipid chain region. The tether layer had a thickness of 18±1 Å and a high hydration of 90±3 %. This much higher hydration, when compared to the DLP tethers presented before, is at least partly attributed to the much longer chain length of the PEG molecules connecting the surface and the lipid bilayer. Interestingly, the thickness of the tether layer is in the same range as the tether layer thickness of the much shorter DLP tethers. The inner headgroup shows a high thickness of 11±1 Å with a low hydration of 14±7 %. The SLD of 1.6±0.2 $\cdot 10^{-6}$ Å^{-2} of this layer is only slightly lower than the SLD of PC headgroups of $1.88 \cdot 10^{-6}$

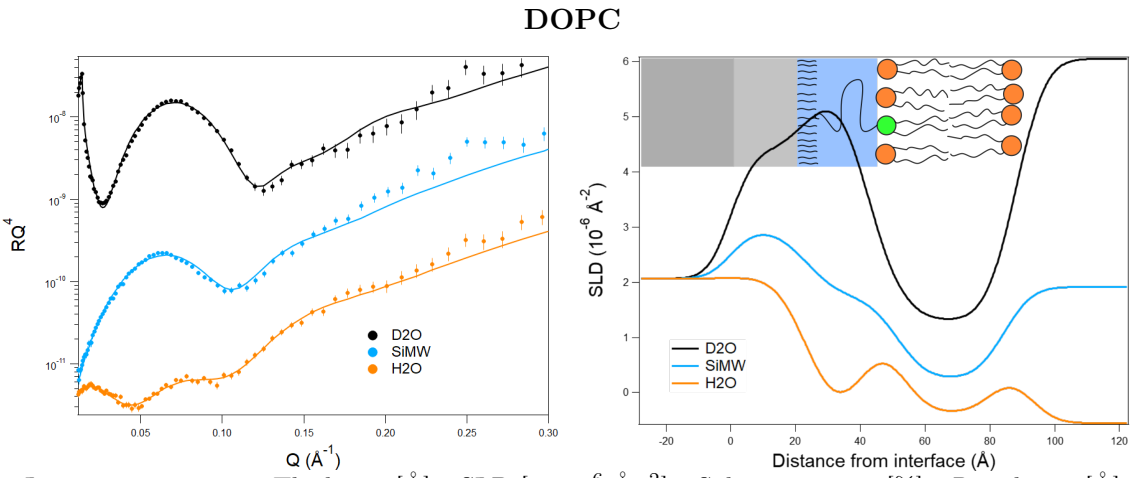

Layer	Thickness [Å]	SLD [$\times 10^{-6}$ Å^{-2}]	Solvent content [%]	Roughness [Å]
SiO_2	23 ± 1	3.47	34 ± 3	6 ± 3
Tethers	18 ± 1	0.6	90 ± 3	8 ± 2
Inner headgroup	11 ± 1	1.6 ± 0.2	14 ± 7	7 ± 1
Inner chain region	16 ± 1	-0.3	25 ± 2	7 ± 1
Outer chain region	16 ± 1	-0.3	25 ± 2	7 ± 1
Outer headgroup	5 ± 1	1.88	20 ± 15	7 ± 1

Figure 4.21: NR measurement of a DOPC membrane on silicon. Top left: Neutron reflectivity curve, top right: The corresponding SLD profile, bottom: Structural parameters obtained from the NR curves.

Å^{-2}. This suggests a moderate amount of PEG chain presence in the inner headgroup layer. Note that, differently to the DLP tethers, this tether architecture features the presence of a PE lipid headgroup in the anchoring part of the molecule. Thus the composition of what is called inner headgroup layer is a combination of the PC lipids composing the bilayer, the PE headgroups from the anchor part of the tether molecule and PEG chains from the tether's spacer group arranging in this layer. Following that, tether presence in the inner headgroup layer is not expected to influence the SLD as strongly as for DLP tethers and thus a high SLD of this layer can still imply a significant fraction of tether molecule insertion into the membrane. The lipid chain regions show a thickness of 16±1 Å, which is well within the expected range. The solvent content of 25±2 % is comparable to the other tBLMs investigated in this thesis. This holds true for the outer headgroup as well, which shows a thickness of 5±1 Å and a solvent content of 20±15 %. In general this tBLM shows a structure which is quite similar to an SLB composed of DOPC lipids apart from the expanded inner headgroup.

DOPC:CL 50:50

Fig. 4.22 shows the resulting reflectivity curves and SLD profiles obtained from the best fits of an NR experiment for a DPN tBLM formed from a 50:50 mixture of DOPC and CL.

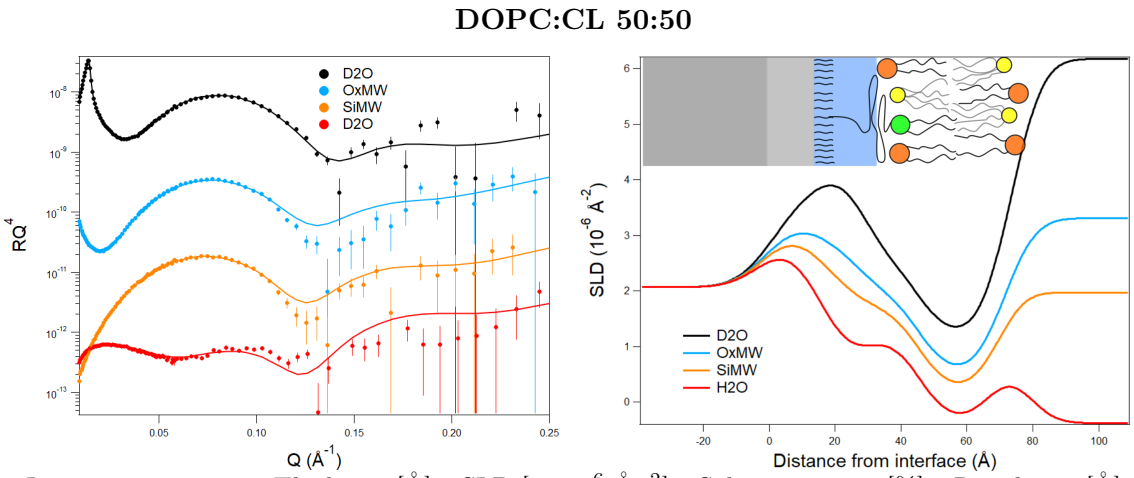

Layer	Thickness [Å]	SLD [$\times 10^{-6}$ Å^{-2}]	Solvent content [%]	Roughness [Å]
SiO_2	16 ± 1	3.47	0	8 ± 1
Tethers	12 ± 1	0.6	70 ± 2	11 ± 1
Inner headgroup	17 ± 1	1.6 ± 0.1	21 ± 3	7 ± 1
Inner chain region	12 ± 1	-0.3	23 ± 1	7 ± 1
Outer chain region	12 ± 1	-0.3	23 ± 1	7 ± 1
Outer headgroup	6± 1	2.4 ± 0.2	27 ± 5	7 ± 1

Figure 4.22: NR measurement of a DOPC:CL 50:50 DPN tBLM on silicon. Top left: Neutron reflectivity curve, top right: The corresponding SLD profile, bottom: Structural parameters obtained from the NR curves.

The model parameters corresponding to the best fits are shown below. This experiment was performed at the FIGARO reflectometer with a characterization at four different contrasts. Data modelling used the standard slab model with the single area representation introduced in section 3.1.4.

A well formed tBLM structure was observed for this membrane containing 50 % CL, showing a surface coverage of roughly 75 %. The tether region is only 12±1 Å thick with a solvent content of 70±2 %. These features were very similar to the DOPC tBLM introduced before and seem to be characteristic for well formed tBLMs with this type of tether architecture. The inner headgroup shows a large thickness of 17±1 Å combined with a hydration of 21±3 % and an SLD of 1.6±0.1 ·10^{-6} Å^{-2}. The SLD is again only slightly below the SLD of a DOPC headgroup. However the thickness is strongly expanded, a behaviour that was already observed for the DLP tethers when large fractions of CL were present. The effect of CL to induce an unordered structure of PEG and lipid headgroups seems to occur in tethers that contain lipids as anchoring moieties as well. The overall SLD of this layer was higher, which is presumably caused by the additional presence of PE headgroups as part of the tether molecule. For the chain region a thickness of 12±1 Å was observed with a hydration of 23±1 %. This was notably thinner than in the case of the pure DOPC tBLM. However, as the inner headgroup consisted of an thick unordered structure, parts of the lipid

chains may have protruded into this region. The overall lipid bilayer thickness, including the inner headgroup layer, stayed in the same range for both lipid compositions. In the outer headgroup layer a thickness of 6±1 Å, a solvent content of 27±5 % and an SLD of 2.4±0.2 $\cdot 10^{-6}$ Å^{-2} were observed. This shows a very similar structure to the DOPC sample again, only the SLD is increased. Considering the higher headgroup SLD of CL when compared to DOPC, this is in agreement with the presence of CL in the headgroup layer and thus the bilayer. Interestingly this is a observation that was not made in the DLP tethers containing CL. In DLP tethers CL caused an increase in outer headgroup thickness while the SLD stayed at values comparable to that of DOPC headgroups.

DOPC:CL 80:20

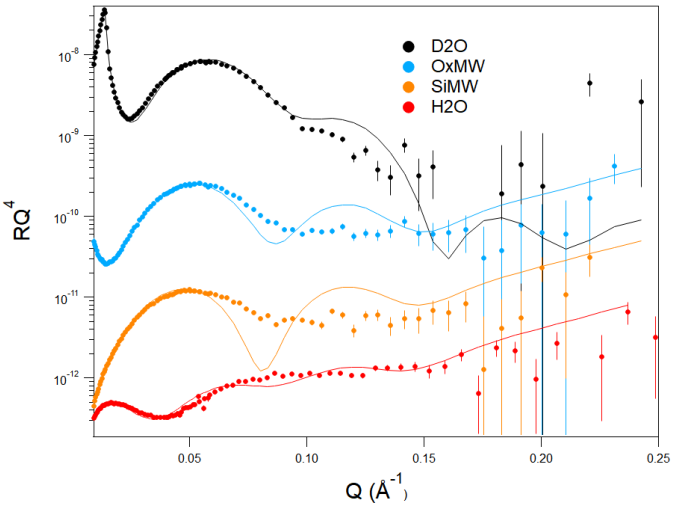

Figure 4.23: NR curves of a DOPC:CL 80:20 DPN tBLM on silicon. The lines show the best fits obtainable with a single area model.

A DOPC:CL 80:20 DPN tBLM was characterized on the FIGARO reflectometer. Reflectivity curves were recorded at four different contrasts. A single area model did not represent the data sufficiently well as is shown in fig. 4.23, however a mixed area model including an area of the sample coated with the lipid membrane and an area not covered by it led to a better representation of the data as shown in fig. 4.24. In applying this two region model, the parameters describing the tether molecule containing sub-membrane space of one region and those describing the tether molecule region not covered by the bilayer of the second region were not connected. This follows from the observation, that the tethers possess a hydrophobic lipid structure at their end that would react quite differently when covered by a lipid bilayer compared to an aqueous medium. In particular the hydrophobic tail of the tether molecule would change its conformation to avoid contact with water. A mixed area model is not available in Motofit. For this reason the software refnx was used for the analysis of this tBLM as described in more detail in section 3.1.4. The first of the two structures used to represent this sample was the same tBLM model as used for the

DOPC:CL 80:20

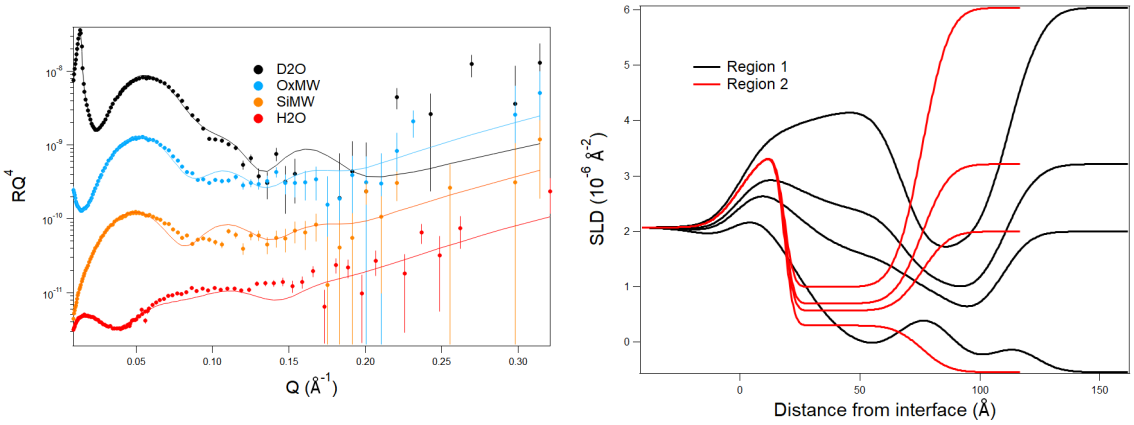

Region 1

Layer	Thickness [Å]	SLD [$\times 10^{-6}$ Å^{-2}]	Solvent content [%]	Roughness [Å]
SiO_2	19 ± 1	3.47	0	9 ± 2
Tethers	49 ± 6	0.5 ± 0.3	67 ± 3	20 ± 1
Inner headgroup	20 ± 7	0.8 ± 0.2	14 ± 19	9 ± 1
Inner chain region	11 ± 3	-0.3	33 ± 8	9 ± 1
Outer chain region	11 ± 3	-0.3	33 ± 8	9 ± 1
Outer headgroup	11 ± 7	1.9 ± 1.1	69 ± 9	9 ± 1
Surface coverage	83 % ± 4 %			

Region 2

Layer	Thickness [Å]	SLD [$\times 10^{-6}$ Å^{-2}]	Solvent content [%]	Roughness [Å]
SiO_2	19 ± 1	3.47	0	9 ± 2
Tethers	57 ± 4	0.4 ± 0.1	11 ± 11	3 ± 5
Surface coverage	17 % ± 4 %			

Figure 4.24: NR measurement of a DOPC:CL 80:20 DPN tBLM on silicon. Top left: Neutron reflectivity curve, top right: The corresponding SLD profile, bottom: Structural parameters obtained from the NR curves.

other DPN samples: a SiO_2 slab at the bottom, followed by a tether slab with the SLD of PEG and four bilayer slabs representing the inner headgroup, the chain regions and the outer headgroup. The region not covered by a bilayer was modelled by a SiO_2 layer that was coupled to the SiO_2 layer of the first region, followed by a tether layer whose thickness and hydration were not linked to the tether layer of the first region.

Fig. 4.24 shows the reflectivity curves together with the best fits obtained from this modelling approach. The SLD profiles for both regions are shown in black (tBLM region) and red (uncovered region). The structural parameters for both regions are also given. The region representing the area covered by the tBLM shows a thick tether layer of 49±6 Å with a high solvent content of 67±3 %. This is significantly thicker than observed for the examples described above. Supposedly, this may be an effect of the preparation process

of the tBLMs. As mentioned in section 2.4.1, when coating the substrates with APTES, different structures than a uniform monolayer of APTES can be formed. An unstructured layer of APTES molecules with a higher thickness may be formed, which can not be distinguished from the tether layer due to a similar average SLD. Such a structure can be an explanation for the observed higher thickness. The inner headgroup layer of the bilayer was highly swollen, showing a thickness of 20±7 Å, while having a low SLD and solvent content of 0.8±0.2 $\cdot 10^{-6}$ Å^{-2} and 14±19 % respectively. This is the typical structure observed for most CL containing samples, as described in the previous sections. The low SLD when compared to the other DPN samples may be explained by a lower fraction of tether molecules being inserted into the bilayer, while PEG still accumulates in its vicinity. However, the fit is not very sensitive to the properties of the inner headgroup layer and thus these parameters should be taken with caution. The chain regions are 11±3 Å thin, which was observed for most CL samples, and show a solvent content of 33±8 %. In the outer headgroup region a large fraction of 69±9 % solvent is found, while the thickness of 11±3 Å and SLD of 1.9±1.1 $\cdot 10^{-6}$ Å^{-2} is rather comparable to the outer headgroup structure of DLP tBLMs than the other DPN tBLM containing high amounts CL. Hence a shifted arrangement of the PC and CL headgroups may be the cause. This tBLM structure covers 83 % of the surface. The remaining 17 % feature only a SiO_2 and a tether layer. The tether layer of 57±4 Å is even thicker than the 47±6 Å layer below the membrane and interestingly shows a very low solvent content of 11±11 %. The SLD of 0.4±0.1 $\cdot 10^{-6}$ Å^{-2} is slightly lower than the SLD of PEG, which accounts for the presence of alkyl chains of the coiled lipid anchor moieties in this region, which have an SLD of -0.3$\cdot 10^{-6}$ Å^{-2}. A possible explanation could be that in order to avoid contact with water, the DSPE lipids at the end of the tethering molecules may hide their tails among the PEG chains, thus expelling water molecules. It is not clear if this happened before the deposition of the lipid membrane, causing the incomplete coverage of the lipid bilayer, or if it is a consequence of differences in the deposition process. Further studies are necessary to clarify this observation.

4.2.2 NhaA incorporation into DPN tBLMs

The NhaA protein was incorporated into the DOPC:CL 50:50 tBLM sample described above and shown in fig. 4.22. In this case the detergent mediated incorporation method led to good results (see section 2.6.2). A solution of roughly 65 μg/ml of NhaA protein was added to the sample cell in H_2O buffer together with DDM at a concentration of 20 % of the CMC. The protein detergent mixture was incubated for 30 minutes, followed by rinsing of the cell with buffer. Fig. 4.25 shows reflectivity curves for both the pristine tBLM and the tBLM after exposure to NhaA. The exposure to the protein clearly has an effect on the tBLM system. The data was modelled using the same procedure as described in section 3.1.4. The incorporated protein replaced part of the lipid bilayer with a volume fraction, that was constrained to the same value among the different slabs representing the bilayer.

Fig. 4.26 shows the reflectivity curves with the best fits, the resulting SLD profiles and the corresponding model parameters. Note that the SLDs of the different bilayer slabs are the effective SLD of each slab, which is the SLD of the bilayer components and the protein

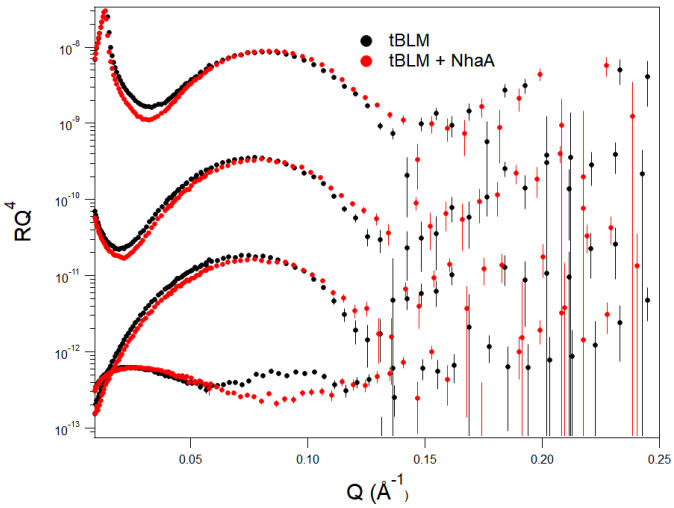

Figure 4.25: NR curves of a pure DOPC:CL 50:50 DPN tBLM (black curves) compared to the same sample with incorporated NhaA (red curves)

fraction combined. They are given for the D_2O contrast, as the SLD value of the protein depends on the degree of deuteration of the solvent. In fig. 4.27 the fit parameters and volume fraction distributions of the different tBLM components are compared for the tBLM and tBLM with incorporated NhaA. The incorporation process caused the replacement of ca. 20 % of the tBLM volume with protein (pink curve in volume fraction graph). When compared to the structure of the pristine tBLM, only minor structural changes were observed. The tether layer, inner headgroup and chain regions showed basically no change. The outer headgroup layer showed a slight increase in thickness and a large increase in hydration. However, the fit was not very sensitive to the outer headgroup thickness and solvent content as visible from the large errors. The increase in outer headgroup hydration is a feature often observed when incorporation protein into tBLMs as this process usually causes slight damage to the membrane, which leads to the removal of some lipids and a more open structure of the outer headgroup. Compared to other protein incorporation studies and especially compared to the incorporation of NhaA into DLP tBLMs the structural changes were minimal.

4.2.3 Summary

DPN tBLMs of different lipid composition were successfully formed and characterized. This shows that the method for surface functionalization with APTES, followed by tether molecule adsorption and subsequent tBLM formation by rapid solvent exchange is a viable procedure for tBLM production. The tBLMs formed using this procedure and surface chemistry usually showed a sub-membrane space of 10-20 Å despite the long PEG chain length of almost 13 nm. The thickness of this sub-membrane space did not vary significantly from the sub-membrane space thickness of tBLMs formed with tether molecules containing

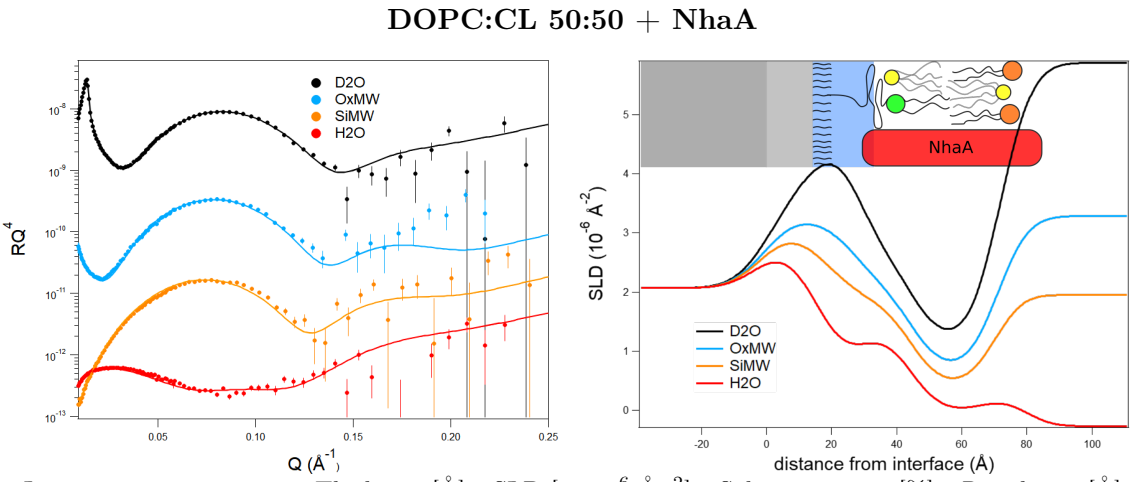

Layer	Thickness [Å]	SLD [$\times 10^{-6}$ Å^{-2}]	Solvent content [%]	Roughness [Å]
SiO_2	16 ± 3	3.47	0	8 ± 2
Tethers	12 ± 2	0.6	85 ± 5	12 ± 3
Inner headgroup	17 ± 1	1.8 ±0.3	21 ± 4	7 ± 3
Inner chain region	13 ± 1	0.3 ±0.1	17 ± 2	7 ± 3
Outer chain region	13 ± 1	0.3 ±0.1	17 ± 2	7 ± 3
Outer headgroup	7 ± 4	2.3 ± 1.5	71 ± 14	7 ± 3
Protein volume fraction	0.19 ± 0.01			

Figure 4.26: NR measurement of a DOPC:CL 50:50 DPN tBLM with incorporated NhaA on silicon. Top left: Neutron reflectivity curve, top right: The corresponding SLD profile, bottom: Structural parameters obtained from the NR curves.

PEG chains of much shorter length. The DLP tethers presented in the previous section 4.1, feature 11 monomer long PEG chains as compared to the 45 monomer units of the DPN tethers and showed a similar sub-membrane space thickness. All investigated samples with DPN tether architecture showed very high solvent content in the sub-membrane space of 60 to 90 %. This conforms to literature that suggests a higher hydration of tethers with longer PEG chains as spacer units of the tether molecules (e.g. [29]). A possible explanation for that is a lower tether molecules density on the surface, that is induced by the fact that longer chains block a larger surface area and thus prevent attachment of further tether molecules in this area. Based on the structure of the pure DOPC sample, bilayers that are structurally very close to SLBs can be formed using this tBLM architecture. The inner headgroup seems to be slightly extended due to interaction with the PEG chains below the bilayer.

The DOPC:CL 80:20 bilayer showed a structure different to the other samples shown. While the general bilayer properties are comparable to others, the thickness of the sub-membrane space was much higher and part of the surface showed no bilayer coverage at all. This may be an effect originating from the surface functionalization with APTES. Formation of a uniform APTES monolayer is a complex task and thicker layers can be formed unintentionally,

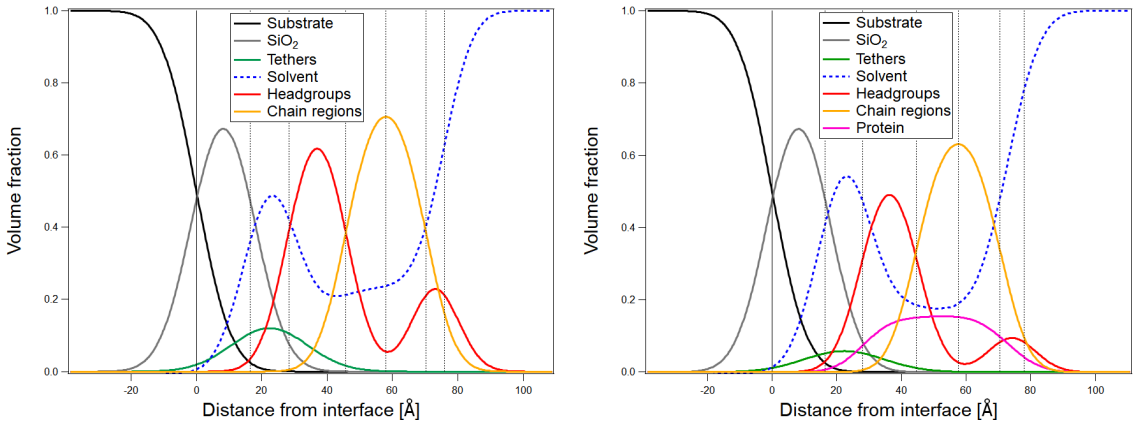

	tBLM		tBLM + NhaA	
	Thickness [Å]	Solvent [%]	Thickness [Å]	Solvent [%]
Tethers	12 ±1	70 ±2	12 ± 2	85 ± 5
Inner headgroup	17 ±1	21 ± 3	17 ± 1	21 ± 4
Inner chain region	12 ±1	23 ±1	13 ± 1	17 ± 2
Outer chain region	12 ±1	23 ±1	13 ± 1	17 ± 2
Outer headgroup	6 ±1	27 ±5	7 ± 4	71 ± 14

Figure 4.27: Volume fraction distribution of the different system components of a pure DOPC:CL 50:50 DPN tBLM (top left) and the same sample after NhaA incorporation. The table shows a comparison of the fit parameters with and without NhaA.

which causes a change in sub-membrane space structure. Optimization of the APTES layer deposition as the crucial step in tBLM formation will be needed to increase reliability of this tBLM production method.

The effect of large fractions of CL in tBLM structure was further investigated using these tBLMs. CL induced a thickening of the inner headgroup layer. This layer contained certain fractions of PEG from the sub-membrane space. The chain regions on the other hand were thinner than e.g. the aforementioned pure DOPC sample. Considering the thickening of the inner headgroup layer and the thinning of the chain regions, the overall membrane thickness remained largely unchanged. It has to be mentioned, that the two chain regions can not be distinguished from each other and were assumed to be symmetric in the data analysis. Thus, the thinning of the chain regions may well be mainly an effect in the inner inner leaflet, which intertwines to the combined PEG-inner headgroup layer. In general CL content induced changes, which are at large comparable to the changes observed in DLP tethers with high CL content.

NhaA was successfully incorporated into a DPN tBLM, which shows that these membranes can form an approximated natural environment for membrane proteins. The incorporation process caused minor changes to the membrane and kept the structure mostly intact. Incor-

poration of 20 vol% of NhaA was observed. Compared to that, protein incorporation into DLP tBLMs caused large structural changes. However, the incorporated fractions into DLP tBLMs were significantly higher than in the DPN tBLM (50 % in DLP tBLM vs 20 % in DPN tBLM). Incorporation at this low level may leave enough lipid bilayer structure intact to maintain an unaltered membrane structure, while larger fraction cause major changes.

Chapter 5

Summary & Conclusion

Within the framework of this thesis, two different types of tBLM architectures were investigated. Both systems were used to characterize the changes that an increasing amount of cardiolipin has on the tethered bilayer structure. Furthermore, NhaA incorporation was successfully demonstrated and quantified in both tBLM architectures.

DLP tBLMs are a tethered bilayer system that is connected to a gold surface via a PEG chain consisting of 11 ethylene oxide units. This allowed the electrophysiological characterization with electrochemical impedance spectroscopy, using the gold substrate as one of the electrodes. Due to the planar surface, neutron reflectometry could be used to determine the nanostructure of the system. These measurements revealed a thin sub-membrane space thickness of approximately one nanometer for all investigated samples of this type, which is significantly less than what had been previously postulated from other indirect means. All samples showed a consistently low solvent content of the sub-membrane space. A high tether molecule content was observed in the inner headgroup layer of the bilayers. Interestingly, the tether concentration showed no significant influence on the bilayer structure in general, neither on the solvent content in the sub-membrane space nor on the tether content of the inner headgroup layer.

The DPN tether system is a modified tBLM system that combines frequently used tether molecules, featuring a 45 unit PEG spacer, with a novel surface functionalization and tBLM formation method. These tBLMs were formed on silicon surfaces, which avoids the strong influence of the gold layer that was invariably observed in the NR experiments featuring DLP tBLMs. The results of this thesis provide the first detailed nanostructural characterisation of this system with varying lipid composition. The tBLMs were formed successfully using the rapid solvent exchange method and showed a surface coverage that was comparable to the established DLP tBLM system. They commonly showed a thin sub-membrane space dimension on the order of one nanometer. Unlike DLP tBLMs however, the solvent content of this sub-membrane space was consistently very high, usually around 70-80%.

The structural differences between the two tether systems largely conformed to expectations. A higher solvent content in the sub-membrane space, as observed in DPN tBLMs when compared to DLP tBLMs, has been reported previously for tether architectures that use tether molecules with longer PEG spacer chains. While the reason for this is still to be identified, it is considered likely that, at least in the case of the systems investigated here, longer PEG chains occupy a larger area on the substrate and therefore cause a generally lower tether density on the surface, which in turn leads to a higher water content below the membrane. Furthermore, the length of the PEG spacer did not seem to influence the thickness of the sub-membrane space significantly, as the two tether systems, one of which has a PEG chain of four times the length than the other, showed a similar sub-membrane space thickness. This could be attributed to coiling of the PEG chains, but may also be caused by the assumed differences in surface coverage of the different tether molecules.

While generally displaying a highly reproducible structure of the membranes, both tBLM systems showed differing phenomena at times. For DLP tBLMs the appearance of a Bragg peak like structure was observed in several samples in NR experiments as described in appendix A.1. The position of this peak indicates a repeating structure of approximately 5-6 nm. QCM-D experiments, which were performed to investigate this feature, showed an adsorbed mass that corresponds to 2-3 times the mass that is expected for a lipid bilayer (shown in appendix A.2). The nature of the phenomenon, as well as the experimental parameters that lead to its appearance, could not be identified yet, although it is likely to be due to the formation of partial multi-bilayers. In DPN tBLMs, a significantly different structure of the sub-membrane space compared to the other measured samples was observed in one of the presented tBLMs, which is described in section 4.2.1. This sample could not be analysed as one continuous structure, but made a mixed area model necessary. A part of the surface was covered by a tBLM, but other regions only showed a dense tether molecule layer with low solvent content. The sub-membrane space of the region covered by a tBLM showed a significantly higher thickness than the other observed samples of roughly five nanometers, which is presumably caused by the deposition of an APTES layer that is thicker than one monolayer. The observation of these features shows that tBLMs are highly complex systems, whose properties and influencing factors are not yet completely understood. Special care must be taken in their preparation in order to ensure reproducibility.

One of the aims of this thesis was to investigate the effects of different amounts of cardiolipin on the structure of the tethered bilayers. CL is a lipid with a unique structure that has been shown to interact with a variety of membrane proteins. While the usually occurring and studied fractions of CL are on the order of 10-20 %, CL fractions up to 80 % were investigated in this thesis. The possibility to produce tBLMs with high fractions of CL was shown for both investigated tether systems. Changing the concentration of CL had a substantial effect on the lipid bilayer properties. DLP tBLMs with high CL fractions were electrically much more sealing than tBLMs from pure phospholipids. Nano-structural NR investigations revealed a dense accumulation of PEG molecules in the inner headgroup region with low solvent content, which may induce this electrophysiological behaviour. This phenomenon was accompanied by a thinning of the chain regions and often an expansion

of the outer headgroup region, which is interpreted as a shifted arrangement of the CL and PC headgroups. In general, large fractions of CL led to an altered structure in both tBLM systems. Interestingly, the observations were very similar for the two investigated tBLM systems. They differ in the structure of the membrane inserting anchor but both use a PEG chain as spacer unit which allows for the accumulation of PEG below the membrane, therefore this phenomenon appears to be largely independent of anchor structure.

The sodium proton antiporter NhaA was chosen to investigate membrane protein incorporation into tBLM systems. Its electrogenic nature makes it an attractive choice due to possible future applications in bio-inspired devices. NhaA was successfully incorporated into both tBLM systems using different incorporation methods. The incorporated volume fraction was as high as 50% in the DLP tBLMs, while in DPN tBLMs, a lower fraction of 20% was observed. As a consequence, the incorporation caused measurable changes in membrane structure at high incorporation fractions in DLP tBLMs, while the changes in DPN tBLMs with lower incorporated fractions were less pronounced. Most notable in the DLP tBLM structure was an increase in chain region thickness to accommodate the thicker membrane protein. Interestingly, the protein incorporation process led to the disappearance of the unusually thick inner headgroup layer that consisted of accumulated PEG in the vicinity of the inner headgroups. In DPN tBLMs the incorporation at lower fractions of 20% only caused minor changes in tBLM structure, which shows that NhaA incorporation in general does not disrupt the lipid bilayer structure significantly. Only higher fractions of NhaA induce large significant changes, as the resulting tBLM is determined by protein structure just as much as by lipid structure. The activity of the NhaA protein was investigated by EIS measurements but could not be confirmed, as shown in section 4.1.5. This may have several reasons as hypothesized in the section. Further experiments on this topic are necessary to determine the cause.

This thesis has produced novel nanostructural characterizations of two types of tBLM systems. Both investigated tBLM systems showed highly promising structures as model membrane systems for protein incorporation studies and as model systems to study bilayer properties themselves. Nonetheless, the results of this thesis also raise several questions. Leading from these nanostructural characterisations are questions concerning the specific influences of different components of tBLMs but also external factors, both during the tBLM formation process or on the already formed tBLM. The novel DPN tBLMs have been shown to be a robust sample system that is suitable for membrane protein incorporation and will be interesting for neutron reflectometry studies, because they do not show the strong influence that is caused by the gold layer which other tBLM systems require. The use of doped silicon substrates could allow the electrophysiological characterization of membrane properties and incorporated protein activity to further develop this system as a platform for membrane protein studies. For this it will be important to further determine the conditions under which a uniform monolayer of APTES is formed on the surface. The peculiar interaction between CL and the PEG chains of the tether molecules is a phenomenon that should be further investigated. This could be done by carrying out a similar study on lipids with a comparable headgroup structure like phosphoglycerols or different spacer units other

than PEG. Moreover, tBLMs with high CL fractions demonstrated suitability for protein incorporation and could be used in the future to investigate the effect of higher CL content on different membrane proteins that interact with CL. Finally, using simultaneous in situ EIS and NR measurements on tBLMs would enable a direct relationship to be established between electrophysiological behaviour and nanostructure. EIS measurements have shown a certain statistical variability in lipid bilayer properties which impedes comparison between results obtained from different techniques. This could be diminished when performing EIS and NR directly on the same sample. First experiments in this direction were performed in this thesis, however, the large surface required for NR experiments increases the complexity of EIS data interpretation significantly. To conclude, building upon the nanostructural characterisations described in this thesis provides the perspective for several rich areas of ongoing research to enhance the depth of knowledge of tethered lipid bilayer membrane systems that incorporate membrane proteins.

Chapter 6

Résumé

Le but du travail présenté dans cette thèse était la caractérisation structurelle des bicouches lipidiques amarrées de composition variable et l'étude de l'incorporation des protéines membranaires. Ce sujet très spécifique a été motivé par les développements de différents domaines de recherche allant de la biologie à la bio-ingénierie en passant par la physique. Au cœur de cette étude se trouvent les bicouches lipidiques. Elles sont la caractéristique constitutive de toutes les membranes cellulaires et donc des structures qui définissent les limites de tous les êtres vivants.

Le concept de base selon lequel une forme de membrane entoure les cellules et les sépare de leur environnement remonte à plus de 250 ans [1]. Une compréhension détaillée de la structure de ces membranes est cependant un développement relativement récent. Bien que les premières idées sur la nature bicouche lipidique des membranes cellulaires aient été proposées à la fin du XIXe siècle, il a fallu attendre 1972, lorsque Singer et Nicholson ont développé le modèle de la mosaïque fluide [2], pour arriver à la compréhension et aux concepts actuels de la membrane cellulaire. Une membrane cellulaire est constituée de nombreux composants différents qui s'assemblent en une structure complexe. Son unité de base est constituée de lipides, des molécules qui possèdent une région de chaîne hydrophobe et un groupe de tête hydrophile. Les lipides sont organisés en une structure à double couche, la région hydrophobe étant tournée vers l'intérieur, ce qui forme une barrière pour l'eau permettant d'isoler l'intérieur de la cellule du monde extérieur. Les membranes cellulaires sont toutefois beaucoup plus complexes que ce composant de base. Alors que la membrane elle-même est principalement constituée de centaines de lipides différents, de stérols, de protéines membranaires, de peptides, de sucres et d'autres composants, la forme de la membrane cellulaire est fortement influencée par la structure cytosquelettique sous la membrane, ainsi que par le glycocalyx externe [3]. Dans le modèle de la mosaïque fluide, les différents composants sont bien structurés à travers la membrane cellulaire, mais peuvent diffuser dans la direction latérale, ce qui entraîne un comportement de type fluide pour les molécules de la bicouche.

Alors que la nature complexe des membranes cellulaires donne lieu à des propriétés évidemment fascinantes, puisqu'elle constitue la base de la vie avancée, leurs propriétés biophysiques fondamentales sont difficiles à mesurer in situ. C'est pourquoi des systèmes membranaires modèles sont nécessaires afin de déterminer le rôle ou la structure de chaque composant de la membrane cellulaire. Ces systèmes simplifiés ne comprennent qu'une petite partie des composants qui constituent une membrane cellulaire naturelle et ne présentent donc qu'un nombre limité de ses propriétés. Ils sont cependant beaucoup plus faciles à caractériser avec des méthodes biophysiques et peuvent servir à éclairer des processus isolés. De nombreux systèmes modèles différents ont été développés au fil des ans, qui présentent différentes propriétés et modélisent différentes caractéristiques d'une membrane cellulaire. La principale motivation derrière l'utilisation de ces différents modèles de membranes est double. Premièrement, l'utilisation d'un modèle de membrane doit être adapté au processus ou à la structure biologique qui doit être étudié. Selon la nature du sujet étudié, les différentes caractéristiques d'une membrane cellulaire doivent être appariées ou approximées pour son observation. Deuxièmement, un système modèle doit être adapté afin d'être accessible aux différentes méthodes expérimentales. Bien que des systèmes très complexes voisins d'une membrane cellulaire naturelle puissent être produits, ils sont inutiles si aucune information ne peut en être extraite avec le matériel expérimental disponible. Certaines méthodes de caractérisation exigent que les membranes soient conformes à une géométrie particulière, de nombreux systèmes membranaires modèles sont donc spécifiquement conçus en tenant compte de ces contraintes. Les bicouches lipidiques sont l'un des systèmes membranaires modèles les plus simples et peuvent aller de systèmes sphériques comme les vésicules, les micelles ou les bicelles à des systèmes planaires comme les bicouches autoportantes, les piles de bicouches ou les bicouches simples sur une surface plane [6]. Parmi ceux-ci, les systèmes membranaires modèles planaires ont l'avantage d'être très bien adaptés à l'étude avec des méthodes de caractérisation nanostructurale et électrochimique.

À la lumière des considérations exposées ci-dessus, un système membranaire modèle planaire constitué de membranes bicouches lipidiques amarrées (tBLM) a été sélectionné pour ce travail. Les tBLM sont constituées de bicouches lipidiques qui sont chimiquement greffées sur une surface plane. Les molécules de greffage sont constituées d'un ancrage hydrophobe qui s'insère dans la bicouche lipidique et est relié à la surface par une molécule hydrophile en forme de chaîne. Structurellement, les tBLM peuvent imiter toutes les propriétés biologiques que les systèmes modèles planaires présentent en général. En outre, les molécules de greffage insérées peuvent imiter les situations dans lesquelles des structures s'attachent à une membrane in vivo. Cela peut être le cas pour les points d'attache cytosquelettiques dans la membrane cellulaire, ou dans des situations telles que la liaison de neurotransmetteurs, dans lesquelles des ancres protéiques s'insérant dans une membrane induisent la fusion de vésicules avec une membrane. De plus, la fixation à une surface plane rend les tBLMs accessibles à une série de méthodes expérimentales sensibles aux interfaces. Ceci a été exploité par l'utilisation de la réflectométrie neutronique dans cette thèse. En plus de cette structure favorable à la recherche expérimentale, les tBLM sont très robustes à la fois dans le temps et contre les influences extérieures. Cela permet des études et des traitements à long terme qui endommageraient d'autres types de systèmes modèles. Ainsi,

la robustesse des tBLM ouvre un champ de dispositifs biotechnologiques. Les biocapteurs et autres dispositifs qui utilisent des systèmes membranaires modèles doivent fonctionner sur de longues périodes. Comme la plupart des autres systèmes membranaires modèles n'ont pas la stabilité requise, le développement des tBLM a conduit à des avancées dans le domaine des dispositifs d'inspiration biologique. Ces trois raisons en font un système membranaire modèle intéressant à étudier.

Les tBLMs offrent une grande liberté de conception car il existe de nombreuses façons de les créer et de nombreuses compositions spécifiques des molécules qui relient la bicouche lipidique à la surface. C'est un avantage évident qui a été exploité dans une multitude d'études. Malgré l'expansion rapide de leur utilisation et de leurs recherches, les détails nanostructuraux de nombreux systèmes tBLM n'ont souvent pas été définis avec précision. Ceci est toutefois important, car l'exploitation des tBLM pour des applications plus sophistiquées nécessite une compréhension détaillée de la nanostructure des tBLM. Les chaînes DLP, l'un des deux systèmes tBLM étudiés dans le cadre de cette thèse, sont un bon exemple. Ils utilisent une surface en or comme support, ce qui donne accès à des méthodes de caractérisation électrochimique. Malgré 20 ans de développement, les propriétés nanostructurales des systèmes DLP ne sont pas couramment décrites, même si leurs propriétés électrophysiologiques sont largement exploitées. Cette situation a motivé les recherches contenues dans cette thèse, car la connaissance des propriétés structurelles fera progresser l'interprétation des résultats expérimentaux obtenus à l'aide de ce système. En outre, en raison du grand nombre d'architectures différentes, de nombreuses façons de préparer les tBLM et de nombreuses structures spécifiques restent inexplorées. Cela offre la possibilité d'améliorer les systèmes existants par la modification des composants et des procédures expérimentales. C'est la raison pour laquelle le choix s'est porté sur la caractérisation des tBLMs DSPE-PEG-NHS (DPN), le second système d'attache des tBLM étudié dans cette thèse. Il diffère des tBLM DLP par la structure des molécules utilisées permettant de greffer la bicouche à la surface. L'architecture est similaire aux systèmes tBLM qui ont été décrits précédemment, mais elle diffère dans la fonctionnalisation de la surface, ce qui peut la rendre intéressante pour des applications spécifiques. Ces DPN tBLM sont supportés par une surface en silicium, qui est plus facile à obtenir que les surfaces en or en terme de qualité requise et qui facilite l'interprétation des données obtenues lors des expériences de diffusion.

Les tBLM sont exploitées depuis les années 1990 pour étudier les propriétés fonctionnelles des protéines membranaires [7]. En général, la plupart des protéines membranaires ont besoin d'un environnement de bicouche lipidique pour fonctionner, donc pour leur étude, des systèmes membranaires modèles sont nécessaires. C'est notamment le cas des transporteurs membranaires qui ont le rôle important de transloquer les ions à travers les membranes bicouches lipidiques. Naturellement, une barrière bicouche lipidique est nécessaire pour pouvoir déterminer tout mouvement à travers celle-ci. Une tBLM constitue l'élément de base idéal pour construire ces systèmes membranaires modèles complexes de transport d'ions. En raison de leur nature robuste, ils peuvent résister aux processus d'incorporation des protéines membranaires de transport d'ions. Ces processus nécessitent la perturbation,

mais pas la dissolution, des lipides dans la bicouche et impliquent souvent l'utilisation de détergents. La connexion à une surface par les molécules d'amarrage fournit la robustesse nécessaire à la construction de ce système complet de protéines + tBLM, ce qui fait défaut aux autres systèmes modèles planaires. Cette propriété a été exploitée dans cette thèse afin d'étudier une protéine spécifique de transport d'ions, l'échangeur sodium-hydrogène NhaA. NhaA est un transporteur électrogène, ce qui signifie qu'il transporte plus d'ions dans une direction à travers la membrane que dans l'autre. Cette propriété le rend intéressant pour la troisième gamme d'applications des tBLM mentionnée ci-dessus : l'utilisation dans les dispositifs biomimétiques.

Au sein du groupe de recherche Systèmes Nanobiotechnologiques et Biomimétiques de l'Université de Grenoble (SyNaBi), un dispositif biomimétique est en cours de développement qui utilise ce transport d'ions à travers une membrane. Le concept se compose de deux compartiments qui sont divisés par une bicouche lipidique avec NhaA incorporé. La protéine transporte les ions sodium à travers la membrane, créant ainsi un potentiel transmembranaire. Le placement d'électrodes dans chaque compartiment permet de récolter le potentiel ionique induit et de le transformer en un potentiel électrique qui peut être utilisé pour la production d'électricité [8]. Ce concept pourrait être utilisé à l'avenir pour un dispositif implantable qui alimenterait des implants médicaux en utilisant des substances présentes dans le corps (des ions de sodium dans ce cas). L'optimisation de ce système est limitée par un manque de compréhension détaillée de l'interaction entre le NhaA et son environnement bicouche lipidique. Ceci est important car la structure d'une membrane influence fortement l'incorporation et la fonction des protéines. Comme mentionné précédemment, la structure de l'environnement de la bicouche lipidique est déterminée non seulement par la composition lipidique, mais aussi par l'architecture de l'amarrage lorsqu'un tBLM est utilisé comme système modèle. Le développement de ce dispositif a servi de motivation supplémentaire pour l'étude des propriétés des systèmes de tBLM et en particulier pour le choix de le NhaA comme protéine de transport d'ions électrogène. Dans le cadre de cette thèse, l'interaction entre l'incorporation de NhaA et la composition lipidique de la tBLM, ainsi que l'architecture d'amarrage, ont été étudiées. La caractérisation de la composition lipidique a été centrée sur les membranes contenant de grandes fractions de cardiolipine (CL), un lipide ayant une structure et des propriétés uniques. Ce lipide peut non seulement influencer l'incorporation des protéines, mais aussi affecter les structures des tBLM elles-mêmes. Ces considérations ont conduit aux trois points d'intérêt abordés dans cette thèse : le type d'architecture des tBLM, leur composition lipidique et l'incorporation de NhaA.

L'étude des systèmes tBLM nécessite des techniques expérimentales adaptées pour fournir des informations sur les systèmes d'interface, car la connexion à une surface est un facteur déterminant des tBLM. Le choix d'une surface plane permet l'utilisation de techniques structurelles à haute résolution comme la réflectométrie neutronique (NR), qui est l'une des principales techniques utilisées dans cette thèse. La NR donne des informations structurelles moyennes sur le système tBLM avec une précision sub-nanométrique. Cette technique peut donc être utilisée pour caractériser les dimensions et la composition des différentes parties de

la bicouche lipidique ou de la couche de liaison et, comme la NR est sensible à la composition moléculaire d'un système, elle permet également de déterminer la présence de protéines et le degré d'incorporation des protéines. En outre, une conception plane, en particulier avec une surface conductrice en or comme support, permet de placer des électrodes des deux côtés du système pour une caractérisation électrophysiologique par spectroscopie d'impédance électrochimique (EIS). Il s'agit d'une méthode établie pour déterminer les paramètres DLP tBLM [9] et permet donc de comparer les informations obtenues sur les tBLM contenant du cardiolipine dans cette thèse à des études avec différentes compositions lipidiques.

Les **objectifs de cette thèse** étaient donc les suivants :

- L'étude de deux systèmes d'architecture tBLM différents et de leurs propriétés structurelles et différences spécifiques : DLP tBLMs et DSPE-PEG-NHS tBLMs.
- La variation du contenu en CL dans les deux systèmes tBLM et la caractérisation des effets que cela a sur la structure et les propriétés bicouches.
- L'incorporation du canal ionique NhaA dans ces systèmes de tBLM, pour étudier si elle est affectée par la CL et quels changements structurels l'incorporation de NhaA provoque dans les deux systèmes de tBLM.

Les DLP tBLM sont un système de bicouche amarré qui est relié à une surface d'or par une chaîne PEG composée de 11 unités d'oxyde d'éthylène. Cela a permis la caractérisation électrophysiologique par spectroscopie d'impédance électrochimique, en utilisant le substrat d'or comme l'une des électrodes. Ces mesures ont révélé une fine épaisseur de l'espace sous-membranaire d'environ un nanomètre pour tous les échantillons étudiés de ce type, ce qui est nettement inférieur à ce qui avait été postulé précédemment par d'autres moyens indirects. En raison de la surface plane, la réflectométrie neutronique a pu être utilisée pour déterminer la nanostructure du système. Tous les échantillons ont montré une teneur en solvant constamment faible de l'espace sub-membranaire. Une teneur élevée en molécules de liaison a été observée dans la couche du groupe de tête interne des bicouches. Il est intéressant de noter que la concentration de molécules de liaison n'a pas eu d'influence significative sur la structure des bicouches en général, ni sur la teneur en solvant dans l'espace sous-membranaire, ni sur la teneur en molécules de liaison de la couche de groupe de tête interne.

Le système d'amarrage DPN est un système tBLM modifié qui combine des molécules d'amarrage fréquemment utilisées, comportant un espaceur PEG de 45 unités, avec une méthode nouvelle de fonctionnalisation de surface et de formation de tBLM. Ces tBLM ont été formés sur des surfaces de silicium, ce qui évite la forte influence de la couche d'or qui a été invariablement observée dans les expériences NR comportant des DLP tBLM. Les résultats de cette thèse fournissent la première caractérisation nanostructurale détaillée de ce système avec une composition lipidique variable. Les tBLM ont été formés avec succès en utilisant la méthode d'échange rapide de solvant et ont montré une couverture de surface comparable au système établi de DLP tBLM. Ils ont généralement montré une dimension fine de l'espace sous-membranaire de l'ordre du nanomètre. Toutefois, contrairement aux

DLP tBLM, la teneur en solvant de cet espace sub-membranaire était toujours très élevée, généralement de l'ordre de 70 à 80 %.

Les différences structurelles entre les deux systèmes d'amarrage ont été largement conformes aux attentes. Une teneur en solvant plus élevée dans l'espace sous-membranaire, telle qu'observée dans les tBLM de DPN par rapport aux tBLM de DLP, a été rapportée précédemment pour les architectures d'amarrage qui utilisent des molécules de liaison avec des chaînes PEG plus longues. Bien que la raison de ce phénomène reste à déterminer, il est considéré comme probable que, au moins dans le cas des systèmes étudiés ici, les chaînes PEG plus longues occupent une plus grande surface sur le substrat et provoquent donc une densité d'attache généralement plus faible à la surface, ce qui entraîne à son tour une teneur en eau plus élevée sous la membrane. En outre, la longueur de l'espaceur en PEG ne semble pas avoir une influence significative sur l'épaisseur de l'espace sous-membranaire, car les deux systèmes d'amarrage, dont l'un possède une chaîne de PEG quatre fois plus longue que l'autre, présentent une épaisseur similaire de l'espace sous-membranaire. Cela pourrait être attribué à l'enroulement des chaînes de PEG, mais pourrait également être le résultat des différences présumées de couverture de surface des différentes molécules d'amarrage.

Tout en présentant généralement une structure des membranes très reproductible, les deux systèmes de tBLM ont parfois montré des phénomènes différents. Pour les DLP tBLM, l'apparition d'une structure semblable à un pic de Bragg a été observée dans plusieurs échantillons des expériences NR. La position de ce pic indique une structure répétitive d'environ 5-6 nm. Les expériences QCM-D, qui ont été réalisées pour étudier cette caractéristique, ont montré une masse adsorbée qui correspond à 2 à 3 fois la masse prévue pour une bicouche lipidique. La nature du phénomène, ainsi que les paramètres expérimentaux qui le conduisent, n'ont pas encore pu être identifiés, bien qu'il soit probablement dû à la formation de multicouches partielles. Dans les tBLM de DPN, une structure de l'espace sub-membranaire significativement différente de celle des autres échantillons mesurés a été observée dans l'un des tBLM présentés. Cet échantillon n'a pas pu être analysé comme une structure continue, mais a rendu nécessaire un modèle de zone mixte. Une partie de la surface était occupée par un tBLM, mais d'autres régions ne présentaient qu'une couche dense de molécules d'ancrage à faible teneur en solvant. L'espace sub-membranaire de la région couverte par un tBLM présentait une épaisseur nettement plus élevée que les autres échantillons observés, d'environ cinq nanomètres, ce qui est probablement dû au dépôt d'une couche d'APTES plus épaisse qu'une monocouche d'APTES. L'observation de ces caractéristiques montre que les tBLM sont des systèmes très complexes, dont les propriétés et les facteurs d'influence ne sont pas encore complètement compris. Un soin particulier doit être apporté à leur préparation afin d'en assurer la reproductibilité.

L'un des objectifs de cette thèse était d'étudier les effets de différentes quantités de cardiolipine sur la structure des bicouches amarrées. La CL est un lipide dont la structure unique a été démontrée comme interagissant avec une variété de protéines membranaires. Alors que les fractions de CL habituellement présentes et étudiées sont de l'ordre de 10 à 20 %, des fractions de CL allant jusqu'à 80 % ont été étudiées dans le cadre de cette thèse. La possibilité de produire des tBLMs avec des fractions élevées de CL a été démontrée pour les

deux systèmes d'amarrage étudiés. La modification de la concentration de CL a eu un effet substantiel sur les propriétés de la bicouche lipidique. Les DLP tBLMs avec des fractions élevées de CL étaient électriquement beaucoup plus isolant que les tBLMs d'autres phospholipides, comme le montre une série d'expériences d'EIS. Les études nanostructurales de NR ont révélé une accumulation dense de molécules de PEG dans la région du groupe de tête interne avec une faible teneur en solvant, ce qui pourrait induire ce comportement électrophysiologique. Ce phénomène s'est accompagné de la réduction des régions de la chaîne et souvent de l'expansion de la région du groupe de tête externe, ce qui est interprété comme un arrangement décalé des groupes de tête CL et PC. En général, de grandes fractions de CL ont conduit à une structure modifiée dans les deux systèmes de tBLM. Il est intéressant de noter que les observations étaient très similaires pour les deux systèmes tBLM étudiés. Il est intéressant de noter que les observations étaient très similaires pour les deux systèmes tBLM étudiés. Ils diffèrent dans la structure de l'ancrage d'insertion de la membrane, mais tous deux utilisent une chaîne de PEG comme unité espaceur qui permet l'accumulation de PEG sous la membrane, ce phénomène semble donc être largement indépendant de la structure de l'ancrage.

L'échangeur sodium-hydrogène NhaA a été choisi pour étudier l'incorporation de protéines membranaires dans les systèmes tBLM. Sa nature électrogène en fait un choix intéressant en raison des futures applications possibles dans les dispositifs bio-inspirés. Le NhaA a été incorporé avec succès dans les deux systèmes de tBLM en utilisant différentes méthodes d'incorporation. La fraction volumique incorporée s'élevait à 50 % dans les DLP tBLM, tandis que dans les DPN tBLM, une fraction inférieure de 20 % a été observée. En conséquence, l'incorporation a entraîné des changements mesurables de la structure de la membrane pour les fractions d'incorporation élevées dans les DLP tBLM, tandis que les changements dans les DPN tBLM avec des fractions d'incorporation plus faibles étaient moins prononcés. Le plus notable dans la structure des DLP tBLM était une augmentation de l'épaisseur de la région de la chaîne lipidique pouvant accueillir la protéine de membrane plus épaisse. Il est intéressant de noter que le processus d'incorporation de la protéine a conduit à la disparition de la couche exceptionnellement épaisse du groupe de tête interne qui était constituée de PEG accumulé à proximité des groupes de tête internes. Dans les DPN tBLM, l'incorporation à des fractions inférieures de 20 % n'a provoqué que des changements mineurs dans la structure des tBLM, ce qui montre que l'incorporation de NhaA en général ne perturbe pas de manière significative la structure de la bicouche lipidique. Seules les fractions plus élevées de NhaA induisent des changements significatifs, car la tBLM résultante est déterminée par la structure des protéines tout autant que par celle des lipides. L'activité de la protéine NhaA a été étudiée par des mesures EIS mais n'a pas pu être confirmée. Ceci pour plusieurs raisons, allant de l'inactivité réelle du protéine au choix des techniques expérimentales. D'autres expériences sur ce sujet sont nécessaires pour en déterminer la cause.

Cette thèse a fourni de nouvelles caractérisations nano-structurales de deux types de systèmes tBLM. Les deux systèmes tBLM étudiés présentent des caractéristiques très prometteuses en tant que systèmes modèles de membranes pour les études d'incorporation de

protéines et en tant que systèmes modèles pour l'étude des propriétés des bicouches elles-mêmes. Néanmoins, les résultats de cette thèse soulèvent également plusieurs questions. Ces caractérisations nano-structurales conduisent à des questions concernant les influences spécifiques des différents composants des tBLM mais aussi des facteurs externes, à la fois pendant le processus de formation des tBLM ou sur les tBLM déjà formées. Les nouveaux tBLM DPN se sont révélés être un système expérimental robuste qui convient à l'incorporation de protéines membranaires et qui sera intéressant pour les études de réflectométrie neutronique, car ils ne montrent pas la forte influence de la couche d'or dont ont besoin des autres systèmes de tBLM. L'utilisation de substrats en silicium dopé pourrait permettre la caractérisation électrophysiologique des propriétés de la membrane et de l'activité des protéines incorporées pour développer davantage ce système en tant que plate-forme pour les études des protéines membranaires. Pour cela, il sera important de déterminer davantage les conditions dans lesquelles une monocouche uniforme d'APTES est formée à la surface. L'interaction particulière entre la CL et les chaînes PEG des molécules d'attache est un phénomène qui devrait être étudié plus en détail. Cela pourrait être fait en réalisant des études similaires sur des lipides ayant une structure de groupe de tête comparable comme les phosphoglycérols ou différentes unités d'espacement autres que le PEG. En outre, les tBLM ayant des fractions de CL élevées ont démontré leur aptitude à l'incorporation de protéines et pourraient être utilisées à l'avenir pour étudier l'effet d'une teneur en CL plus élevée sur différentes protéines membranaires qui interagissent avec la CL. Enfin, l'utilisation de mesures simultanées in situ d'EIS et de NR sur les tBLM permettrait d'établir une relation directe entre le comportement électrophysiologique et la nanostructure. Les mesures EIS ont montré une certaine variabilité statistique des propriétés de la bicouche lipidique qui empêche la comparaison entre les résultats obtenus par différentes techniques. Cette variabilité pourrait être réduite en effectuant l'EIS et la NR directement sur le même échantillon. Des premières expériences dans ce sens ont été réalisées dans le cadre de cette thèse, cependant, la grande surface requise pour les expériences NR augmente considérablement la complexité de l'interprétation des données EIS. En conclusion, la mise en place des caractérisations nanostructurales décrites dans cette thèse ouvre la perspective de plusieurs domaines de recherche riches en cours pour améliorer la profondeur des connaissances sur les systèmes membranaires bicouches à lipides amarrées qui incorporent des protéines membranaires.

Appendix

A.1 DLP tBLM multilayer features

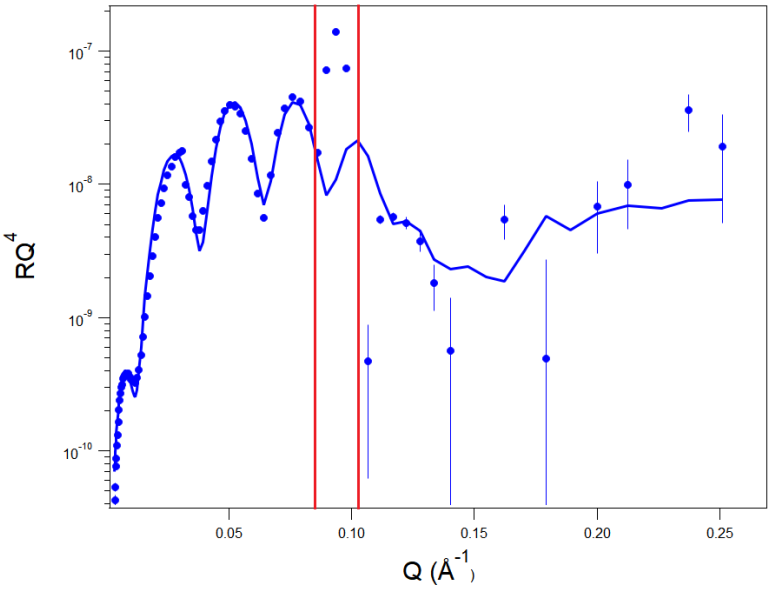

Figure A.1.1: D_2O NR curve of a sample showing the "multilayer peak" indicated in red.

Despite having proven to be a suitable method for membrane production, the utilized rapid solvent exchange methods resulted in unusual structures at times. Fig. A.1.1 shows the reflectivity curve in D_2O of a DLP tBLM which shows a feature that has been observed multiple times. While the general curve shapes corresponds to a tBLM with a structure similar to the ones presented above and can be modelled as such, a peak is visible at approximately 0.1 $Å^{-1}$. This assumed Bragg peak indicates a repetitive structure of a dimension of roughly 50-60 Å. However, multiple bilayers could not represent the curves well, indicating that another type of structure is present, possibly a mixture of tethered bilayer and multiple bilayers. This phenomenon seemed to be independent of lipid composition and will need further investigation to be understood. As it is, it represents an experimental uncertainty in DLP tBLM preparation.

A.2 QCM-D of DLP tBLMs

To investigate the DLP tBLM formation process, QCM-D experiments have been performed. As QCM-D allows to monitor the mass as well as the viscoelastic properties during the process, the different steps like tether molecule adsorption, lipid adsorption and the actual bilayer formation step by rapid solvent exchange can be followed. The frequency shift of the oscillation quartz is directly related to the adsorbed mass, while the dissipation factor gives information on the viscoelasticity (see section 3.3)

This kind of information is on one hand important for the tBLM preparation protocols, as it allows to optimize the incubation times according to adsorption behaviour. One the other hand the amount of adsorbed mass is useful for the interpretation of data obtained through other experimental techniques. Knowing the amount of tether molecules on the surface helps in interpreting the sub-membrane space structure. Finally the Bragg peak-like features which were observed in several NR experiments were investigated by QCM-D.

The QCM-D experiments presented here have been performed with the Q-sense instrument described in section 3.3 at room temperature. All QCM-D crystals were cleaned according to the cleaning protocol in the appendix A.3 prior to use.

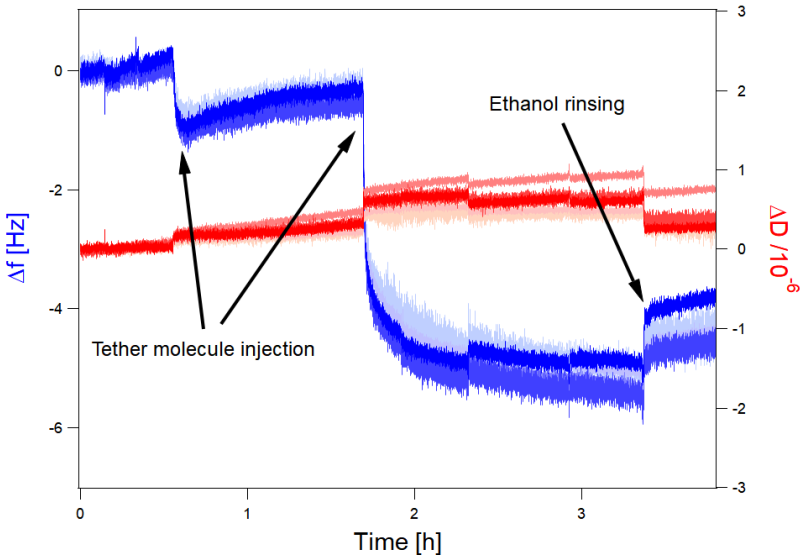

Figure A.2.1: QCM-D curves of a T40 DLP tether molecule adsorption process. Blue curves represent the different frequency overtones with the darkest blue being the 3rd overtone. Red curves show the dissipation factor, the darkest red showing again the 3rd overtone.

Fig. A.2.1 shows a QCM-D experiment following the adsorption process of tether molecules on a gold coated QCM-D chip. The whole process has been carried out with ethanol as a solvent, including the baseline calibration. At the point marked by the first arrow on the left a small amount of T40 mixture was injected into the sample chamber and

left for adsorption. A nearly instantaneous frequency shift of roughly 1 Hz was observed accompanied by a negligible change in dissipation. When the sample showed no further changes, an excess amount of tether molecules was injected so that the whole surface could be covered. While a sudden change of frequency could be observed again, it took roughly 30 minutes to reach a steady state. As the tether molecules were available in excess, this means that the maximum surface coverage was reached. The slowing adsorption speed conforms with the assumption that the whole surface was covered, as it is statistically less likely for dissolved tether molecules to come into contact with an uncovered part of the surface. In addition to that, the length of the tether molecules will cause them to occupy more space on the surface temporarily, which could be freed after some time and thus made available for delayed further adsorption. After removing the remaining unbound tether molecules from the sample cell by rinsing with ethanol, the frequency shift reached a value of roughly -5 Hz. During the whole process only minor changes in the dissipation were observed, which implies that the adsorbed mass was mostly rigid. With this assumption, the Sauerbrey equation can be used to estimate the adsorbed mass as shown in section 3.3, which yielded an adsorbed mass of $\approx$ 90 ng/cm^2. With an average molecular mass of a T40 mixture of 568.04 g/mol this leads to an area per molecule of 1 nm^2. As the exact molecular surface areas of tether and spacer molecules are not known, an precise surface coverage can not be determined, but a large fraction of the surface was certainly covered by tether molecules. While the surface of just the grafting group is definitely smaller (a benzene ring has a diameter of 2.5 Å), if one takes into account the larger surface that a flexible molecule occupies, at such a surface density adsorption of further molecules is most likely prevented by the adsorbed flexible molecules.

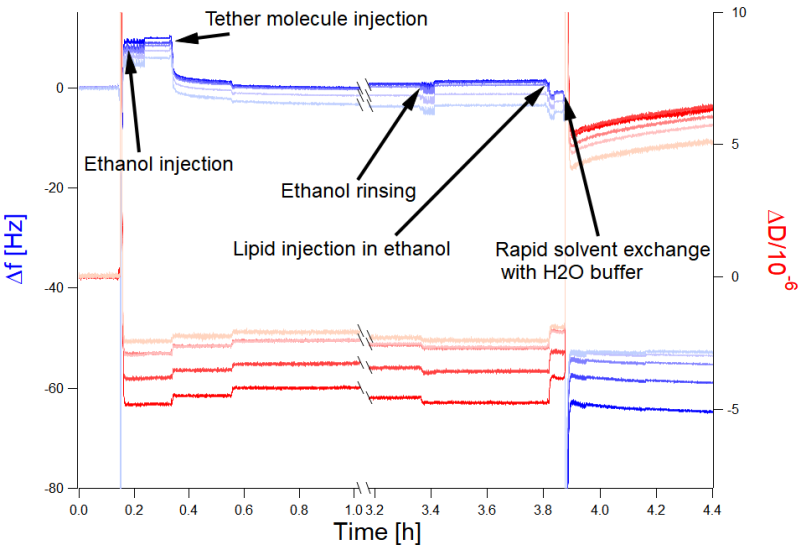

Figure A.2.2: QCM-D curves of a DOPC DLP tBLM formation. Blue curves represent the different frequency overtones with the darkest blue being the 3rd overtone. Red curves show the dissipation factor, the darkest red showing again the 3rd overtone.

Fig. A.2.2 shows the DLP tBLM formation process with QCM-D. A T40 DOPC tBLM was formed at a pH of 7.4 in the standard buffer of 10 mM HEPES with 150 mM NaCl at room temperature. Note that this measurement started with a baseline in H_2O and was later switched to ethanol for the tether procedure. Thus the frequency shifts during the part of the process in ethanol have to be determined from a baseline which is shifted by roughly +10 Hz from the H_2O baseline and will be less precise. Upon tether injection a frequency shift of around 10 Hz is observed, twice the amount when compared to the sample mentioned above. Upon addition of 3.4 mM lipid solution to the chamber a small additional shift in frequency is observed. This confirms, that lipids arrange in the vicinity of the tether molecules on the surface while still dissolved in ethanol. Upon flushing with buffer a large frequency shift down to ≈-60 Hz (from the H_2O baseline) occurs, showing that lipid mass from the solution is attaching to the surface. This frequency shift corresponds to ≈1100 ng/cm^2. That is more than twice the adsorbed mass which would be expected for a SLB (usually showing a frequency shift of around 25 Hz which corresponds to 450 ng/cm^2, see e.g. [50]). When subtracting the 10 Hz shift caused by the mass of the adsorbed tether molecules, it still is on the order of two bilayers. One explanation for this high value could be that a double bilayer has formed on the surface. The frequency shift is accompanied in this case by a dissipation shift of $\approx 6 \cdot 10^{-6}$. That is a high value which suggests the presence of material with viscoelastic properties. Thus the presence of non-lamellar structures like liposomes or micelles is possible. However, the high dissipation can also arise from the contribution of the hydrated sub-membrane space. Even with low water contents of ≈20 % as shown from the NR experiments, it contains a significant amount of water that is trapped in a hydrogel-like structure below the membrane. As this participates in the oscillation of the crystal, the frequency will be affected. From the QCM-D experiments it is not possible to identify which of these assumptions hold true. However, the large adsorbed mass confirms the presence of a further structure on some DLP tBLMs, which is in agreement with the Bragg peak-like feature observed in the NR data.

A.3 Cleaning protocols

Gold coated blocks for NR experiments were cleaned in a multi-step procedure before usage in NR experiments to remove any remaining organic molecules and to prepare them for tether molecule coating. A first step consisted of exposure to UV-ozone for 20 minutes (UV/ozone ProCleaner Plus) or to air plasma for 3 minutes (Harrick plasma cleaner). Alternatively, piranha solution was used to remove any organic molecules from the surface. This was done by carefully submerging the gold coated blocks into a 1:3 mixture of H_2O_2 and H_2SO_4 that was kept below 80 °C for roughly one minute. Further cleaning steps consisted in ultra sonication in 2 % Neutracon solution, MilliQ water, chloroform, acetone and ethanol for 15 minutes each. Samples were kept in ethanol until the tether molecule deposition was performed.

The QCM-chips were first UV/ozone treated for 10 minutes, followed by submersion in a diluted 5:3:1 mixture of MilliQ:H_2SO_4:H_2O_2. Subsequently they were rinsed with MilliQ water and sonicated in MilliQ and ethanol for 15 minutes.

Silicon blocks for NR experiments were cleaned using piranha solution. A concentrated piranha solution consisting of one third H_2O_2 and two thirds H_2SO_4 was carefully prepared and kept at a temperature of no more than 80 °C. Silicon blocks were slowly submerged in the solution and kept for 15 minutes. After removal from the solution they were rinsed with water and dried in a vacuum oven at 80 °C for 15 minutes to remove any remaining solvent.

The peek component of the solid liquid cell and the O-rings were sonicated for 15 minutes in 2 % Neutracon solution followed by ultra-sonication in MilliQ water for the same amount of time. Subsequently they were stored in MilliQ water until use. The tubings were rinsed with large amounts of MilliQ and ethanol repeatedly and then stored in MilliQ until they were used.

Bibliography

[1] A. Nollet. *Part of a Letter from Abbè Nollet, of the Royal Academy of Sciences at Paris, and F.R.S. to Martin Folkes Esq; President of the same, concerning Electricity.* 1748. DOI: 10.1098/rstl.1748.0018.

[2] S. Singer and G. L. Nicolson. 'The Fluid Mosaic Model of the Structure of Cell Membranes'. In: *Science* 175.4023 (1972), pp. 720–731. DOI: 10.1126/science.175.4023.720.

[3] B. Alberts et al. *Molecular Biology of the Cell.* 2014, p. 1464. ISBN: 978-0-815-34432-2.

[4] O. G. Mouritsen and Luis A. Bagatolli. *Life - As A Matter Of Fat.* 2005. ISBN: 3-540-23248-6. DOI: 10.1007/b138577.

[5] *Cell membrane.* URL: https://en.wikipedia.org/wiki/Cell_membrane (visited on 15/04/2020).

[6] Y. H. M. Chan and S. G. Boxer. 'Model membrane systems and their applications'. In: *Current Opinion in Chemical Biology* 11.6 (2007), pp. 581–587. DOI: 10.1016/j.cbpa.2007.09.020.

[7] B. A. Cornell et al. 'A biosensor that uses ion-channel switches.' In: *Nature* 387.6633 (1997), pp. 580–583. DOI: 10.1038/42432.

[8] D. K. Martin et al. 'Ion-Transporting Supported and Tethered Lipid Bilayers That Incorporate Biological Membrane Transport Proteins'. In: *Liposomes, Lipid Bilayers and Model Membranes From Basic Research to Application.* 2016, pp. 383–400.

[9] D. J. McGillivray et al. 'Structure of functional Staphylococcus aureus α-hemolysin channels in tethered bilayer lipid membranes'. In: *Biophysical Journal* 96.4 (2009), pp. 1547–1553. DOI: 10.1016/j.bpj.2008.11.020.

[10] P. Mueller et al. 'Reconstitution of Cell Membrane Structure in vitro and its Transformation into an Excitable System'. In: *Nature* 196 (1962), pp. 1048–1050. DOI: 10.1038/194979a0.

[11] E. Sackmann. 'Supported membranes: Scientific and practical applications'. In: *Science* 271.5245 (1996), pp. 43–48. DOI: 10.1126/science.271.5245.43.

[12] F. Blachon et al. 'Nanoroughness Strongly Impacts Lipid Mobility in Supported Membranes'. In: *Langmuir* 33.9 (2017), pp. 2444–2453. DOI: 10.1021/acs.langmuir.6b03276.

[13] M. Tanaka and E. Sackmann. 'Polymer-supported membranes as models of the cell surface'. In: *Nature* 437.7059 (2005), pp. 656–663. DOI: 10.1038/nature04164.

[14] O. Worsfold, N. H. Voelcker and T. Nishiya. 'Biosensing using lipid bilayers suspended on porous silicon'. In: *Langmuir* 22.16 (2006), pp. 7078–7083. DOI: 10.1021/la060121y.

[15] G. Fragneto, T. Charitat and J. Daillant. 'Floating lipid bilayers: Models for physics and biology'. In: *European Biophysics Journal* 41.10 (2012), pp. 863–874. DOI: 10.1007/s00249-012-0834-4.

[16] J. Y. Wong et al. 'Polymer-Cushioned Bilayers. I. A Structural Study of Various Preparation Methods Using Neutron Reflectometry'. In: *Biophysical Journal* 77.3 (1999), pp. 1445–1457. DOI: 10.1016/S0006-3495(99)76992-4.

[17] I. K. Vockenroth et al. 'Stable insulating tethered bilayer lipid membranes.' In: *Biointerphases* 3.2 (2008), FA68–FA73. DOI: 10.1116/1.2912097.

[18] H. Lang, C. Duschl and H. Vogel. 'A New Class of Thiolipids for the Attachment of Lipid Bilayers on Gold Surfaces'. In: *Langmuir* 10.1 (1994), pp. 197–210. DOI: 10.1021/la00013a029.

[19] N. Bunjes et al. 'Thiopeptide-supported lipid layers on solid substrates'. In: *Langmuir* 13.23 (1997), pp. 6188–6193. DOI: 10.1021/la9703171.

[20] V. Atanasov et al. 'Membrane on a chip: a functional tethered lipid bilayer membrane on silicon oxide surfaces.' In: *Biophysical Journal* 89.3 (2005), pp. 1780–1788. DOI: 10.1529/biophysj.105.061374.

[21] S. Hertrich et al. 'Highly hydrated deformable polyethylene glycol-tethered lipid bilayers'. In: *Langmuir* 30.31 (2014), pp. 9442–9447. DOI: 10.1021/la4045804.

[22] L. Becucci, R. J. Faragher and A. Schwan. 'The effect of the hydrophilic spacer length on the functionality of a mercury-supported tethered bilayer lipid membrane'. In: *Bioelectrochemistry* 101 (2015), pp. 92–96. DOI: 10.1016/j.bioelechem.2014.08.012.

[23] M. L. Wagner and L. K. Tamm. 'Tethered polymer-supported planar lipid bilayers for reconstitution of integral membrane proteins: Silane-polyethyleneglycol-lipid as a cushion and covalent linker'. In: *Biophysical Journal* 79.3 (2000), pp. 1400–1414. DOI: 10.1016/S0006-3495(00)76392-2.

[24] Y. Xue et al. 'Quantifying thiol-gold interactions towards the efficient strength control.' In: *Nature Communications* 5 (2014), pp. 1–9. DOI: 10.1038/ncomms5348.

[25] G. Valincius, T. Meskauskas and F. Ivanauskas. 'Electrochemical impedance spectroscopy of tethered bilayer membranes'. In: *Langmuir* 28.1 (2012), pp. 977–990. DOI: 10.1021/la204054g.

[26] S. Lecuyer, G. Fragneto and T. Charitat. 'Effect of an electric field on a floating lipid bilayer: A neutron reflectivity study'. In: *European Physical Journal E* 21.2 (2006), pp. 153–159. DOI: 10.1140/epje/i2006-10054-8.

[27] J. Lin et al. 'Impedance spectroscopy of bilayer membranes on single crystal silicon'. In: *Biointerphases* 3.2 (2008), FA33–FA40. DOI: 10.1116/1.2896117.

[28] S. Terrettaz, M. Mayer and H. Vogel. 'Highly electrically insulating tethered lipid bilayers for probing the function of ion channel proteins'. In: *Langmuir* 19.14 (2003), pp. 5567–5569. DOI: 10.1021/la034197v.

[29] A. Junghans and I. Köper. 'Structural analysis of tethered bilayer lipid membranes'. In: *Langmuir* 26.13 (2010), pp. 11035–11040. DOI: 10.1021/la100342k.

[30] G. Krishna et al. 'Tethered bilayer membranes containing ionic reservoirs: Selectivity and conductance'. In: *Langmuir* 19.6 (2003), pp. 2294–2305. DOI: 10.1021/la026238d.

[31] W. Knoll et al. 'Functional tethered lipid bilayers'. In: *Reviews in Molecular Biotechnology* 74.3 (2000), pp. 137–158. DOI: 10.1016/S1389-0352(00)00012-X.

[32] C. Rossi et al. 'Surface response methodology for the study of supported membrane formation'. In: *J. Phys. Chem. B* 111.26 (2007), pp. 7567–7576. DOI: 10.1021/jp0686792.

[33] J. Andersson and I. Köper. 'Tethered and polymer supported bilayer lipid membranes: Structure and function'. In: *Membranes* 6.30 (2016), pp. 1–14. DOI: 10.3390/membranes6020030.

[34] R. Budvytyte et al. 'Structure and properties of tethered bilayer lipid membranes with unsaturated anchor molecules'. In: *Langmuir* 29.27 (2013), pp. 8645–8656. DOI: 10.1021/la401132c.

[35] R. M. Epand. 'Biophysical studies of lipopeptide-membrane interactions'. In: *Peptide Science* 43.1 (1997), pp. 15–24. DOI: 10.1002/(SICI)1097-0282(1997)43:1<15::AID-BIP3>3.0.CO;2-3.

[36] C. G. Cranfield et al. 'Evidence of the Key Role of H3O+ in Phospholipid Membrane Morphology'. In: *Langmuir* 32.41 (2016), pp. 10725–10734. DOI: 10.1021/acs.langmuir.6b01988.

[37] F. Giess et al. 'The Protein-Tethered Lipid Bilayer: A Novel Mimic of the Biological Membrane'. In: *Biophysical Journal* 87.5 (2004), pp. 3213–3220. DOI: 10.1529/biophysj.104.046169.

[38] F. Heinrich et al. 'A new lipid anchor for sparsely tethered bilayer lipid membranes'. In: *Langmuir* 25.7 (2009), pp. 4219–4229. DOI: 10.1021/la8033275.

[39] D. J. McGillivray et al. 'Molecular-scale structural and functional characterization of sparsely tethered bilayer lipid membranes.' In: *Biointerphases* 2.1 (2007), pp. 21–33. DOI: 10.1116/1.2709308.

[40] C. G. Cranfield et al. 'Transient potential gradients and impedance measures of tethered bilayer lipid membranes: Pore-forming peptide insertion and the effect of electroporation'. In: *Biophysical Journal* 106.1 (2014), pp. 182–189. DOI: 10.1016/j.bpj.2013.11.1121.

[41] R. Richter, A. Mukhopadhyay and A. Brisson. 'Pathways of lipid vesicle deposition on solid surfaces: a combined QCM-D and AFM study.' In: *Biophysical Journal* 85.5 (2003), pp. 3035–3047. DOI: 10.1016/S0006-3495(03)74722-5.

[42] T. Ragaliauskas et al. 'Fast formation of low-defect-density tethered bilayers by fusion of multilamellar vesicles'. In: *Biochimica et Biophysica Acta - Biomembranes* 1859.5 (2017), pp. 669–678. DOI: 10.1016/j.bbamem.2017.01.015.

[43] C. Rossi et al. 'Differential Mechanisms for Calcium-Dependent Protein/Membrane Association as Evidenced from SPR-Binding Studies on Supported Biomimetic Membranes'. In: *Biochemistry* 42.51 (2003), pp. 15273–15283. DOI: 10.1021/bi035336a.

[44] M. Chadli et al. 'New Tethered Phospholipid Bilayers Integrating Functional G-Protein-Coupled Receptor Membrane Proteins'. In: *Langmuir* 33.39 (2017), pp. 10385–10401. DOI: 10.1021/acs.langmuir.7b01636.

[45] A. O. Hohner, M. P. C. David and J. O. Rädler. 'Controlled solvent-exchange deposition of phospholipid membranes onto solid surfaces'. In: *Biointerphases* 5.1 (2010), pp. 1–8. DOI: 10.1116/1.3319326.

[46] A. Laganowsky et al. 'Membrane proteins bind lipids selectively to modulate their structure and function'. In: *Nature* 510.7503 (2014), pp. 172–175. DOI: 10.1038/nature13419.

[47] S. M. Schiller et al. 'Archaea analogue thiolipids for tethered bilayer lipid membranes on ultrasmooth gold surfaces'. In: *Angewandte Chemie - International Edition* 42.2 (2003), pp. 208–211. DOI: 10.1002/anie.200390080.

[48] R. L. Naumann et al. 'Tethered lipid bilayers on ultraflat gold surfaces'. In: *Langmuir* 19.13 (2003), pp. 5435–5443. DOI: 10.1021/la0342060.

[49] S. R. Jadhav et al. 'Fabrication of highly insulating tethered bilayer lipid membrane using yeast cell membrane fractions for measuring ion channel activity'. In: *Journal of Colloid and Interface Science* 322.2 (2008), pp. 465–472. DOI: 10.1016/j.jcis.2008.02.064.

[50] H. P. Wacklin. 'Composition and asymmetry in supported membranes formed by vesicle fusion'. In: *Langmuir* 27.12 (2011), pp. 7698–7707. DOI: 10.1021/la200683e.

[51] J. F. Nagle and S. Tristram-Nagle. 'Structure of lipid bilayers'. In: *Biochim. Biophys. Acta* 1469 (2000), pp. 159–195. DOI: 10.1016/s0304-4157(00)00016-2.

[52] S. Tristram-Nagle, H. I. Petrache and J. F. Nagle. 'Structure and Interactions of Fully Hydrated Dioleoylphosphatidylcholine Bilayers'. In: *Biophysical Journal* 75.2 (1998), pp. 917–925. DOI: 10.1016/S0006-3495(98)77580-0.

[53] P. L. Yeagle. 'Cholesterol and the cell membrane'. In: *BBA - Reviews on Biomembranes* 822.3-4 (1985), pp. 267–287. DOI: 10.1016/0304-4157(85)90011-5.

[54] H. Alobeedallah, B. A. Cornell and H. Coster. 'The Effect of Cholesterol on the Dielectric Structure of Lipid Bilayers'. In: *The Journal of Membrane Biology* 251.1 (2018), pp. 153–161. DOI: 10.1007/s00232-017-0007-6.

[55] M. C. Pangborn. 'Isolation and Purification of a Serologically Active Phospholipid From Beef Heart'. In: *J. Biol. Chem.* 143 (1942), pp. 247–256.

[56] J. J. Maguire et al. 'Known unknowns of cardiolipin signaling: The best is yet to come'. In: *BBA - Molecular and Cell Biology of Lipids* 1862.1 (2017), pp. 8–24. DOI: 10.1016/j.bbalip.2016.08.001.

[57] R. H. Houtkooper and F. M. Vaz. 'Cardiolipin, the heart of mitochondrial metabolism'. In: *Cellular and Molecular Life Sciences* 65.16 (2008), pp. 2493–2506. DOI: 10.1007/s00018-008-8030-5.

[58] R. N. A. H. Lewis and R. N. McElhaney. 'The physicochemical properties of cardiolipin bilayers and cardiolipin-containing lipid membranes'. In: *BBA - Biomembranes* 1788.10 (2009), pp. 2069–2079. DOI: 10.1016/j.bbamem.2009.03.014.

[59] G. Daum. 'Lipids of mitochondria'. In: *BBA - Reviews on Biomembranes* 822.1 (1985), pp. 1–42. DOI: 10.1016/0304-4157(85)90002-4.

[60] M. Schlame and M. Ren. 'Barth syndrome, a human disorder of cardiolipin metabolism'. In: *FEBS Letters* 580.23 (2006), pp. 5450–5455. DOI: 10.1016/j.febslet.2006.07.022.

[61] H. K. Saini-Chohan et al. 'Cardiolipin biosynthesis and remodeling enzymes are altered during development of heart failure'. In: *Journal of Lipid Research* 50.8 (2009), pp. 1600–1608. DOI: 10.1194/jlr.M800561-JLR200.

[62] M. Schlame, D. Rua and M. L. Greenberg. 'The biosynthesis and functional role of cardiolipin'. In: *Progress in Lipid Research* 39.3 (2000), pp. 257–288. DOI: 10.1016/S0163-7827(00)00005-9.

[63] L. D. Renner and D. B. Weibel. 'Cardiolipin microdomains localize to negatively curved regions of Escherichia coli membranes'. In: *Proceedings of the National Academy of Sciences of the United States of America* 108.15 (2011), pp. 6264–6269. DOI: 10.1073/pnas.1015757108.

[64] A. Shibata et al. 'Significant stabilization of the posphatidylcholine bilayer structure by incorporation of small amounts of cardiolipin'. In: *BBA - Biomembranes* 1192 (1994), pp. 71–78. DOI: 10.1016/0005-2736(94)90144-9.

[65] J. D. Unsay et al. 'Cardiolipin effects on membrane structure and dynamics.' In: *Langmuir* 29.51 (2013), pp. 15878–15887. DOI: 10.1021/la402669z.

[66] T. N. Zeczycki et al. 'Increasing levels of cardiolipin differentially influence packing of phospholipids found in the mitochondrial inner membrane'. In: *Biochemical and Biophysical Research Communications* 450.1 (2014), pp. 366–371. DOI: 10.1016/j.bbrc.2014.05.133.

[67] A. L. Boscia et al. 'X-ray structure, thermodynamics, elastic properties and MD simulations of cardiolipin/dimyristoylphosphatidylcholine mixed membranes'. In: *Chemistry and Physics of Lipids* 178 (2014), pp. 1–10. DOI: 10.1016/j.chemphyslip.2013.12.010.

[68] J. Pan et al. 'Structural and mechanical properties of cardiolipin lipid bilayers determined using neutron spin echo, small angle neutron and X-ray scattering, and molecular dynamics simulations.' In: *Soft Matter* 11.1 (2015), pp. 130–138. DOI: 10.1039/c4sm02227k.

[69] M. Ren, C. K. Phoon and M. Schlame. 'Metabolism and function of mitochondrial cardiolipin'. In: *Progress in Lipid Research* 55.1 (2014), pp. 1–16. DOI: 10.1016/j.plipres.2014.04.001.

[70] N. C. Robinson. 'Functional binding of cardiolipin to cytochrome c oxidase'. In: *Journal of Bioenergetics and Biomembranes* 25.2 (1993), pp. 153–163. DOI: 10.1007/BF00762857.

[71] Y. C. Awasthi et al. 'Tightly bound cardiolipin in cytochrome oxidase'. In: *BBA - Bioenergetics* 226.1 (1971), pp. 42–52. DOI: 10.1016/0005-2728(71)90176-9.

[72] M. Zhang, E. Mileykovskaya and W. Dowhan. 'Gluing the respiratory chain together: Cardiolipin is required for supercomplex formation in the inner mitochondrial membrane'. In: *Journal of Biological Chemistry* 277.46 (2002), pp. 43553–43556. DOI: 10.1074/jbc.C200551200.

[73] K. Gupta et al. 'The role of interfacial lipids in stabilizing membrane protein oligomers'. In: *Nature* 541.7637 (2017), pp. 421–424. DOI: 10.1038/nature20820.

[74] M. Schlame, L. Horvàth and L. Vìgh. 'Relationship between lipid saturation and lipid-protein interaction in liver mitochondria modified by catalytic hydrogenation with reference to cardiolipin molecular species.' In: *The Biochemical Journal* 265.1 (1990), pp. 79–85. DOI: 10.1042/bj2650079.

[75] B. Raguse et al. 'Tethered lipid bilayer membranes: formation and ionic reservoir characterization'. In: *Langmuir* 14.3 (1998), pp. 648–659. DOI: 10.1021/la9711239.

[76] G. Krishna et al. 'Tethered Bilayer Membranes Containing Ionic Reservoirs: The Interfacial Capacitance'. In: *Langmuir* 17 (2001), pp. 4858–4866. DOI: 10.1021/la001480a.

[77] W. Hoiles et al. 'An engineered membrane to measure electroporation: Effect of tethers and bioelectronic interface'. In: *Biophysical Journal* 107.6 (2014), pp. 1339–1351. DOI: 10.1016/j.bpj.2014.07.056.

[78] W. Hoiles et al. 'The effect of tethers on artificial cell membranes: A coarse-grained molecular dynamics study'. In: *PLOS ONE* 11.10 (2016), pp. 1–20. DOI: 10.1371/journal.pone.0162790.

[79] M. Maccarini et al. 'Nanostructural determination of a lipid bilayer tethered to a gold substrate'. In: *The European Physical Journal E* 39.12 (2016), p. 123. DOI: 10.1140/epje/i2016-16123-5.

[80] M. Maccarini et al. 'Functional Characterization of Cell-Free Expressed OprF Porin from Pseudomonas aeruginosa Stably Incorporated in Tethered Lipid Bilayers'. In: *Langmuir* 33 (2017), pp. 9988–9996. DOI: 10.1021/acs.langmuir.7b01731.

[81] S. Park et al. 'Probing the influence of tether density on tethered bilayer lipid membrane (tBLM)-peptide interactions'. In: *Applied Materials Today* 18 (2020), p. 100527. DOI: 10.1016/j.apmt.2019.100527.

[82] C. G. Cranfield et al. 'The Assembly and Use of Tethered Bilayer Lipid Membranes'. In: *Methods in Membrane Lipids*. 2015, pp. 45–53. DOI: 10.1007/978-1-4939-1752-5_4.

[83] *DSPE-PEG-NHS NSP-Functional Polymers and Copolymers*. URL: https://www.nanosoftpolymers.com/product/dspe-peg-nhs/ (visited on 10/03/2020).

[84] G. Fragneto et al. 'Neutrons and Model Membranes: Moving towards Complexity'. In: *Current Opinion in Colloid & Interface Science* (2018). DOI: 10.1016/j.cocis.2018.10.003.

[85] C. Rossi et al. 'A Tethered Bilayer Assembled on Top of Immobilized Calmodulin to Mimic Cellular Compartmentalization'. In: *PLoS ONE* 6.4 (2011), pp. 1–7. DOI: 10.1371/journal.pone.0019101.

[86] J. Kim et al. 'Formation, structure, and reactivity of amino-terminated organic films on silicon substrates'. In: *Journal of Colloid and Interface Science* 329.1 (2009), pp. 114–119. DOI: 10.1016/j.jcis.2008.09.031.

[87] M. Zhu, M. Z. Lerum and W. Chen. 'How to Prepare Reproducible, Homogeneous, and Hydrolytically Stable Aminosilane-derived Layers on Silica'. In: *Langmuir* 28.1 (2012), pp. 416–423. DOI: 10.1021/la203638g.

[88] R. G. Acres et al. 'Molecular structure of 3-aminopropyltriethoxysilane layers formed on silanol-terminated silicon surfaces'. In: *Journal of Physical Chemistry C* 116.10 (2012), pp. 6289–6297. DOI: 10.1021/jp212056s.

[89] S. U. Argekar, T. L. Kirley and D. W. Schaefer. 'Determination of structure-property relationships for 3-aminopropyltriethoxysilane films using x-ray reflectivity'. In: *Journal of Materials Research* 28.8 (2013), pp. 1118–1128. DOI: 10.1557/jmr.2013.54.

[90] A. Coutable et al. 'Preparation of tethered-lipid bilayers on gold surfaces for the incorporation of integral membrane proteins synthesized by cell-free expression'. In: *Langmuir* 30.11 (2014), pp. 3132–3141. DOI: 10.1021/la5004758.

[91] H. M. Keizer et al. 'Functional ion channels in tethered bilayer membranes - Implications for biosensors'. In: *ChemBioChem* 8.11 (2007), pp. 1246–1250. DOI: 10.1002/cbic.200700094.

[92] L. Becucci et al. 'An electrochemical investigation of sarcolipin reconstituted into a mercury-supported lipid bilayer'. In: *Biophysical Journal* 93.8 (2007), pp. 2678–2687. DOI: 10.1529/biophysj.107.109280.

[93] H. Nanda et al. 'Electrostatic interactions and binding orientation of HIV-1 matrix studied by neutron reflectivity'. In: *Biophysical Journal* 99.8 (2010), pp. 2516–2524. DOI: 10.1016/j.bpj.2010.07.062.

[94] R. L. Naumann et al. 'Proton transport through a peptide-tethered bilayer lipid membrane by the H+-ATP synthase from chloroplasts measured by impedance spectroscopy'. In: *Biosensors and Bioelectronics* 17.1-2 (2002), pp. 25–34. DOI: 10.1016/S0956-5663(01)00182-8.

[95] R. L. Naumann et al. 'Kinetics of valinomycin-mediated K+ion transport through tethered bilayer lipid membranes'. In: *Journal of Electroanalytical Chemistry* 550-551 (2003), pp. 241–252. DOI: 10.1016/S0022-0728(03)00013-5.

[96] J. Li-Fries. 'Ion Channels in Mixed Tethered Bilayer Lipid Membranes'. PhD thesis. Mainz, 2007.

[97] I. C. West and P. Mitchell. 'Proton/sodium ion antiport in Escherichia coli.' In: *The Biochemical Journal* 144.1 (1974), pp. 87–90. DOI: 10.1042/bj1440087.

[98] D. Taglicht, E. Padan and S. Schuldiner. 'Overproduction and Purification of a Functional Na+/H+ Antiporter Coded by nhaA (ant) from Escherichia coli'. In: *The Journal of Biological Chemistry* 266.17 (1991), pp. 11289–11294.

[99] E. Padan et al. 'Alkaline pH homeostasis in bacteria: New insights'. In: *BBA - Biomembranes* 1717.2 (2005), pp. 67–88. DOI: 10.1016/j.bbamem.2005.09.010.

[100] C. L. Brett, M. Donowitz and R. Rao. 'Evolutionary origins of eukaryotic sodium/proton exchangers'. In: *American Journal of Physiology - Cell Physiology* 288.2 57-2 (2005), pp. C223–C239. DOI: 10.1152/ajpcell.00360.2004.

[101] C. Hunte et al. 'Structure of a Na+/H+ antiporter and insights into mechanism of action and regulation by pH.' In: *Nature* 435.7046 (2005), pp. 1197–1202. DOI: 10.1038/nature03692.

[102] E. Padan. 'The enlightening encounter between structure and function in the NhaA Na+-H+ antiporter'. In: *Trends in Biochemical Sciences* 33.9 (2008), pp. 435–443. DOI: 10.1016/j.tibs.2008.06.007.

[103] C. Lee et al. 'Crystal structure of the sodium–proton antiporter NhaA dimer and new mechanistic insights'. In: *The Journal of General Physiology* 144.6 (2014), pp. 529–544. DOI: 10.1085/jgp.201411219.

[104] A. Rimon, T. Tzubery and E. Padan. 'Monomers of the NhaA Na+/H+ antiporter of Escherichia coli are fully functional yet dimers are beneficial under extreme stress conditions at alkaline pH in the presence of Na+ or Li+'. In: *Journal of Biological Chemistry* 282.37 (2007), pp. 26810–26821. DOI: 10.1074/jbc.M704469200.

[105] T. Mager et al. 'Transport mechanism and pH regulation of the Na+/H+ antiporter NhaA from Escherichia coli: An electrophysiological study'. In: *Journal of Biological Chemistry* 286.26 (2011), pp. 23570–23581. DOI: 10.1074/jbc.M111.230235.

[106] M. Appel et al. 'Conformations of NhaA, the Na/H Exchanger from Escherichia coli, in the pH-Activated and Ion-Translocating States'. In: *Journal of Molecular Biology* 386.2 (2009), pp. 351–365. DOI: 10.1016/j.jmb.2008.12.042.

[107] Y. Huang et al. 'Mechanism of pH-dependent activation of the sodium-proton antiporter NhaA'. In: *Nature Communications* 7 (2016), pp. 1–10. DOI: 10.1038/ncomms12940.

[108] E. Padan. 'Functional and structural dynamics of NhaA, a prototype for Na+ and H+ antiporters, which are responsible for Na+ and H+ homeostasis in cells'. In: *Biochimica et Biophysica Acta - Bioenergetics* 1837.7 (2014), pp. 1047–1062. DOI: 10.1016/j.bbabio.2013.12.007.

[109] P. Dibrov et al. '2-Aminoperimidine, a specific inhibitor of bacterial NhaA Na+/H+ antiporters'. In: *FEBS Letters* 579.2 (2005), pp. 373–378. DOI: 10.1016/j.febslet.2004.11.098.

[110] L. Galili et al. 'Unraveling functional and structural interactions between transmembrane domains IV and XI of NhaA Na+/H+ antiporter of Escherichia coli'. In: *Journal of Biological Chemistry* 279.22 (2004), pp. 23104–23113. DOI: 10.1074/jbc.M400288200.

[111] E. Padan et al. 'NhaA crystal structure: functional-structural insights.' In: *The Journal of Experimental Biology* 212 (2009), pp. 1593–1603. DOI: 10.1242/jeb.026708.

[112] A. Ben Tahar et al. 'A PANI supported lipid bilayer that contains NhaA transporter proteins provides a basis for a biomimetic biocapacitor'. In: *Chemical Communications* 55.87 (2019), pp. 13152–13155. DOI: 10.1039/c9cc05569j.

[113] T. Flinois et al. 'Assisted lipid deposition by reductive electrochemical aryldiazonium grafting and insertion of the antiport NhaA protein in this stable biomimetic membrane'. In: *Colloids and Surfaces B: Biointerfaces* 190 (2020), p. 110924. DOI: 10.1016/j.colsurfb.2020.110924.

[114] J. Kubicek et al. 'Expression and purification of membrane proteins'. In: *Methods in Enzymology* 541 (2014), pp. 117–140. DOI: 10.1016/B978-0-12-420119-4.00010-0.

[115] A. M. Seddon, P. Curnow and P. J. Booth. 'Membrane proteins, lipids and detergents: Not just a soap opera'. In: *BBA - Biomembranes* 1666.1-2 (2004), pp. 105–117. DOI: 10.1016/j.bbamem.2004.04.011.

[116] A. Berquand et al. 'Influence of calcium on direct incorporation of membrane proteins into in-plane lipid bilayer'. In: *Ultramicroscopy* 107.10-11 (2007), pp. 928–933. DOI: 10.1016/j.ultramic.2007.04.008.

[117] R. Budvytyte et al. 'Modification of Tethered Bilayers by Phospholipid Exchange with Vesicles'. In: *Langmuir* 29 (2013), pp. 4320–4327. DOI: 10.1021/la304613a.

[118] D. Zuber et al. 'Kinetics of charge translocation in the passive downhill uptake mode of the Na+/H+antiporter NhaA of Escherichia coli'. In: *BBA - Bioenergetics* 1709.3 (2005), pp. 240–250. DOI: 10.1016/j.bbabio.2005.07.009.

[119] E. Fermi and W. H. Zinn. *Reflection of neutron on mirrors*. Tech. rep. 1946, pp. 1–4.

[120] J. Chadwick. 'Possible existence of a Neutron'. In: *Nature* 129.3252 (1932), p. 312. DOI: 10.1038/129312a0.

[121] H. Schober. 'An introduction to the theory of nuclear neutron scattering in condensed matter'. In: *Journal of Neutron Research* 17.3-4 (2014), pp. 109–357. DOI: 10.3233/JNR-140016.

[122] T. Russel. 'X-ray and neutron reflectivity for the investigation of polymers'. In: *Materials Science Reports* 5.4 (1990), pp. 171–271. DOI: 10.1016/S0920-2307(05)80002-7.

[123] G. Fragneto. 'Neutron reflectivity at the solid/liquid interface: Examples of applications in biophysics'. In: *Journal of Physics: Condensed Matter* 13.21 (2001), pp. 4973–4989. DOI: 10.1088/0953-8984/13/21/322.

[124] R. Cubitt and G. Fragneto. 'Chapter 2.8.3 Neutron Reflection: Principles and Eexamples of Applications'. In: *Scattering*. 2002, pp. 1198–1208.

[125] A.-J. Dianoux and G. Lander. *Neutron Data Booklet*. 2003. ISBN: 0780388593.

[126] F. Cousin and A. Menelle. 'Neutron reflectivity'. In: *EPJ Web of Conferences* 104 (2015), pp. 1–22. DOI: 10.1051/epjconf/201510401005.

[127] F. Cousin and A. Chennevière. 'Neutron reflectivity for soft matter'. In: *EPJ Web of Conferences* 188 (2018). DOI: 10.1051/epjconf/201818804001.

[128] L. G. Parratt. 'Surface studies of solids by total reflection of x-rays'. In: *Phys. Rev.* 95.2 (1954), pp. 359–369. DOI: 10.1103/PhysRev.95.359.

[129] M. Born et al. *Principles of Optics: Electromagnetic Theory of Propagation, Interference and Diffraction of Light*. 7th ed. Cambridge University Press, 1999. DOI: 10.1017/CBO9781139644181.

[130] L. Névot and P. Croce. 'Caractérisation des surfaces par réflexion rasante de rayons X. Application à l'étude du polissage de quelques verres silicates'. In: *Rev. Phys. Appl. (Paris)* 15.3 (1980), pp. 761–779. DOI: 10.1051/rphysap:01980001503076100.

[131] T. Saerbeck et al. 'Recent upgrades of the neutron reflectometer D17 at ILL'. In: *Journal of Applied Crystallography* 51.2 (2018), pp. 249–256. DOI: 10.1107/S16005767180023 9X.

[132] *FIGARO - Fluid Interfaces Grazing Angles ReflectOmeter*. URL: https://www.ill.eu/fr/utilisateurs/instruments/instruments-list/figaro/description/instrument-layout/ (visited on 03/03/2020).

[133] R. A. Campbell et al. 'FIGARO: The new horizontal neutron reflectometer at the ILL'. In: *European Physical Journal Plus* 126.11 (2011), pp. 1–22. DOI: 10.1140/epjp/i2011-11107-8.

[134] J. Penfold et al. 'Recent advances in the study of chemical surfaces and interfaces by specular neutron reflection'. In: *Journal of the Chemical Society - Faraday Transactions* 93.22 (1997), pp. 3899–3917. DOI: 10.1039/a702836i.

[135] P. Gutfreund et al. 'Towards generalized data reduction on a time-of-flight neutron reflectometer'. In: *Journal of Applied Crystallography* 51 (2018), pp. 1–10. DOI: 10.1107/S160057671800448X.

[136] O. Arnold et al. 'Mantid - Data analysis and visualization package for neutron scattering and μ SR experiments'. In: *Nuclear Instruments and Methods in Physics Research, Section A: Accelerators, Spectrometers, Detectors and Associated Equipment* 764 (2014), pp. 156–166. DOI: 10.1016/j.nima.2014.07.029.

[137] A. R. Nelson. 'Co-refinement of multiple-contrast neutron/X-ray reflectivity data using MOTOFIT'. In: *Journal of Applied Crystallography* 39.2 (2006), pp. 273–276. DOI: 10.1107/S0021889806005073.

[138] A. R. Nelson and S. W. Prescott. 'Refnx: Neutron and X-ray reflectometry analysis in python'. In: *J. Appl.Cryst.* 52 (2019), pp. 193–200. DOI: 10.1107/S1600576718017296.

[139] O. Heavens. 'Optical Properties of Thin Films'. In: *Reports on Progress in Physics* 23.1 (1960), pp. 1–65. DOI: 10.1088/0034-4885/23/1/301.

[140] M. Björck. 'Fitting with differential evolution: An introduction and evaluation'. In: *Journal of Applied Crystallography* 44.6 (2011), pp. 1198–1204. DOI: 10.1107/S0021889811041446.

[141] Kenneth Levenberg. 'A Method for the Solution of Certain Non-Linear Problems in Least Squares'. In: *Quarterly of Applied Mathematics* 2 (1944), pp. 164–168. DOI: 10.1090/qam/10666.

[142] D. W. Marquardt. 'An algorithm for least-squares estimation of nonlinear parameters'. In: *Journal of the Society for Industrial and Applied Mathematics* 11.2 (1963), pp. 431–441. DOI: 10.1137/0111030.

[143] T. Krist, M. Brière and L. Cser. 'H in Ti thin films'. In: *Thin Solid Films* 228.1-2 (1993), pp. 141–144. DOI: 10.1016/0040-6090(93)90583-B.

[144] A. Paul et al. 'Substrate-stress-induced magnetic and nonmagnetic structural correlations in Fe/Si multilayers'. In: *Journal of Applied Crystallography* 48 (2015), pp. 1023–1033. DOI: 10.1107/S1600576715009942.

[145] *Biomolecular Scattering Length Density Calculator*. URL: http://psldc.isis.rl.ac.uk/Psldc/ (visited on 03/04/2020).

[146] A. J. Bard and L. R. Faulkner. *Electrochemical Methods Fundamentals and Applications*. John Wiley & Sons, Inc., 2001, p. 833. ISBN: 0-471-04372-9.

[147] M. E. Orazem and B. Tribollet. *Electrochemical Impedance Spectroscopy*. John Wiley & Sons, Inc., 2008, pp. 1–525. ISBN: 9780470041406.

[148] J. Bisquert and F. Fabregat-Santiago. 'Impedance spectroscopy: A general introduction and application to dye-sensitized solar cells'. In: *Dye-sensitized solar cells*. EPFL Press, 2010. Chap. 12, pp. 1–99.

[149] D. D. MacDonald. 'Reflections on the history of electrochemical impedance spectroscopy'. In: *Electrochimica Acta* 51.8-9 (2006), pp. 1376–1388. DOI: 10.1016/j.electacta.2005.02.107.

[150] D. W. Deamer and J. Bramhall. 'Permeability of lipid bilayers to water and ionic solutes'. In: *Chemistry and Physics of Lipids* 40.2-4 (1986), pp. 167–188. DOI: 10.1016/0009-3084(86)90069-1.

[151] C. Steinem et al. 'Impedance analysis of supported lipid bilayer membranes: a scrutiny of different preparation techniques.' In: *BBA* 1279.2 (1996), pp. 169–180. DOI: 10.1016/0005-2736(95)00274-X.

[152] H. Fricke. 'The electric capacity of suspensions with special reference to blood'. In: *Journal of General Physiology* 9.2 (1925), pp. 137–152. DOI: 10.1085/jgp.9.2.137.

[153] G. Wiegand et al. 'Electrical properties of supported lipid bilayer membranes'. In: *Journal of Physical Chemistry B* 106.16 (2002), pp. 4245–4254. DOI: 10.1021/jp014337e.

[154] G. Valincius et al. 'Electrochemical Impedance Spectroscopy of Tethered Bilayer Membranes: An Effect of Heterogeneous Distribution of Defects in Membranes'. In: *Electrochimica Acta* 222 (2016), pp. 904–913. DOI: 10.1016/j.electacta.2016.11.056.

[155] K. J. Kwak et al. 'Formation and finite element analysis of tethered bilayer lipid structures'. In: *Langmuir* 26.23 (2010), pp. 18199–18208. DOI: 10.1021/la1021802.

[156] G. Valincius and M. Mickevicius. 'Tethered Phospholipid Bilayer Membranes. An Interpretation of the Electrochemical Impedance Response'. In: *Advances in Planar Lipid Bilayers and Liposomes*. Vol. 21. 2015, pp. 27–61. ISBN: 9780128021163. DOI: 10.1016/bs.adplan.2015.01.003.

[157] J. K. Kendall et al. 'Effect of the structure of cholesterol-based tethered bilayer lipid membranes on ionophore activity'. In: *ChemPhysChem* 11.10 (2010), pp. 2191–2198. DOI: 10.1002/cphc.200900917.

[158] M. L. Taylor, S. Sharifi and D. D. Macdonald. 'Optimization of Impedance Models with Differential Evolution'. In: *ECS Trans.* 50.31 (2013), pp. 131–139. DOI: 10.1149/05031.0131ecst.

[159] S. Maher et al. 'Micron dimensioned cavity array supported lipid bilayers for the electrochemical investigation of ionophore activity'. In: *Bioelectrochemistry* 112 (2016), pp. 16–23. DOI: 10.1016/j.bioelechem.2016.07.002.

[160] G. Sauerbrey. 'Verwendung von Schwingquarzen zur Wägung dünner Schichten und zur Mikrowägung'. In: *Zeitschrift für Physik* 155.2 (1959), pp. 206–222. DOI: 10.1007/BF01337937.

[161] P. L. Konash and G. J. Bastiaans. 'Piezoelectric crystals as detectors in liquid chromatography'. In: *Analytical Chemistry* 52.12 (1980), pp. 1929–1931. DOI: 10.1021/ac50062a033.

[162] M. Laatikainen and M. Lindström. 'Determination of adsorption isotherms with quartz crystal microbalance in liquid phase'. In: *Journal of Colloid And Interface Science* 125.2 (1988), pp. 610–614. DOI: 10.1016/0021-9797(88)90027-6.

[163] F. Höök et al. 'Energy dissipation kinetics for protein and antibody-antigen adsorption under shear oscillation on a quartz crystal microbalance'. In: *Langmuir* 14.4 (1998), pp. 729–734. DOI: 10.1021/la970815u.

[164] D. M. Gryte, M. D. Ward and W.-S. Hu. 'Real-Time Measurement of Anchorage-Dependent Cell Adhesion Using a Quartz Crystal Microbalance'. In: *Biotechnology Progress* 9.1 (1993), pp. 105–108. DOI: 10.1021/bp00019a016.

[165] M. C. Dixon. 'Quartz crystal microbalance with dissipation monitoring: Enabling real-time characterization of biological materials and their interactions'. In: *Journal of Biomolecular Techniques* 19.3 (2008), pp. 151–158.

[166] M. Rodahl et al. 'Simultaneous frequency and dissipation factor QCM measurements of biomolecular adsorption and cell adhesion'. In: *Faraday Discussions* 107 (1997), pp. 229–246. DOI: 10.1039/a703137h.

[167] E. Briand et al. 'Combined QCM-D and EIS study of supported lipid bilayer formation and interaction with pore-forming peptides.' In: *The Analyst* 135.2 (2010), pp. 343–350. DOI: 10.1039/b918288h.

[168] C. Montis et al. 'Nucleolipid bilayers: A quartz crystal microbalance and neutron reflectometry study'. In: *Colloids and Surfaces B: Biointerfaces* 137 (2016), pp. 203–213. DOI: 10.1016/j.colsurfb.2015.07.039.

[169] N. Kučerka et al. 'Lipid Bilayer Structure Determined by the Simultaneous Analysis of Neutron and X-Ray Scattering Data'. In: *Biophysical Journal* 95.5 (2008), pp. 2356–2367. DOI: 10.1529/biophysj.108.132662.

[170] R. Vácha et al. 'Effects of alkali cations and halide anions on the DOPC lipid membrane'. In: *Journal of Physical Chemistry A* 113.26 (2009), pp. 7235–7243. DOI: 10.1021/jp809974e.